ANL-7176

339
4-11-66

ANL-7176

MASTER

Argonne National Laboratory

REACTOR DEVELOPMENT PROGRAM

PROGRESS REPORT

February 1966

DISCLAIMER

LEGAL NOTICE

Printed in USA. Price $4.00 . Available from the Clearinghouse for Federal Scientific and Technical Information, National Bureau of Standards, U. S. Department of Commerce, Springfield, Virginia

ANL-7176
Reactor Technology
(TID-4500)
AEC Research and
Development Report

ARGONNE NATIONAL LABORATORY
9700 South Cass Avenue
Argonne, Illinois 60439

REACTOR DEVELOPMENT PROGRAM PROGRESS REPORT

February 1966

Albert V. Crewe, Laboratory Director
Stephen Lawroski, Associate Laboratory Director

Division	Director
Chemical Engineering	R. C. Vogel
Idaho	M. Novick
Metallurgy	F. G. Foote
Reactor Engineering	L. J. Koch
Reactor Physics	R. Avery
Remote Control	R. C. Goertz

Report coordinated by
R. M. Adams and A. Glassner

Issued March 23, 1966

Operated by The University of Chicago
under
Contract W-31-109-eng-38
with the
U. S. Atomic Energy Commission

FOREWORD

The Reactor Development Program Progress Report, issued monthly, is intended to be a means of reporting those items of significant technical progress which have occurred in both the specific reactor projects and the general engineering research and development programs. The report is organized in a way which, it is hoped, gives the clearest, most logical overall view of progress. The budget classification is followed only in broad outline, and no attempt is made to report separately on each sub-activity number. Further, since the intent is to report only items of significant progress, not all activities are reported each month. In order to issue this report as soon as possible after the end of the month editorial work must necessarily be limited. Also, since this is an informal progress report, the results and data presented should be understood to be preliminary and subject to change unless otherwise stated.

The issuance of these reports is not intended to constitute publication in any sense of the word. Final results either will be submitted for publication in regular professional journals or will be published in the form of ANL topical reports.

The last six reports issued in this series are:

August 1965	ANL-7090
September 1965	ANL-7105
October 1965	ANL-7115
November 1965	ANL-7122
December 1965	ANL-7132
January 1966	ANL-7152

REACTOR DEVELOPMENT PROGRAM

Highlights of Project Activities for February 1966

EBR-II

The scheduled maintenance and modification program during reactor shutdown is in progress. New dip ring heaters have been installed in the rotating plug seal trough, and the primary-tank heater thimbles have been replaced with ones of new design. The primary system is being held at 280°F for current work.

The fuel-transfer arm, which had been operating with difficulty over an extended period of time, was removed into an inert-atmosphere, neoprene-nylon bag, cleaned, and inspected. It was found that the bell crank had broken loose at the pivot point of vertical-horizontal movement. This is being corrected by redesign and replacement of the bell crank. The procedure has been valuable in demonstrating that components can be removed from the reactor to facilitate repairs when required.

ZPPR

A supplement to the ZPPR Preliminary Safety Analysis Report, submitted to the AEC on February 3, 1966, describes a new backup containment structure and provides answers to questions raised by various Commission review bodies. The report on the coring of the Gravel Gertie structure was also forwarded to AEC this month.

ZPR-3

The first phase of the SEFOR critical experiments, run as part of the AEC assistance program to the SEFOR project, was completed. In addition to experiments with the unsegmented SEFOR core, Doppler experiments were performed on a basis that did not interrupt the planned experimental program. Work was begun on experiments with a SEFOR two-segment fuel-element design.

PLUTONIUM RECYCLE PROGRAM (EBWR)

The unrodded and unpoisoned plutonium zone in the EBWR had been found experimentally to have a multiplication constant of 1.001 when loaded with twenty-two assemblies. A four-group, two-dimensional diffusion-theory calculation for this configuration yielded a multiplication constant of 1.008. In the calculation the control-rod followers were assumed to be made of Zircaloy; actually, the lower 15 in. of the followers are of stainless steel. Calculations will be made to estimate the reactivity effect due to the stainless steel.

ERRATUM to ANL-7152

Page 7, paragraph 5, sentence 3, reading "The fuel had received... subassembly." should read: "The fuel had received 0.1-0.2 a/o burnup on the initial irradiation and ~1.0 a/o burnup on the reprocessed subassembly."

TABLE OF CONTENTS

TABLE OF CONTENTS

TABLE OF CONTENTS

I. LIQUID-METAL-COOLED REACTORS

A. EBR-II

1. Operations

Work on planned maintenance and modifications, started after the scheduled shutdown on January 23 (see Progress Report for January 1966, ANL-7152, p. 1) is continuing.

Work has begun to replace the 200 dip ring heaters in the large and small rotating plug seals. The replacement heaters are clad in Type 405 stainless steel instead of Type 304 because of the better compatibility of the former with the tin-bismuth alloy in the rotating seal.

After the heat transfer systems were cooled to 350°F, the secondary system was drained and cooled to room temperature. The steam system was cooled, drained, and all major components were opened for inspection. Examination of the main condensers, No. 2 feedwater heater, and the steam drum revealed no evidence of pitting or corrosion.

The temperature of the primary system was reduced to 280°F, and the primary-tank heater thimbles were replaced with ones of new design (see Section I.A.4).

2. Removal of Fuel-transfer Arm

During cooling of the primary system, the locking-pin actuating arm in the fuel-transfer mechanism became difficult to operate, despite frequent programmed exercising. When checked with a specially fabricated tool that duplicated the upper adapter of a subassembly, it was found that difficulty existed in engaging and disengaging, and that the "sensing" feature of the mechanism that indicates the presence of a subassembly was missing.

On February 19, the transfer arm and its shielding plug were removed by raising them into a specially fabricated neoprene-nylon bag that maintained the inert gas atmosphere. The operation was performed in a routine manner as planned and proved valuable in demonstrating that equipment can be removed from the tank when necessary to facilitate repairs of vital components.

Adhered sodium was permitted to oxidize in air and then cleaned from the assembly. When the inspection port between the horizontal and vertical shafts of the transfer mechanism was cut open, the bell crank at the pivot point of the locking pin and sensing rod mechanism was observed to have failed. In addition, an aluminum-bronze bushing at the base of the vertical shaft was badly deteriorated. A newly redesigned bell crank was fabricated and is being installed.

Radioactivity associated with the removal of the transfer arm was very low. Induced activity in the stainless steel of the mechanism was less than one mR/hr, beta and gamma, on contact. The maximum activity on the carrier block after sodium removal was 12 mR/hr at 2 in. Sodium activity had decayed to 10^{-2} μCi/g, primarily due to Na^{22}.

3. Maintenance and Minor Modifications

A number of maintenance jobs, minor modifications, and tests have been accomplished during this shutdown period. These include the following:

Test and lapping of the steam-drum safety valves; overhaul of the turbine-driven feedwater pump; mechanical modification to the fuel-unloading-machine position-indicating system; cleaning of condensed sodium from the N-1 and N-2 argon inlet and outlet nozzles on the primary tank; maintenance on nuclear and process instrumentation; rebuilding the startup feedwater pump; overhaul of the gland seal exhauster; many other minor items.

Mechanical installation of the replacement feedwater-pressure control valve has been completed and control-system installation started.

4. Reactor Improvements

Replacement of the primary-tank heater thimbles went smoothly, and new silicon-controlled rectifiers were installed for the heater-power-control systems. After test these were placed in operation. Work is in progress to eliminate noise from this power source in the low-level nuclear instrumentation.

5. Reactor Physics and Kinetics

a. Computer Calculations. Work is being performed on digital simulation of reactor kinetics for programming with the 1604 computer when it becomes available.

Work is also being done on analog estimation of the accuracy of kinetics analyses. The existing analog equipment shows fluctuations which may be difficult to eliminate.

A program for a 91-subassembly (Mark I-A) core with 14 experimental subassemblies "homogenized" in Row 4 was sent to the Applied Mathematics Division for computation of power generation in the core and blanket. The results will be used for determining temperatures and burnup rates in the larger core.

The substitution worth of a subassembly (blanket to enriched) in Row 6 was calculated by Mach-1 code to be 0.30%; the average of previously measured values is 0.31%.

b. Fuel-pin Failure. A proposal is being considered to investigate the consequences of actual failure of a fuel pin. It involves the reirradiation of a bare Mark-I pin which has already reached a maximum burnup of 1.2 a/o. The irradiation will continue until the specimen fails as indicated by the fission product-monitoring systems, or it will be removed for inspection if no such indication is received after reasonable additional burnup.

To attain representative operating temperatures, the test specimen would be located at the center of a cluster of six unirradiated Mark-I-A fuel pins. Autocatalytically propagated failure effects would be limited by surrounding the test cluster with a ring of 12 stainless-steel-filled dummy pins. Following failure, the reactor would be shut down and the test subassembly removed for inspection.

c. Heat Transfer. The use of a steady-state heat transfer program written for the 1620 computer allows an analysis of expected performance (flow and temperature pattern) of all subassemblies scheduled for insertion into the core. Also, the ARGUS program for transient analysis has been applied to the 70 and 52% enriched driver subassemblies with an output giving subassembly time-temperature characteristics. The use of ARGUS (transient) and the steady-state programs will allow a complete analysis of the core whenever revised power distribution is required.

6. Experimental Irradiations

a. Neutron Radiography. A procedure was devised for preparing very thin boron oxide-zinc sulphide films for use as neutron-sensitive scintillators. Scintillators of this type appear promising as image converters for neutron radiographic applications.

Calculations were made for the shielding requirements of irradiated experimental fuel capsules. According to the calculations, a dose rate of 11 mR/hr would be observed at a distance of one meter from three capsules with 25 cm of lead and 2 cm of iron as shield materials.

There has been considerable difficulty experienced in bonding a very thin (0.001-in.) layer of boron nitride to a conductor without altering the properties of the boron nitride. Because of these difficulties, delivery of a neutron-sensitive vidicon tube is delayed until early March 1966.

7. Fuel Cycle Facility

Two radial blanket assemblies ("A" type) were dismantled, and rods were prepared for transfer to the TAN hot cell facility for sampling and

examination. One of the assemblies (from Row 6) was removed for blanket surveillance, and the other contained an experimental irradiation (A776X--samples for α measurement).

A new bond-testing machine has been received from the manufacturer. This machine was redesigned to increase the life of the drive mechanism and the eddy-current coils. It will be installed in the Air Cell when out-of-cell testing and calibration are completed.

In an effort to increase production by reducing the work load on the pin-processor machine, four batches (272 pins) of Chicago-produced Mark-I-A fuel pins were loaded into jackets; calculated values of pin volumes rather than volumes obtained by the pin-processing equipment were used. Preliminary bond testing indicated that the rate of acceptance for sodium level in an element is normal.

Work is continuing on identifying the character and nature of the scale found on pins from the first returned subassembly (C-162) fabricated from irradiated fuel (see Progress Report for January 1966, ANL-7152, p. 7). A revised analysis of the scale shows that it contained only 0.8% rather than 10% sodium. Samples of the scale have been submitted for emission spectrographic and X-ray diffraction analysis. Metallographic examination continues.

Transfer of fuel between the reactor and the FCF has been suspended as a result of the maintenance and modification work being done on the reactor.

Production is summarized in Table I.

TABLE I. Production Summary--February 1966

Subassemblies Received*	9
Subassemblies Dismantled	15
Subassemblies Fabricated	11
Subassemblies Transferred to Reactor*	7
Pins Decanned	1210
Melt-refining Runs:	
Irradiated Fuel	9
Recycle Metal	1
Average Pouring Yield	92.9%
Injection-casting Runs	6
Pin Processing: (253 additional Chicago Mark I-A)	
Acceptable Pins	734
Reject Pins	95
Pins Welded	1155
Leak Testing:	
Accepts	1078
Rejects	46
Bond Testing (completed runs):	
Accepts	1233
Rejects	119
Surveillance: C-102, C-135	

*Transfer of fuel between the reactor and FCF has been temporarily suspended as a result of the reactor-modification program.

B. General Fast Reactor Physics

1. ZPR-3

The first phase of the SEFOR critical experiments in ZPR-3 was completed this month. This is the experiment being conducted as part of the Atomic Energy Commission's program of assistance to the Southwest Experimental Fast Oxide Reactor (SEFOR) project. The experiments performed during the first phase of the program were done on a mockup of the SEFOR reactor core with an unsegmented fuel-element design.

Following completion of the first phase, experiments were begun with a SEFOR mockup with a two-segment fuel-element design. This experiment is intended to investigate the change in reactivity due to fuel expansion when measuring the SEFOR Doppler effect. A 2-in. gap is placed in the fuel so that one segment expands into a region of higher reactivity and the other expands into a region of lower worth. Criticality was reached with 327.4 kg of $Pu^{239+241}$. The ZPR-3 control rod was recalibrated, and physics measurements were started.

a. Initial SEFOR Criticality. Following is a detailed description of Assembly 47, a mockup of SEFOR at reactor loading No. 15, the loading at which the assembly was first critical.

An interface view of Half No. 1 of the reactor is shown in Fig. 1. All of the drawer type numbers are shown in their proper locations. Figures 2 through 5 show the actual arrangement of the materials in each type of drawer loading. Half No. 2 of the assembly is loaded as the mirror image of Half No. 1, except for the location of the C-6 and C-16 type drawers in the core. These drawers will be discussed later. Figure 6 is a horizontal view of the reactor showing the location and dimensions of the various regions of the SEFOR mockup.

Two types of plutonium fuel are used in the mockup. The original or "old" fuel on hand was plutonium with 1.1 w/o aluminum jacketed in stainless steel in the form of plates of 1/8-in. nominal thickness. The additional plutonium required for this assembly was obtained as a Pu-U-Mo alloy, called "new." The plutonium enrichment is 20%. It is also canned in stainless steel and is 1/4 in. thick. The new plutonium was loaded in core region 1A and the old plutonium in core region 1B (see Fig. 6) to provide a negative overall temperature coefficient of reactivity for this assembly.

The core drawer loadings are based on a unit of five drawers, C-1 through C-5 and C-11 through C-15. These drawer loadings are shown in Fig. 2. The remaining edge core drawers are shown in Figs. 3 and 4 along with blanket drawer BC-1 which is loaded behind all the core drawers. The control drawers, CC-2 and CC-4, are loaded like C-2 and C-4 plus BC-1, except that one column of 1/8-in. aluminum is removed.

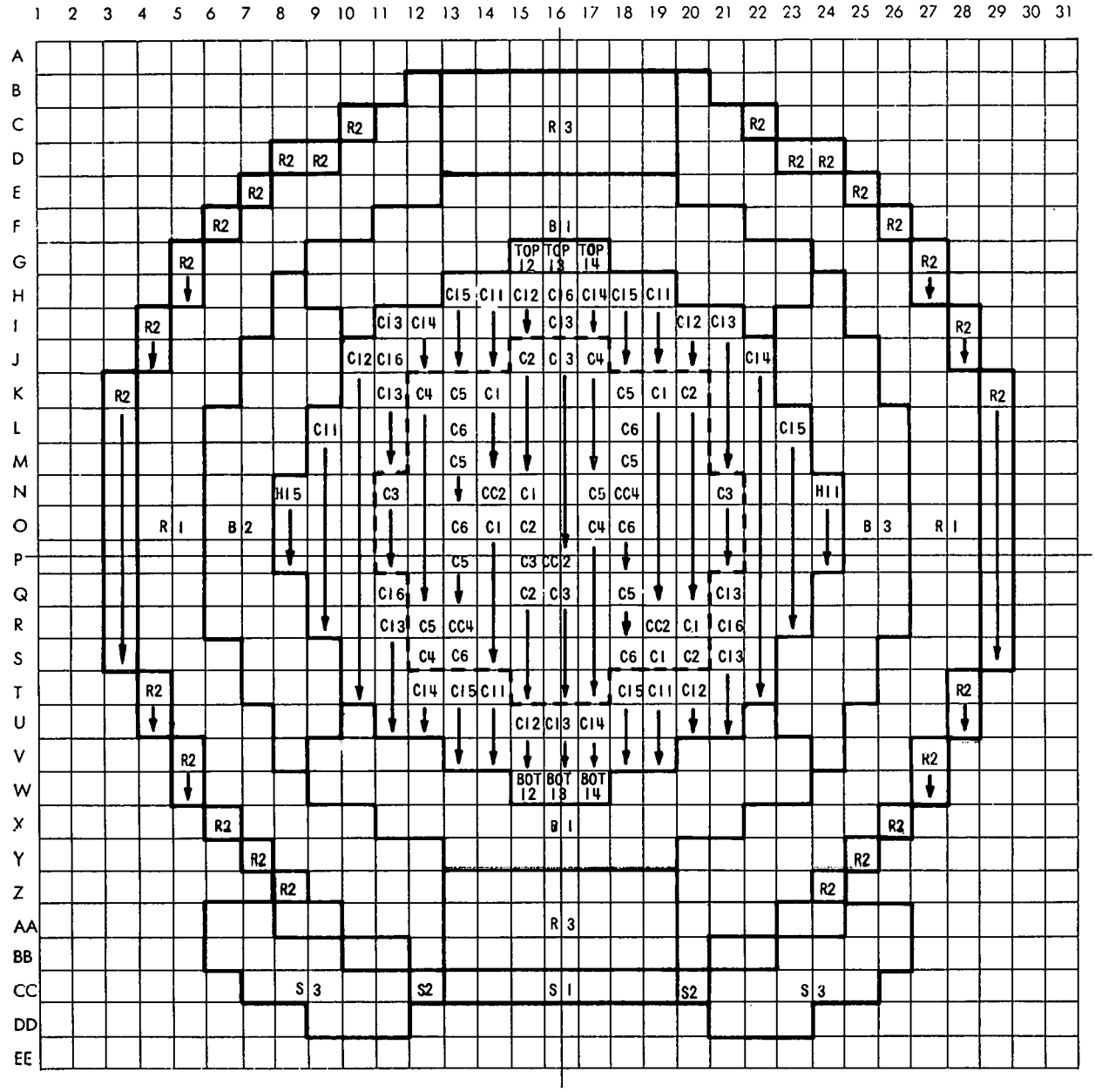

Fig. 1. Interface View of Half No. 1 of Assembly 47, ZPR-3, for Loading No. 15

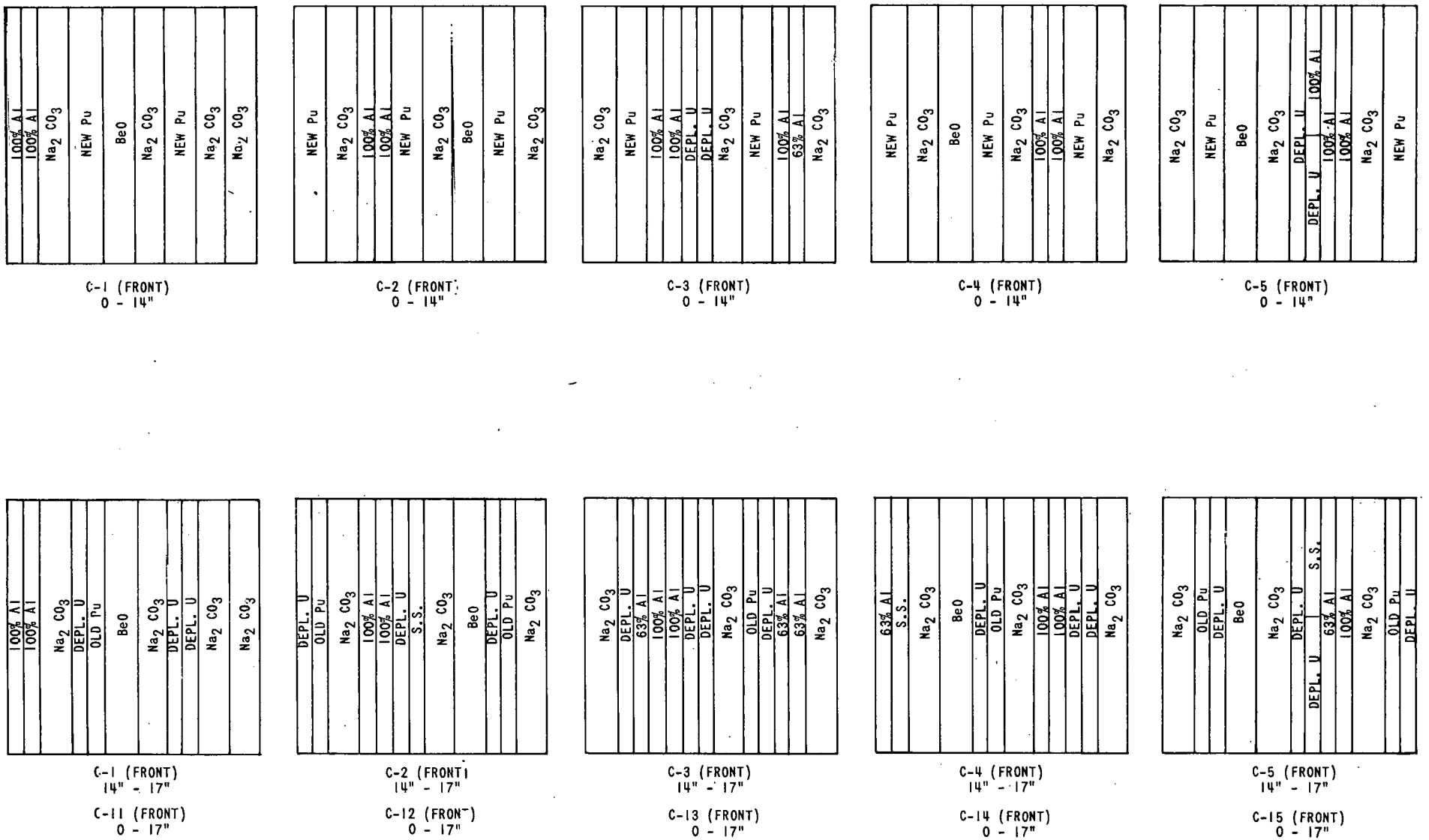

Fig. 2. Drawer Loadings, Assembly 47, ZPR-3

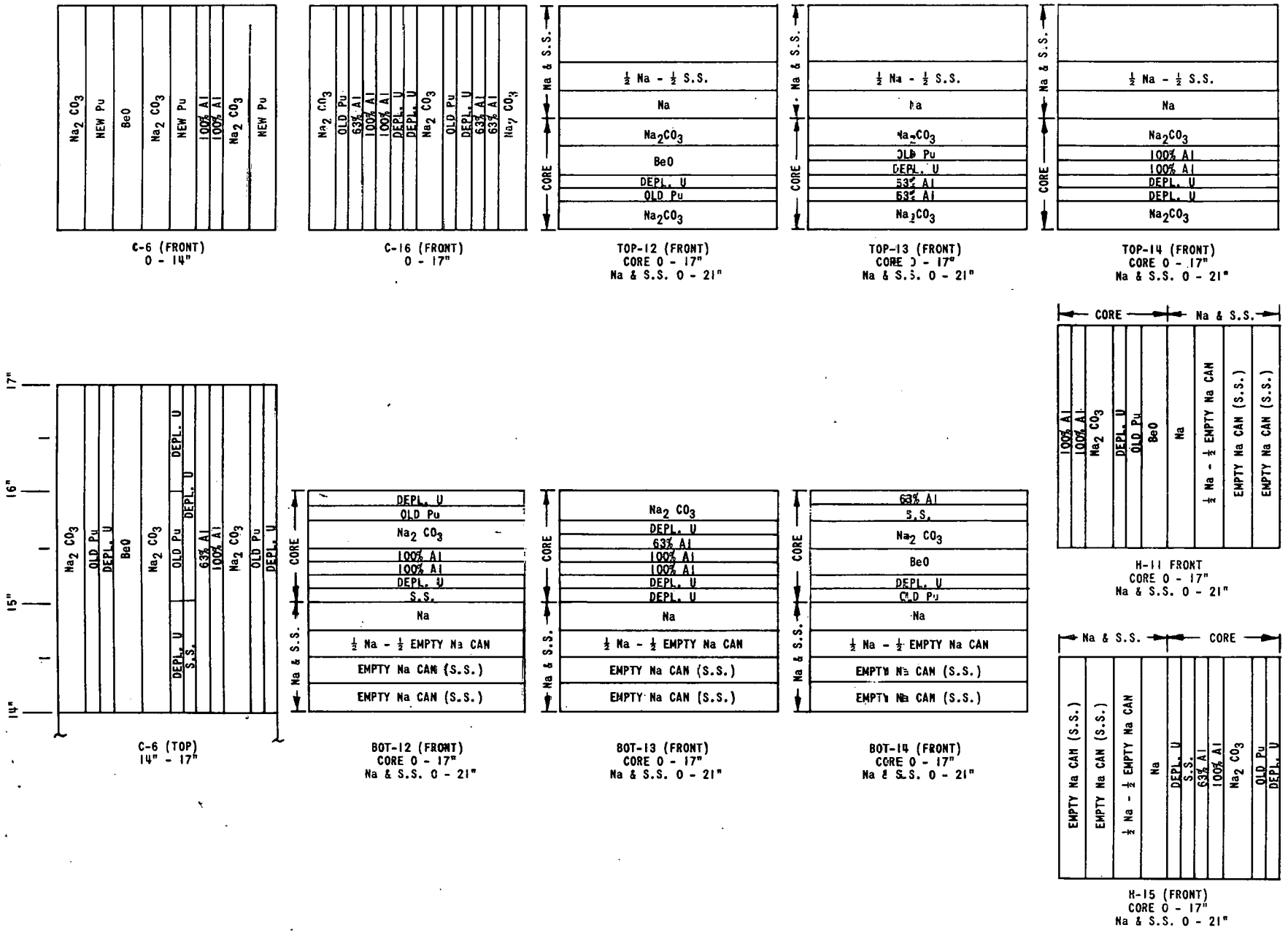

Fig. 3. Drawer Loadings, Assembly 47, ZPR-3

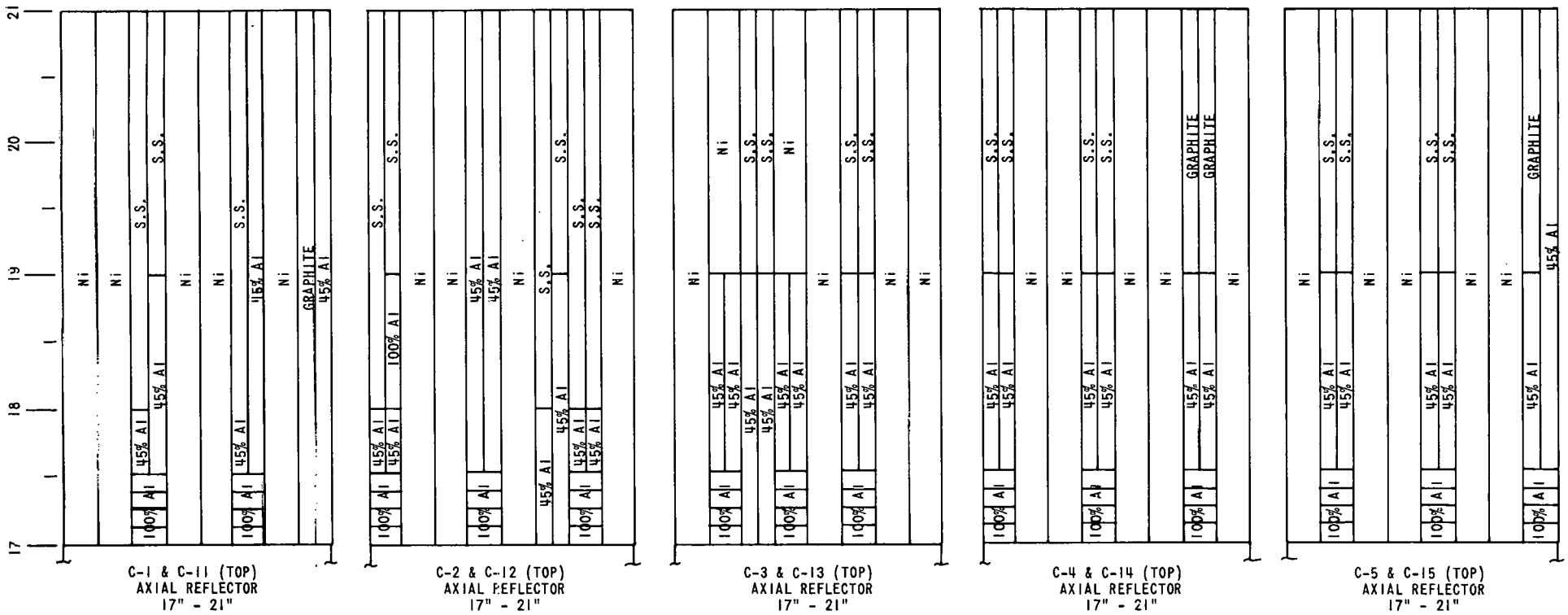

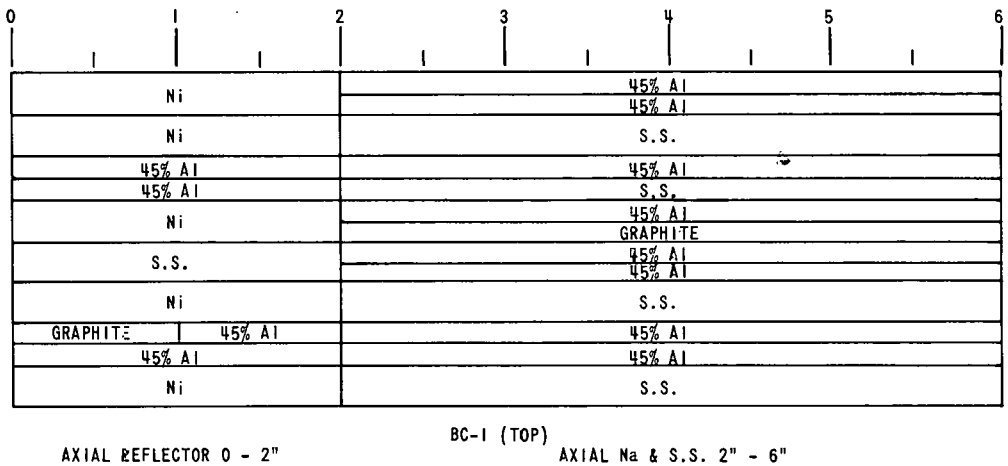

Fig. 4. Drawer Loadings, Assembly 47, ZPR-3

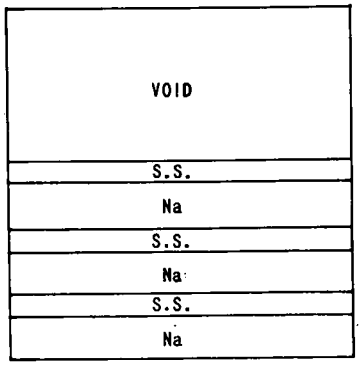

B-1 (FRONT)
RADIAL Na & S.S.
0 - 27"

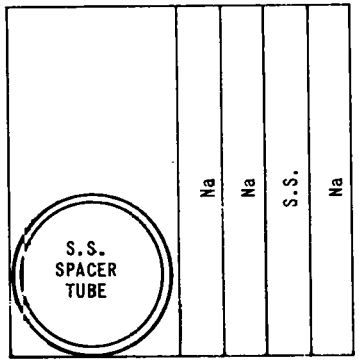

B-2 (FRONT)
RADIAL Na & S.S.
0 - 27"

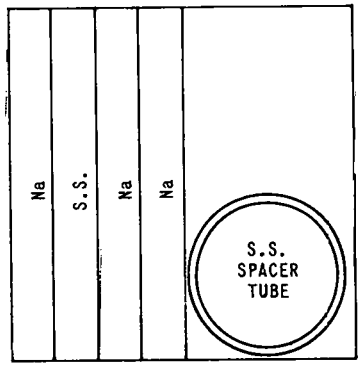

B-3 (FRONT)
RADIAL Na & S.S.
0 - 27"

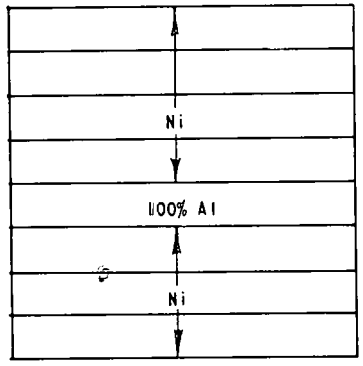

R-1 (FRONT)
RADIAL REFLECTOR
0 - 20"
(NO DRAWER)

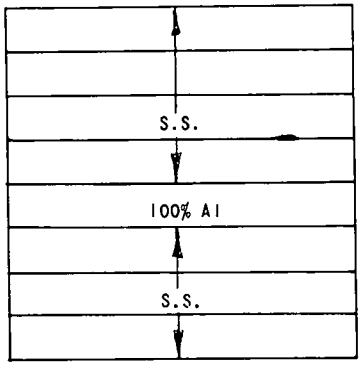

R-2 (FRONT)
RADIAL REFLECTOR
0 - 20"
(NO DRAWER)

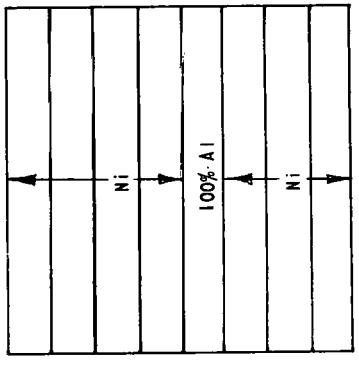

R-3 (FRONT)
RADIAL REFLECTOR
0 - 20"

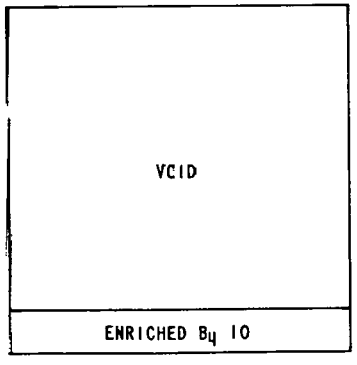

S-1 (FRONT)
BORON CARBIDE SHIELD
0 - 21"

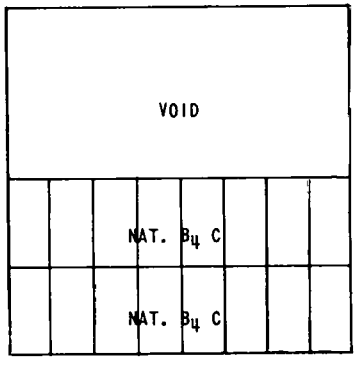

S-2 (FRONT)
BORON CARBIDE SHIELD
0 - 21"

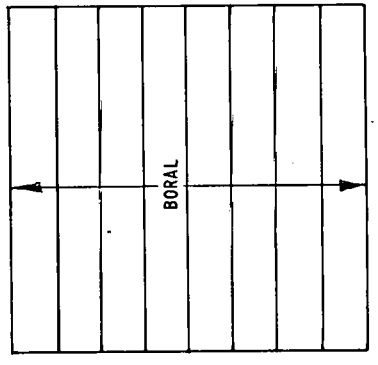

S-3 (FRONT)
BORON CARBIDE SHIELD
0 - 21"

Fig. 5. Drawer Loadings, Assembly 47, ZPR-3

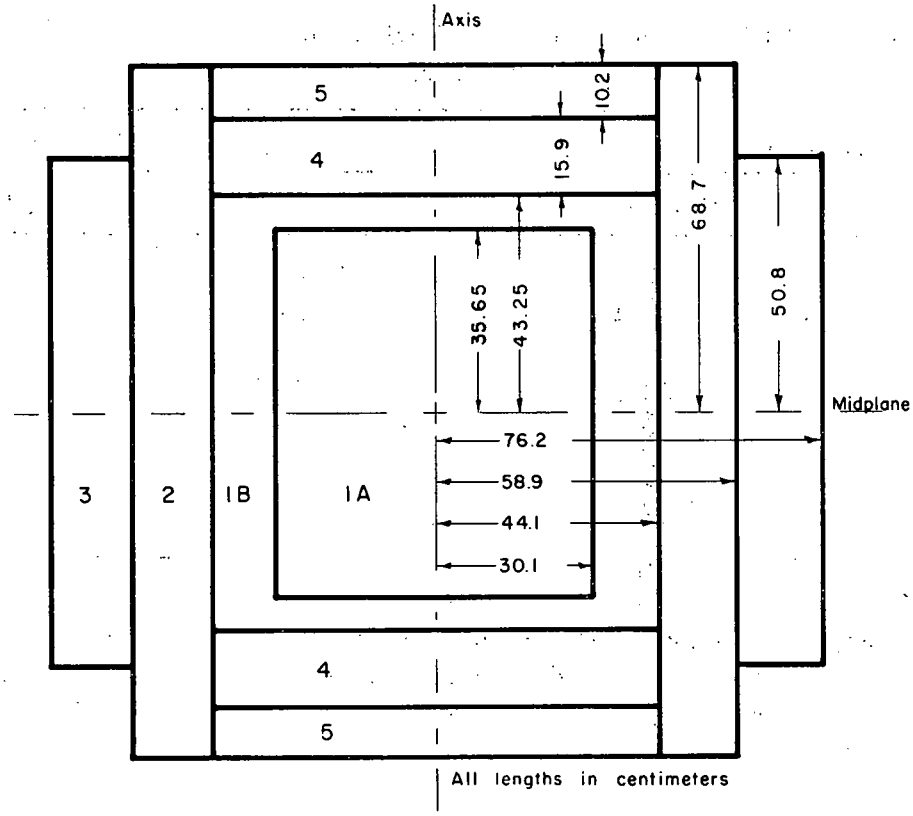

Fig. 6. Horizontal View of Assembly 47 of ZPR-3

On Figs. 2 and 3, front views are given of the various core drawers, with the material in each column labeled. As a further elaboration of these figures, the average quantity of material per lineal inch of each column in the core drawers is given in Table II. The stainless steel associated with drawers and matrix tubes is also given in Table III. The stainless steel alloy is Type 304 and has a nominal composition of 69.7 w/o Fe, 17 w/o Cr, 10.4 w/o Ni, 1.1 w/o Mn, and 0.6 w/o Si.

TABLE II. Composition of Individual Columns

Nominal Material	Column Thickness (in.)	Composition of 2-in.-high Column (g/in. of length)
100% Al	1/8	10.62 Al
63% Al	1/8	6.73 Al
BeO	1/4	8.158-Be, 14.482-O
Na_2CO_3	1/4	6/18-Na, 1.609-C, 6.437-O, 8.60-SS
Depl. U	1/8	73.99-U^{238}, 0.16-U^{235}
New Pu	1/4	18.259-$Pu^{239+241}$, 1.630-Pu^{240}, 79.57-U^{238}, 2.55-Mo, 7.14-SS, 0.17-U^{235}
Old Pu	1/8	32.83-$Pu^{239+241}$, 1.568-Pu^{240}, 0.36-Al, 8.29-SS
SS	1/8	30.71-SS
Drawers and matrix		56.53-SS

TABLE III. Core Drawer Substitutions for Increasing Plutonium Enrichment

Type C-6 for C-5		Type C-16 for C-13	
Half No. 1	Half No. 2	Half No. 1	Half No. 2
1-L-13	2-R-12	1-J-11	2-U-11
1-O-13	2-K-13	1-Q-11	2-U-16
1-S-13	2-N-13	1-H-16	2-K-21
1-L-18	2-Q-13	1-R-21	
1-O-18	2-K-18		
1-P-18	2-M-18		
1-S-18	2-Q-18		
	2-R-18		

Figure 5 shows the drawer loadings for the radial sodium and stainless steel Region 2, the radial reflector Region 3, and the boron carbide shield. Stainless steel was substituted in part of the reflector because there was insufficient nickel on hand.

To achieve criticality in loading No. 15, the plutonium enrichment was increased by substituting core drawers C-6 for C-5 and C-16 for C-13. Table III lists the matrix positions where these substitutions were made.

Table IV lists the actual material composition of the regions in the assembly with all control drawers inserted. With the configuration, the measured multiplication constant, k, was 1.00030 ± 0.00003. The mass of this loading included 314.31 kg $Pu^{239+241}$ in a core volume of 527.6 liters.

TABLE IV. Assembly 47 Composition for Loading No. 15

Reactor Region			Material Composition (g/cc)											
Name	No.	Volume (ℓ)	Pu^{239} + Pu^{241}	Pu^{240}	U^{238}	U^{235}	Bo	O	Mo	C	Na	Al	304 SS	Ni
Core (New Pu)	1A	203.1	0.5875	0.0525	3.06	0.006	0.085	0.416	0.082	0.067	0.253	0.313	1.31	
Core (Old Pu)	1B	324.5	0.6007	0.0287	3.12	0.006	0.081	0.406		0.067	0.252	0.346	1.43	
Radial Na/SS	2	661.5									0.235	0.022	2.16	
Radial Reflector	3(Ni)	579.2										0.276	0.60	6.36
Radial Reflector	3(SS)	155.6										0.274	6.29	
Axial Reflector	4	195.5								0.035		0.239	1.62	4.25
Axial Na/SS	5	127.7								0.075		0.482	3.58	

b. Radial Fission and BF_3 Traverses. To complete the determination of the power distribution in the SEFOR reactor, radial traverses were made to augment the axial traverses previously reported (see Progress Report for January 1966, ANL-7152, pp. 11-13).

The design details of the mockup for both the radial and axial traverses were as described in Section 1.a. U^{238} and Pu^{239} fission counters and a BF_3 proportional counter were used for the traverses. The traverse tube was placed at the radial midplane of the reactor in the front of the drawers in the 16th row in Half No. 2. Figures 7, 8, and 9 show the results of the three traverses with the SEFOR rods Nos. 2 and 3 completely inserted. The slight tilting of the curves is perhaps due to the fact that the fuel columns in the outer core region are not symmetrical about the vertical midplane of the assembly, causing the half of the core nearer rod No. 2 to be loaded a little heavier than the other half of the core. Figure 10 is a Pu^{239} traverse with SEFOR rod No. 3 removed. The peak in the sodium and stainless steel region caused by the nickel reflector is eliminated, as may be seen by comparison with Fig. 7.

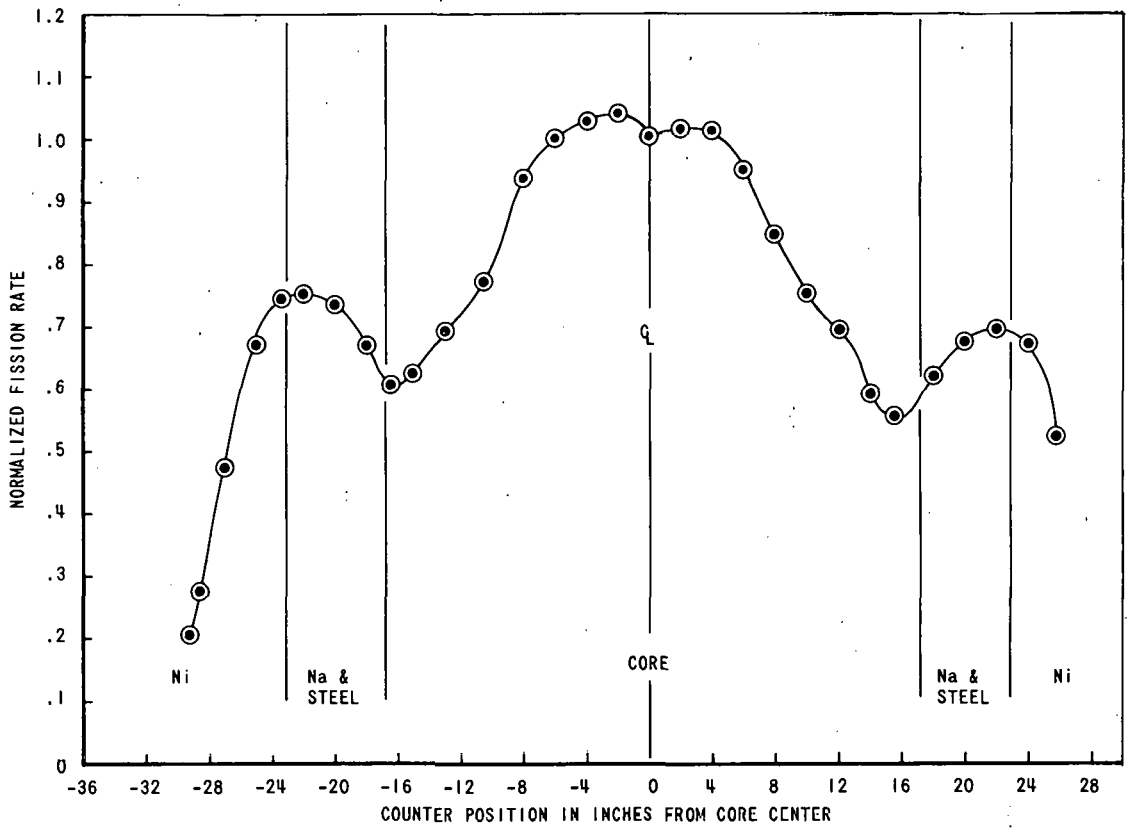

Fig. 7. Radial Traverse with Pu^{239} Fission Counter

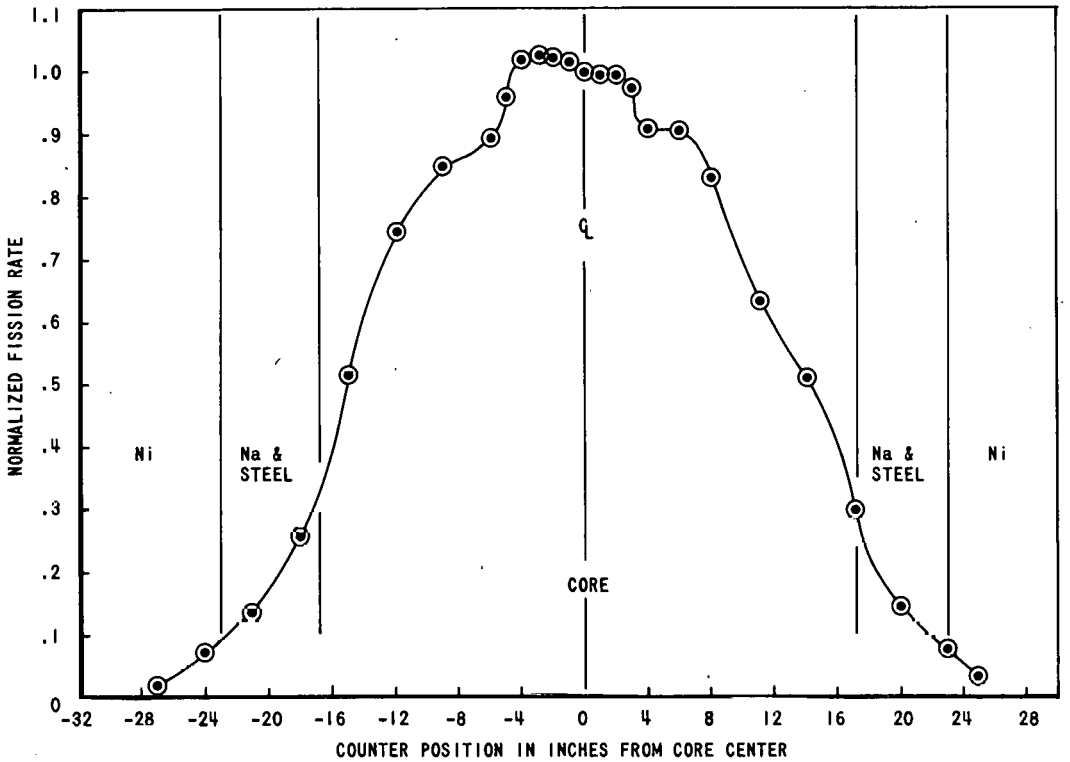

Fig. 8. Radial Traverse with U^{238} Fission Counter

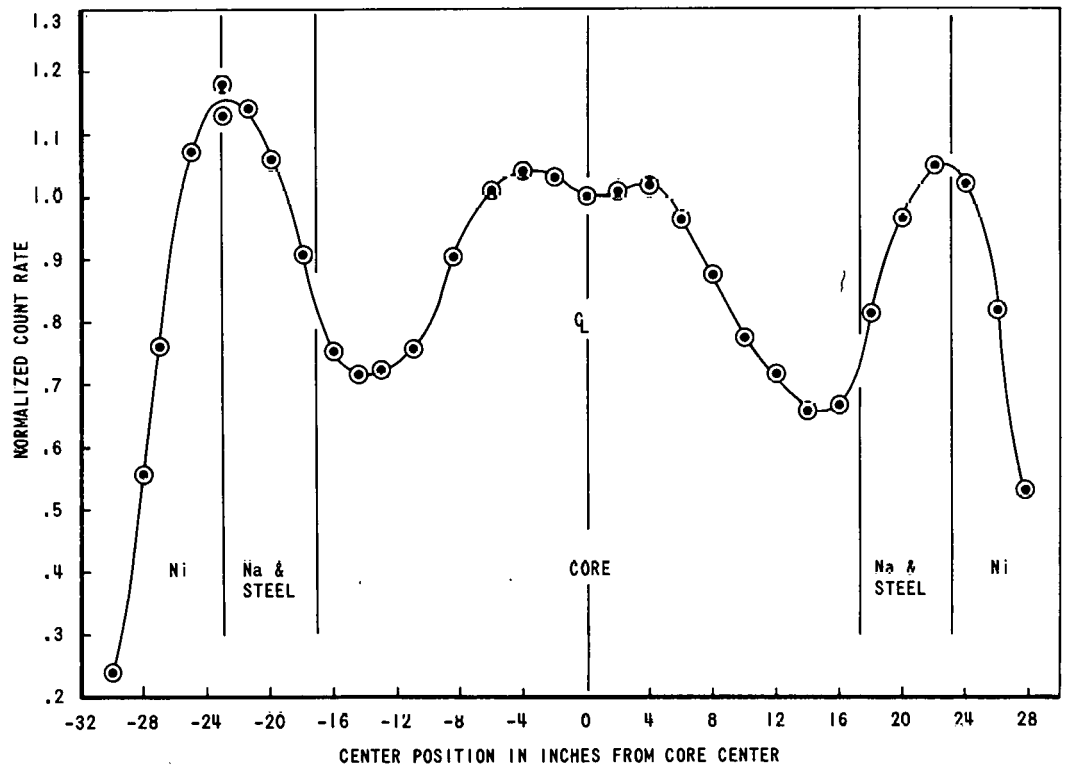

Fig. 9. Radial Traverse with BF_3 Proportional Counter

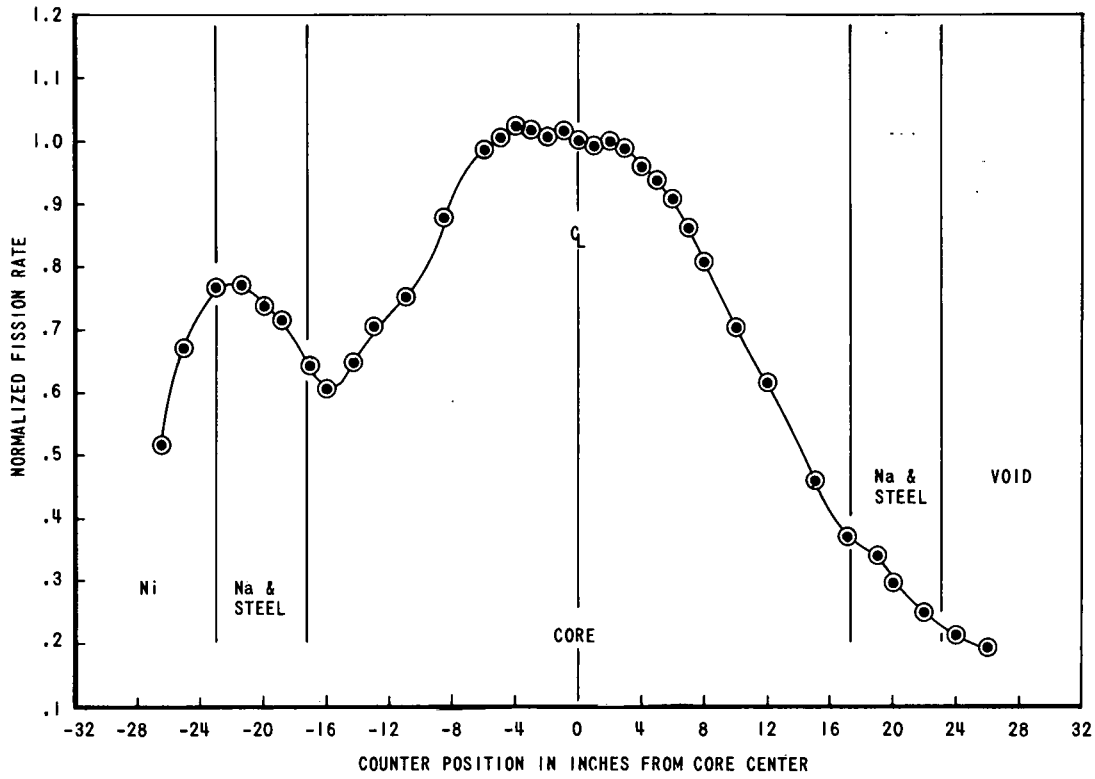

Fig. 10. Radial Traverse with Pu^{239} Fission Counter and SEFOR Rod No. 3 Removed

c. Spectral Indices. Fission ratios were measured at the center of the core to help determine the neutron spectrum at this point. Two gas-flow-type absolute fission counters were placed in the center of the core; one counter contained a U^{235} foil as a standard, and U^{233}, U^{238}, Pu^{239}, and Pu^{240} foils were placed in the other. The results are listed in Table V.

TABLE V. Central Fission Ratios

$\sigma_{28}/\sigma_{25} = 0.0264$
$\sigma_{23}/\sigma_{25} = 1.451$
$\sigma_{49}/\sigma_{25} = 0.9163$
$\sigma_{40}/\sigma_{25} = 0.2006$

d. Measurements of Reactivity Worth. The reactivity worths of many materials of interest to reactor design were measured at the center of the core. Two-inch cubes of materials, either solid material, material in stainless steel cans, or thin samples with 1/8-in. pieces of aluminum to make the 2-in. cube of material required by the changer, were moved in and out of the core by means of a sample changer. Results are given in Table VI. All measurements are compared to a 2-in. void in the center of the core. Since corrections for any aluminum or stainless steel around the samples were made the numbers given are for the materials as listed. Corrections for temperature drift, which was appreciable, were determined by making reference measurements frequently between the sample measurements.

TABLE VI. Measurements of Central Reactivity Worth Relative to Void

Material	Sample Size (in.)	Sample Weight (g)			Material Worth (Ih/kg)
		Material	Aluminum	Stainless	
Al (100%)	2 x 2 x 2	350.5	-	-	-15.0 ± 0.6
Al (45%)	2 x 2 x 2	143.2	-	-	-13.2 ± 1.4
SS	2 x 2 x 2	1026.1	-	-	-10.8 ± 0.2
SS	8--1/4 x 2 x 2 Empty Na cans	166.8	0	0	-11.6 ± 1.2[a]
Fe	2 x 2 x 2	1028.0	-	-	-9.4 ± 0.2
Mo	2 x 2 x 2	1279.8	-	-	-38.0 ± 0.2
Cr	2--1 x 2 x 2 cans	439.2	-	102.4	-10.7 ± 0.5
Mn	2--1 x 2 x 2 cans	597.3	-	102.0	-21.3 ± 0.3
Ni	2 x 2 x 2	1150.4	-	-	-13.8 ± 0.2
Na	2--1 x 2 x 2 cans	91.2	-	195.0	-8.4 ± 3.0
Be	2 x 2 x 2	240.7	-	-	+33.2 ± 0.8
BeO	2 x 2 x 2	361.3	-	-	+4.4 ± 0.6
Al_2O_3	2--1 x 2 x 2 cans	224.2	-	174.1	-15.2 ± 0.9
Fe_2O_3	2--1 x 2 x 2 cans	341.0	-	180.4	-11.7 ± 0.6
Graphite	2 x 2 x 2	196.4	-	-	-9.7 ± 1.0
Zr	2 x 2 x 2	846.0	-	-	-10.7 ± 0.2
Bi	2 x 2 x 2	1276.2	-	-	-2.1 ± 0.2
Ta	2--1 x 2 x 2 cans	1004.0	-	102.4	-103.2 ± 2.0
W	2--1 x 2 x 2 cans	1867.2	-	103.1	-35.6 ± 0.1
B_4C (Enr)[b]	1--1/4 x 2 x 2	32.4	125.4	-	-4300 ± 125
Depl U	2 x 2 x 2	2460.4	-	-	-21.2 ± 0.1
Pu[c]	1--1/4 x 2 x 2 can	93.0	153.1	-	+462 ± 2
Pu[d]	1--1/8 x 2 x 2 can	69.1	135.3	17.9	+448 ± 3
Pu[d]	2--1/8 x 2 x 2 cans	138.1	126.7	35.9	+469 ± 2
Pu[d]	3--1/8 x 2 x 2 cans	207.2	119.0	53.8	+474 ± 1
Pu-U-Mo[e]	1--1/8 x 2 x 2 can	79.9	135.9	14.6	+52.4 ± 2.5
Pu-U-Mo[e]	2--1/8 x 2 x 2 cans	159.8	124.5	29.2	+56.7 ± 1.3
Pu-U-Mo[e]	3--1/8 x 2 x 2 cans	239.7	117.0	43.8	+59.1 ± 0.8
Enr U[f]	1--1/16 x 2 x 2 plate	72.1	146.6	-	+328 ± 3
Enr U[f]	2--1/16 x 2 x 2 plates	144.2	136.0	-	+335 ± 2
Enr U[f]	3--1/16 x 2 x 2 plates	216.4	136.5	-	+331 ± 1

[a] Average of two measurements.

[b] 62.33 w/o B^{10}, 7.01 w/o B^{11}, 30.66 w/o C.

[c] 94.51 a/o Pu^{239}, 5.11 a/o Pu^{240}, 0.38 a/o Pu^{241}.

[d] 95.06 w/o Pu^{239}, 4.55 w/o Pu^{240}, 0.39 w/o Pu^{241}.

[e] 17.86 w/o $Pu^{239+241}$, 1.64 w/o Pu^{240}, 78.0 w/o Depl U, 2.5 w/o Mo.

[f] 93.0 w/o U^{235}.

e. Measurements of Ratio of U^{238} Capture to U^{235} Fission. Natural and enriched uranium foils were irradiated at four radial core positions in the reactor midplane. The fissions and captures in the foils were determined by radiochemical analysis. Fissions were determined by the Mo^{99} production and captures were determined by the Np^{239} production. Table VII lists the results of the analysis. The natural uranium foils were placed in the mirror image positions from the enriched foils, except for sample 1E, which could not be placed in 1-N-17 because the drawer type had been changed. Figure 11 shows the exact position of the foils in the front of the drawers.

TABLE VII. Results of Fission and Capture Analysis of Natural and Enriched Uranium Foils

Foil No.	Foil Size (in., mil)	Enrichment (%)	Location	Foil Wt (g)	Fissions/g	Captures/g ($\times 10^{-9}$)
1E	0.995 dia x 5	93.09	1-Q-17	1.2715	1.29×10^{10}	
2E	0.995 dia x 5	93.07	1-N-16	1.2715	1.32×10^{10}	
3E	1/4 x 1 x 20	93.18	1-N-12	1.5237	1.08×10^{10}	
4E	1/4 x 1 x 20	93.18	1-N-9	1.5752	7.20×10^{9}	
5N	1.0 dia x 10	Natural	2-N-17	2.5000	4.13×10^{8}	2.03
6N	1.0 dia x 10	Natural	2-N-16	2.4378	4.23×10^{8}	1.95
7N	1/2 x 1 x 25	Natural	2-N-12	3.7393	3.86×10^{8}	1.42
8N	1/2 x 1 x 25	Natural	2-N-9	3.7043	2.18×10^{8}	1.08

f. Doppler Effect Measurements. Measurements of the Doppler effect in U^{238} with the SEFOR core were made by means of a newly developed foil-activation technique that requires only a half-hour irradiation at 50 W.

A scintillation counter was used to discriminate against the fission product activity in a highly depleted uranium foil in a fast-neutron spectrum. The gamma counter (developed by Davey of the Idaho Division) uses a combination of a thin lead filter and a thin NaI crystal, and has good efficiency between about 40 and 90 keV. With the aid of a pulse-height analyzer, the 74-keV gamma ray of U^{239} can be counted with only 5 to 20% of the total count arising from fission products. An automatic, two-position changer combined with a Nuclear Data Analyzer Type 180 is used so that two foils may be counted repeatedly in succession with a single detector.

A simple electrically heated resistance furnace is evacuated to eliminate oxidation of the uranium and reduce heat conduction. The resistance coil heats a ceramic element suspended inside the furnace, and one foil is located in a recess in the ceramic. The other (cold) monitor foil is located outside the furnace.

The experiments consist of comparing the U^{239} activity of the inner (furnace) foil and the outer (cold monitor) foil at different temperatures. The foils are 0.005-in. thick and 0.50 in. in diameter, and are identical in weight. The U^{235} content is nominally 0.2%.

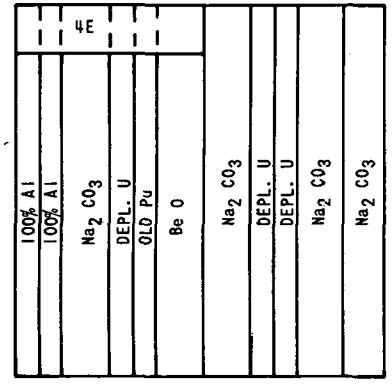

1 - N - 9

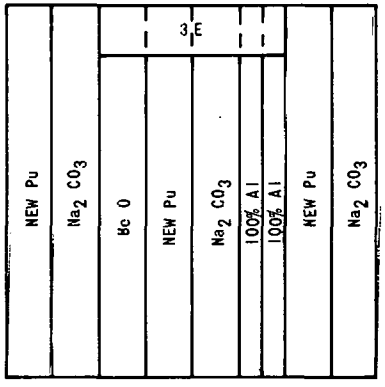

1 - N - 12

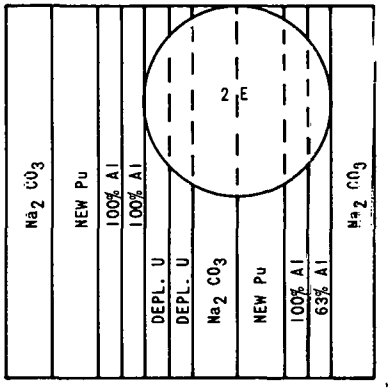

1 - N - 16

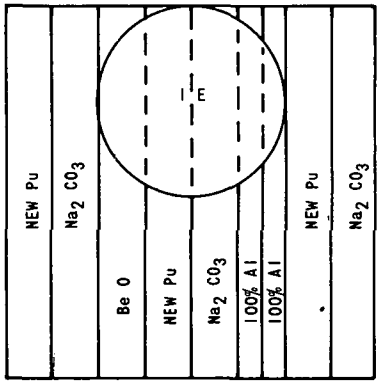

1 - Q - 17

E - ENRICHED U
N - NATURAL U
(SEE TABLE III)

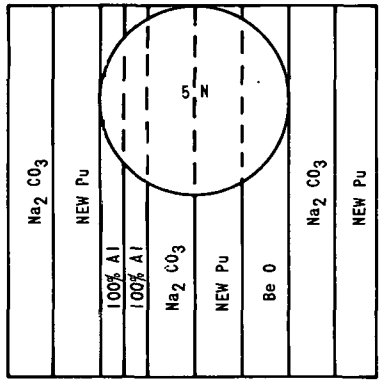

2 - N - 17

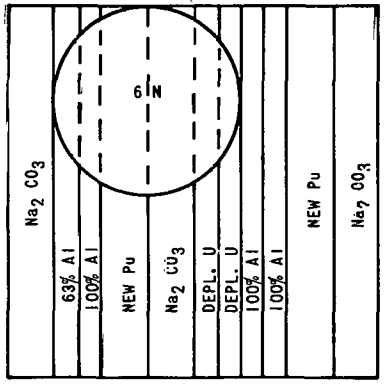

2 - N - 16

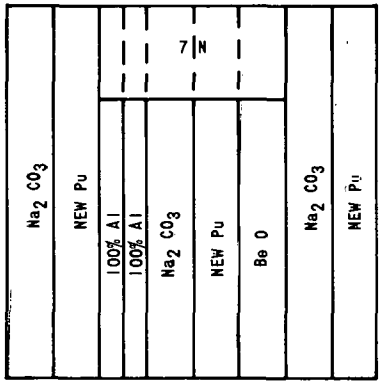

2 - N - 12

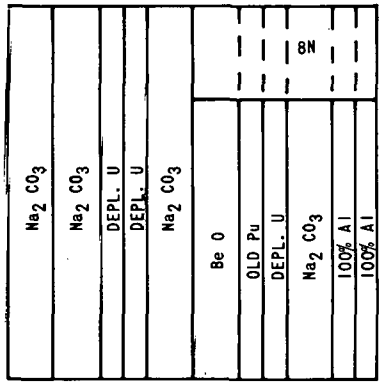

2 - N - 9

Fig. 11. Foil Positions in Front of Drawers in ZPR-3 SEFOR Mockup

Two separate experiments, in which fuel and diluent plates were arranged so that the neutron spectrum at the measuring furnace was as close as practicable to that in a homogeneous reactor, gave a mean increase of $3\frac{1}{2} \pm 1/2\%$ for a temperature rise from 27 to 500°C. A simple calculation, using Argonne's Cross Section Set 224, gave a value of approximately 4% for the same temperature rise. This agreement is encouraging, but should not be overemphasized. A second series of experiments, in which the local fuel and diluent plates were reoriented, gave a measurement approximately twice this value of $3\frac{1}{2}\%$. Clearly, the local environmental effects must be investigated carefully before these activation results can be accepted. Manganese-activation measurements carried out in the same core indicate that Set 224 may be appreciably in error in predicting the low-energy spectrum.

2. ZPR-6

a. Reactivity Worth Measurements. Measurements of reactivity worths with Assembly 4Z continued (see Progress Report for January 1966, ANL-7152, pp. 14-15). Specifically the worths of Na, C, U^{235}, and U^{238} were measured as a function of radius relative to void.

The sodium-void coefficient was also measured as functions of distance in the axial direction. A check of the heterogeneity effects on the sodium void coefficient was made by repeating the measurements with the sodium cans loaded between plates of graphite, the relative positions of the sodium cans and the enriched U^{235} plates being left undisturbed. Only the depleted uranium plates were exchanged with graphite plates. The results of these measurements are currently being analyzed.

b. Shutdown Reactivity as a Function of Time. ZPR-6 utilizes 10 fuel-bearing dual-purpose rods which are ejected from the core when scrammed and 11 (usually 12) B^{10} safety blades which are inserted into the core when scrammed. It is of interest to know the shutdown reactivity as a function of time. It is also of interest to determine whether the sum of the individual rod worths as measured in a critical assembly is equal to the total rod worth as measured during a scram condition. The following work was done with Assembly No. 4Z of ZPR-6.

Measurements of reactivity versus time were made with a BF_3 ionization chamber operating at an initial current level of $\sim 10^{-6}$ Amp, a P2-A Philbrick operational amplifier with a 10^7-ohm-voltage-developing resistor damped by a 100-PF capacitor,[1] a Dymec analog-to-digital converter, and a CDC DDP-24 digital computer. The computer was used on-line to accumulate the data. The reactivity as a function of time was calculated by use of a space-independent, one-energy-group, kinetics code. The calculated results were plotted automatically by a Calcomp plotter.

[1]The amplifier was located in the reactor cell by the chamber to reduce noise and hum pickup.

Figure 12 shows the reactivity-removal rate due to scramming nine dual-purpose rods from full in (0.000 cm) to full out (60.000 cm), and 1 dual-purpose rod from 18.000 to 60.000 cm. Time zero on the chart is ~2 msec before magnet power was removed. Sampling intervals were 5 msec. It is seen that ~50 msec elapsed before the rods started moving; the scram was essentially over in ~220 msec.

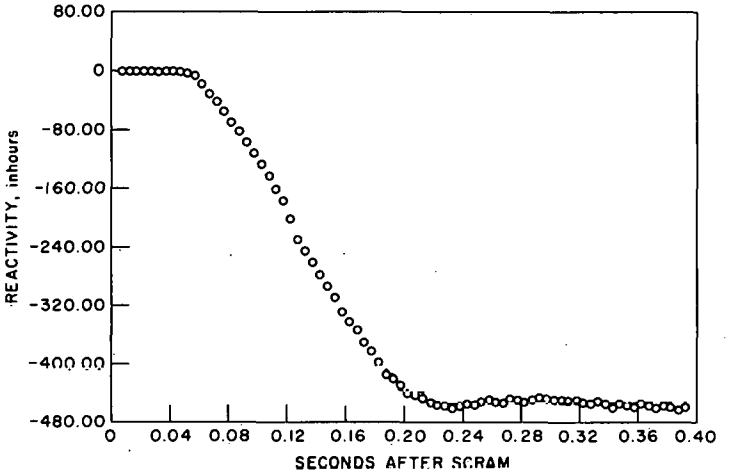

Fig. 12. Rate of Reactivity Removal due to Scram of Dual-purpose Rods

It is noted that there is a slight rise in the curve after 220 msec which subsequently returns to the previous base line. This is attributed to a small amount of 60-cps hum noted on the output of the amplifier when connected to the A to D converter. Hum is known to offset the data in this manner at low signal levels.

Three significant conclusions can be derived from this figure: (1) The reactivity-removal rate as a function of time due to the dual-purpose rods is nearly constant for this core after the rods start moving. (2) It takes ~50 msec before reactivity removal starts.[2] (3) The total measured worth of the rods removed during the scram is ~460 Ih, whereas the total worth obtained by summing the individual rod worths is ~463 Ih. Thus, the total worth agrees within the uncertainty of the rod calibration, which is estimated to be ~±5 Ih. It is not clear at this time whether or not this close agreement is fortuitous.

Figure 13 shows the reactivity-removal rate due to scramming both the dual-purpose rods and the 11 B^{10} safety blades. Again, reactivity removal starts ~50 msec after magnet-power removal and is essentially completed in 240 msec. The time between points is 10 msec in this case. The total worth measured during the scram

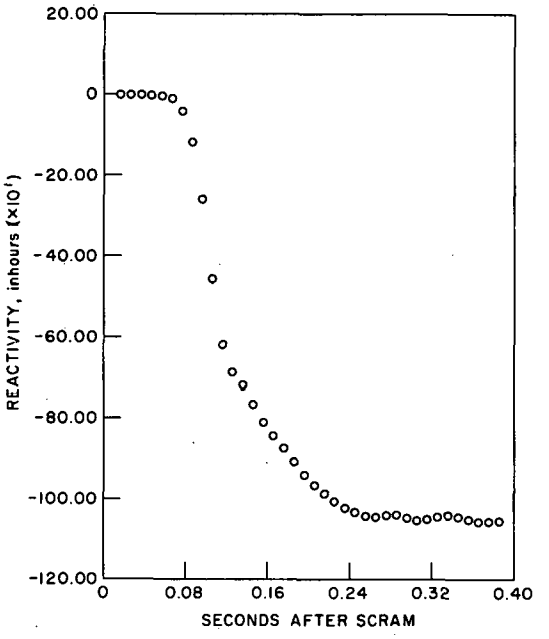

Fig. 13. Rate of Reactivity Removal due to Scram of B^{10} and Dual-purpose Rods

[2] To get total delay in the case of an instrument scram, the instrument and relay response time must be added to this. The relays utilized would add another delay of 20-25 msec.

was ~1040 Ih. For the rod configuration during this scram, the worth of the dual-purpose rods obtained by summing the rods individually, was 367 Ih. Two typical B^{10} rod worths were measured; one value was found to be ~61 Ih and the other ~59 Ih. The other nine B^{10} rods should average approximately the same with 5% or less. Assuming they are the same, the B^{10} rods would be worth ~660 Ih, making the total worth ~1027 Ih. Thus the results obtained from the total scram measurement also agree with the sum of the individual worths within the estimated accuracy of the rod worths.

Figure 14 shows the shutdown reactivity rate due to eleven B^{10} safety blades and one dual-purpose blade (the latter scrammed accidentally). Reactivity removal starts about 50 msec after loss of magnet power. Approximately 90% of the worth is inserted in ~120 msec. The B^{10} rod "bounce" is seen immediately thereafter. The final slow rate of reactivity removal is attributed to the slowing-down action of the pneumatic dampers for the B^{10} rod and the one dual-purpose rod (the damping action for the dual-purpose rods occurs outside the core). From the graph the total worth of the B^{10} blades and the dual-purpose rod is ~725 Ih. The estimated total B^{10} worth of ~660 Ih plus the worth of the dual-purpose rod of 66 Ih compares favorably with this measured value.

The above data were taken with the reactor operating at ~200 W and an ionization-chamber current of $\sim 10^{-6}$ Amp. Figure 15 shows the data obtained with the B^{10} rods when the reactor power was ~10 W and the initial ionization-chamber current $\sim 5 \times 10^{-8}$ Amp. The statistical fluctuations became quite pronounced.

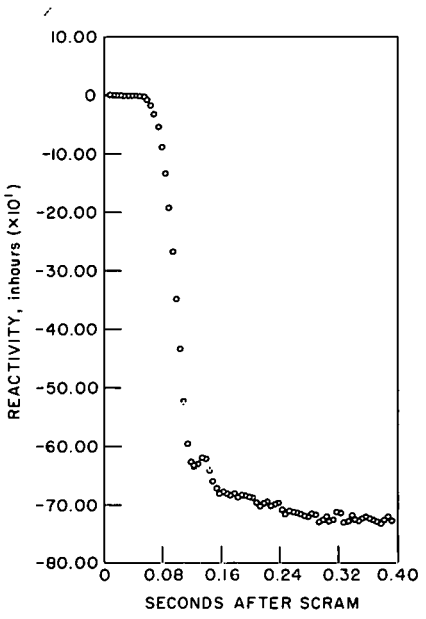

Fig. 14. Rate of Reactivity Removal due to Scram of B^{10} Safety Rods

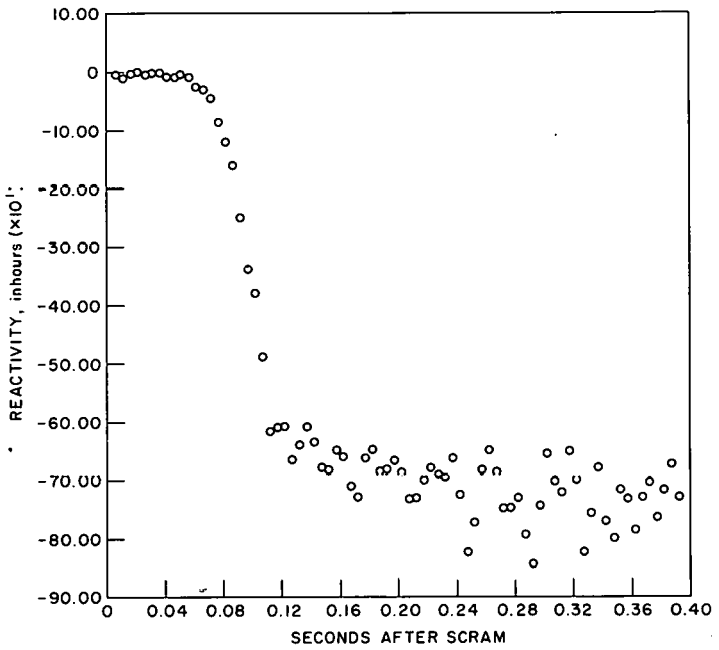

Fig. 15. Rate of Reactivity Removal at Low Power Level due to Scram of B^{10} Safety Rods

3. ZPR-9

Experimental studies with ZPR-9 Assembly No. 8 were completed during this reporting period and a major effort was directed toward converting the ZPR-9 facility to a steel matrix for the small zone studies in the Civilian Power Program.

The final measurements made on the BeO reflected Assembly No. 8 included the hydrogen void experiment, a number of central worth measurements and a series of reactivity and reaction rate traverses. The addition of a 20-mil thick x 2-in. wide strip of polyethylene to each of the core drawers introduced 172.55 g of hydrogen to the core and had a measured worth of +0.61% $\Delta k/k$. Subsequent additions of 154.58 g of hydrogen to the BeO reflector added 0.1% $\Delta k/k$. Other parameters measured on Assembly No. 8 are listed in Table VIII.

TABLE VIII. ZPR-9 Assembly No. 8--Experimentally Measured Parameters

Critical Radius:	31.74 cm
Mass:	278.8 kg U^{235}
Reflector:	11.14 cm BeO plus 47.17 cm Al Isolation Blanket
Edge Fuel Worth:	18.3 Ih/kg of U^{235} relative to BeO

Central Reactivity Worths

C	+8.7 Ih/kg
B^{10}	-2481
U^{235}	168.7
U^{238}	-14.8
H*	+4860
W	-11.6
Re	-47.2

Gap Worth: 1.05% $\frac{\Delta k}{k}$/cm

*Extrapolated to infinite dilution.

All of the physics measurements associated with the rocket program are currently being re-examined and compared to a consistent set of calculations so that the three major objectives of the program (i.e., the magnitude of the reflector oriented control margins, a consistent set of tungsten cross sections, and the effects of hydrogen in a fast core) can be properly evaluated. This summary is being prepared as a topical report.

The major change in the facility will be the replacement of the present aluminum matrix assembly with a stainless steel matrix assembly of approximately 5.5 foot cross sectional area. This is being accomplished in order to be able to obtain the proper composition more representative of dilute fast reactors. Two inch square stainless steel tubes which have been welded in bundles of twenty five which have been on order since April 1965 are currently being received. It is anticipated that all of the required bundles of stainless steel tubes will be delivered by the end of March 1965 for assembly on ZPR-9.

Installation of the stainless steel matrix assembly, Doppler effect equipment and the loading of the core reflector is planned to be completed by the end of April 1966. Loading of the fuel for ZPR-9 Assembly No. 11 for Doppler effect measurements is expected to commence around the first of May 1966.

ZPR-9 Assembly No. 11 will be the first of a series of small (less than 500 kg critical mass) zoned cores primarily for Doppler effect measurements. Its objective will be to test, in conjunction with ZPR-6 Assemblies 4Z and 5, the predictability of Doppler effect measurements for a full size fast reactor based on small zoned core approximations. Assembly No. 11 will have a central zone whose composition will be the same as the central zone of ZPR-6 Assembly No. 4Z, and the uniform full scale composition of Assembly No. 5, a 2600 liter dilute carbide fast reactor. Succeeding cores will have compositional variations simulating the compositions of other large dilute fast reactors for Doppler effect, spectrum and other physics measurements.

4. ZPPR

The supplement to the ZPPR Preliminary Safety Analysis Report was completed and transmitted to the AEC on February 3. It contains a description of a backup containment structure, an analysis of the consequences of the maximum credible accident (fire) in the ZPPR cell, including the capabilities of the backup containment structure, an analysis of the probability of an excursion in the ZPPR reactor, a discussion of the conjectured behavior of the reactor during a hypothetical excursion (design basis accident), and an analysis of the consequences of the hypothetical excursion (design basis accident) which includes inhalation doses at the nearest site boundary and other surrounding areas.

The report on the coring of the Gravel Gertie structure was completed by Eberline and Associates and forwarded to the AEC on February 23.

The following is the current status of the reactor components:

a. Bed and Tables. The detailed drawings of the bed and two tables were approved and returned to the vendor on February 16. Preparations for direct fabrication by the vendor have begun.

b. Matrix Drawers. Two prototype drawers have been accepted. Approval for start of production was given on February 17. The vendor has suggested eliminating the electropolishing operation and substituting a flapper-wheel sanding operation to deburr the holes. The sample provided by the vendor was examined and found to be satisfactory. The requirement of the specifications was to remove the sharp edges and burrs, and the vendor was instructed that either method of finishing was acceptable.

c. Matrix Tubes. Laboratory representatives inspected the vendor's gauges and inspection procedures and found them to be adequate.

The weld height on some tubes ranged from 0.000 to 0.003 in. above the surface in small areas. No weld above surface is permitted. The vendor is setting up a belt sander to grind and obtain a flush surface.

Six hundred and twelve tubes were accepted with minor corrections to be made. Approximately 600 additional tubes were fabricated and were inspected, although 450 of these did not yet have the notch cut in because of a broken notching die, now being repaired. Dimensional measurements were acceptable with the exception of the weld protrusion as explained above. The work is progressing satisfactorily.

Several prospective vendors were visited to explore the possibility of bundling the tubes. The bid package for bundling is being prepared.

d. Fuel-rod Drives. All ten of the fuel-rod drives have been received and are being checked out at ANL.

e. Nuclear Instrumentation. The nuclear instrumentation is approximately half complete. All items have been ordered. One trip circuit has been fabricated to check out the fail-safe features. Tests of individual components indicate no single failure results in a nonfail-safe performance. Testing is continuing.

f. Gamma Monitor Equipment. Three of the seven instruments are complete. All parts are ordered or received.

Other ANL procurement items are delayed pending the release of funds by the AEC.

C. General Fast Reactor Fuel Development

1. Metal Fuels

a. Compatibility of Jacket Materials with Molten U-Pu-Zr and U-Pu-Ti Alloys. The rates at which molten U-Pu-Zr and U-Pu-Ti alloy fuels (see Progress Report for January 1966, ANL-7152, p. 33) dissolve jacket alloys are being determined. Type 304 stainless steel tubes were plunged into molten U-15 w/o Pu-10 w/o Zr; at 1350°C the penetration rate was 0.076 mm/sec and at 1400°C it was 0.136 mm/sec. V-20 w/o Ti tubes were plunged into molten U-15 w/o Pu-6.5 w/o Ti; at 1300°C the penetration rate was 0.0027 mm/sec and at 1450°C, 0.027 mm/sec. V-20 w/o Ti has the better resistance to dissolution.

2. Carbide Fuels

a. Compatibility of (U,Pu)C with Potential Jacket Materials. Because of difficulties involved in the large-scale production of single-phase uranium-plutonium monocarbide, this study is concerned with: (1) the relative compatibility effects of stoichiometric and nonstoichiometric uranium-plutonium carbides with potential commercial jacketing alloys, and (2) possible modification of nonstoichiometric uranium-plutonium carbides to improve compatibility with these alloys.

Compatibility couples, containing both single-phase monocarbide and two-phase hyperstoichiometric carbides, which have been heat-treated at 800°C for 42 days (approximately 1000 hr), are being examined. The single-phase monocarbide contained 4.83 w/o equivalent carbon and the hyperstoichiometric carbide 5.25 w/o equivalent carbon, resulting in a proportionate amount of $(U,Pu)_2C_3$ as a second phase. [Weight percent equivalent carbon = w/o C + (w/o O x 0.79) + (w/o N x 0.857).] The extents of the diffusion zones in three of the alloys were as follows.

	Stoichiometric	Hyperstoichiometric
Hastelloy-X	8 μ	8 μ
Type 304 Stainless Steel	Nil	25 μ
16-25-6 Alloy	27 μ	34 μ

The diffusion zone in the case of Hastelloy-X was in the direction of the fuel and appeared to be unaffected by the presence of the sesquicarbide phase. The reaction product has not as yet been analyzed but is believed to be directly related to the relatively high nickel content of Hastelloy-X. In the cases of Type 304 stainless steel and 16-25-6 alloy, diffusion zones were within the cladding. Presumably, these zones are related to carbon diffusion, and analyses are planned to determine carbon content.

Similar compatibility couples containing 16-15-6 alloy and N-155 alloy are being examined metallographically while one containing Haynes 56 alloy is currently being heat treated.

b. Density and Phase Distribution. Firing studies were initiated to determine the density and phase distribution obtained for pellets formed from mixtures of nonstoichiometric uranium-plutonium carbides and metal powders. A hypostoichiometric uranium-plutonium carbide button was prepared by the arc-melting process. Samples of the button and of -44-μ powder obtained by crushing the button were submitted for chemical analyses, with the following results:

	C (w/o)	O (ppm)	N (ppm)
Arc-Melted Button	4.42	44	330
-44-μ Powder	4.36	1100	540

Pellets containing 0.75 w/o Carbowax 4000 as a binder were pressed from this powder at a pressure of 2815 kg/cm^2. A second set of pellets containing an addition of 3.89 w/o iron powder was prepared in an identical manner. Firings were made in an argon atmosphere and held 3 hr at the maximum firing temperature. Densities obtained were as follows:

	Density (g/cm^3)			% Theoretical Density		
Fuel	1400°C	1500°C	1600°C	1400°C	1500°C	1600°C
Unmodified	10.41	11.05	11.47	76.5	81.3	84.4
Fe Modified	10.31	11.29	11.17	75.9	83.2	82.3

Metallographic examination of the pellets is in progress.

3. Jacket Development

a. Vanadium-base Alloys. Prior screening tests of vanadium-base alloys have indicated that the V-15 w/o Ti-7.5 w/o Cr alloy has a greatly improved creep resistance (Progress Report for June 1965, ANL-7071, p. 21) and a somewhat improved sodium corrosion resistance (Progress Report for April 1965, ANL-7045, p. 20) as compared with the first-generation V-20 w/o Ti alloy.

Scale-up operations for the V-15 w/o Ti-7.5 w/o Cr alloy have been under way for several months. To date, three production-size ingots (9.7 cm in diameter) have been consolidated by double arc melting under a helium-argon atmosphere. All ingots were sound and homogeneous. Analytical results for alloy content and interstitial elements are shown in Table IX. The consolidation technology for this alloy has been satisfactorily established except, perhaps, for minor adjustments or improvements.

TABLE IX. Analytical Results for Arc-cast V-15 w/o Ti-7.5 w/o Cr Alloy Ingots

	Ingot and Location								
	AM64			AM68			AM75		
Element	Top	Middle	Bottom	Top	Middle	Bottom	Top	Middle	Bottom
Titanium, w/o	15.1	14.5	14.8	14.9	14.7	14.6	15.1	14.7	14.7
Chromium, w/o	7.5	7.3	7.8	7.6	7.3	6.9	7.5	7.6	7.5
Carbon, ppm	234	-	265	222	-	226	229	-	187
Oxygen, ppm	772	-	632	810	-	810	660	-	630
Nitrogen, ppm	390	-	410	390	-	440	540	-	360
Hydrogen, ppm	13	-	15	17	-	13	45	-	19
Total Interstitials, ppm	1409	-	1322	1439	-	1489	1474	-	1196

The three ingots have been successfully processed into tubing, rod, and sheet. Primary fabrication is by double extrusion. Billets are "canned" in stainless steel to prevent contamination and extruded at 1100 to 1150°C. Following an arc-cast ingot breakdown extrusion, billets are re-extruded into shapes suitable for secondary fabrication.

Secondary fabrication of rod and sheet by cold rolling has presented no problems if as-extruded material is vacuum annealed at 850 to 900°C prior to cold working to eliminate edge and nose cracking. Extruded tube blanks are annealed and given a light swage over a hardened mandrel to improve wall uniformity and surface quality. The tube blanks, approximately 2.03 cm in OD with a 0.25-cm wall and 100 cm long, are tube-reduced to 1.63-cm OD and 0.13-cm wall on an ANL-designed three-roll tube-reducer. Schematic details of the tube-reducer are shown in Figs. 16 and 17. The tube-reducing operation has significantly reduced the number of processing steps from extruded tube-blank to finished tubing.

The tube-reduced blanks are finished to required final sizes (a typical size being of 0.290-in. OD with 0.015-in. wall) by mandrel or plug drawing and inspected by nondestructive techniques. Tube-reduced blanks are also being furnished to a commercial tube-redraw firm to establish commercial capability in this area.

In conjunction with fabrication development, annealing characteristics of the V-15 w/o Ti-7.5 w/o Cr alloy (and a similar V-15 w/o Ti-5 w/o Cr alloy) have been studied. The change in hardness as a function of annealing temperature is shown in Fig. 18. Although the 700°C anneal for V-15 w/o Ti-7.5 w/o Cr produced a grain morphology characteristic of a fully recrystallized structure, a temperature of 800°C is the more logical recrystallization temperature because of the slightly lower hardness. In the sample annealed at 800°C, the mean grain diameter was 0.006 mm. The increase in hardness observed for anneals at 1000°C and higher, especially at 1250°C, is thought to be due to a change in the nature and morphology of the precipitate. This has been observed in metallographic examination but requires further confirmation by other techniques.

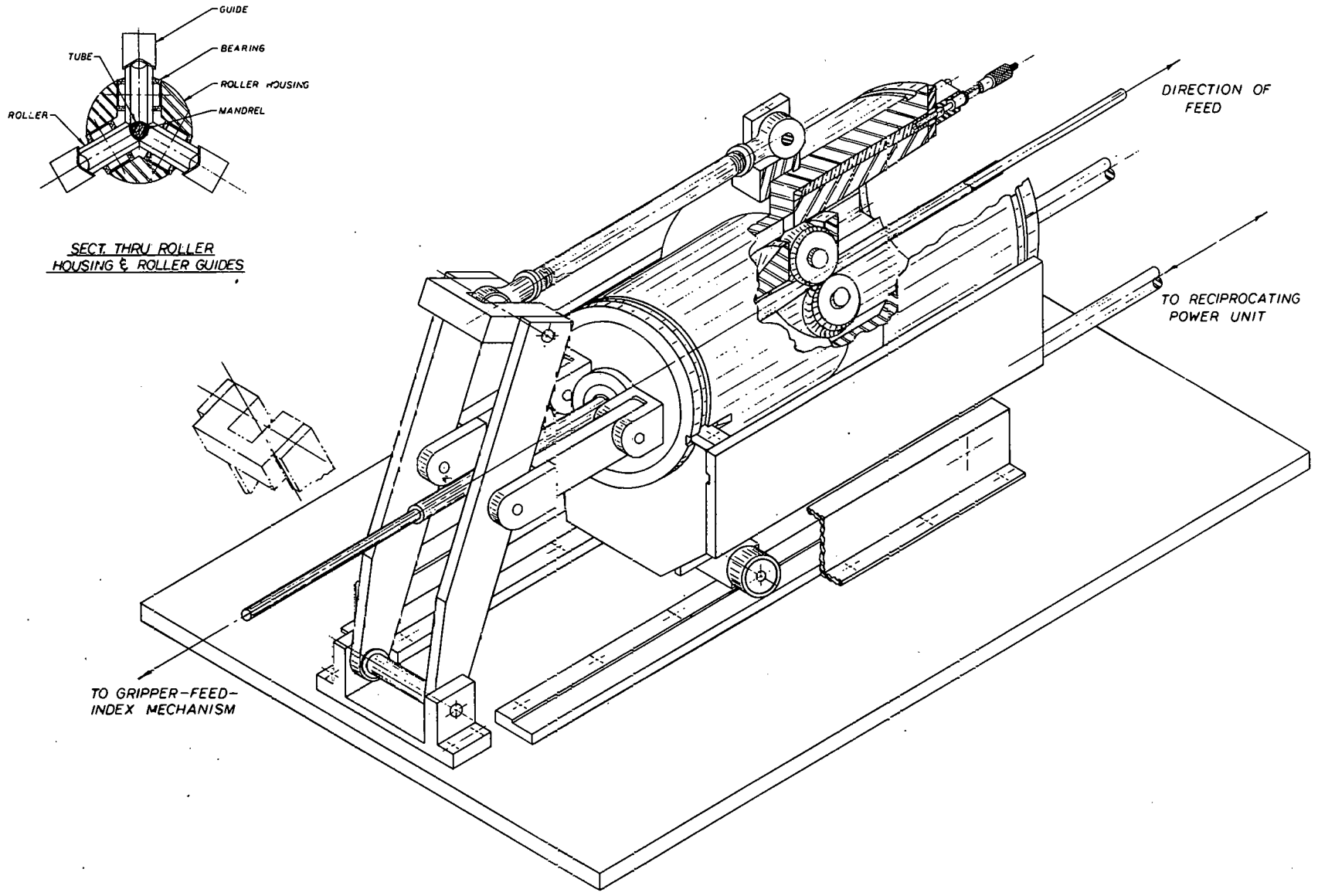

Fig. 16. Schematic Arrangement of the ANL Three-roll Tube-reducer. (Present starting tube size is 2.5-cm dia.)

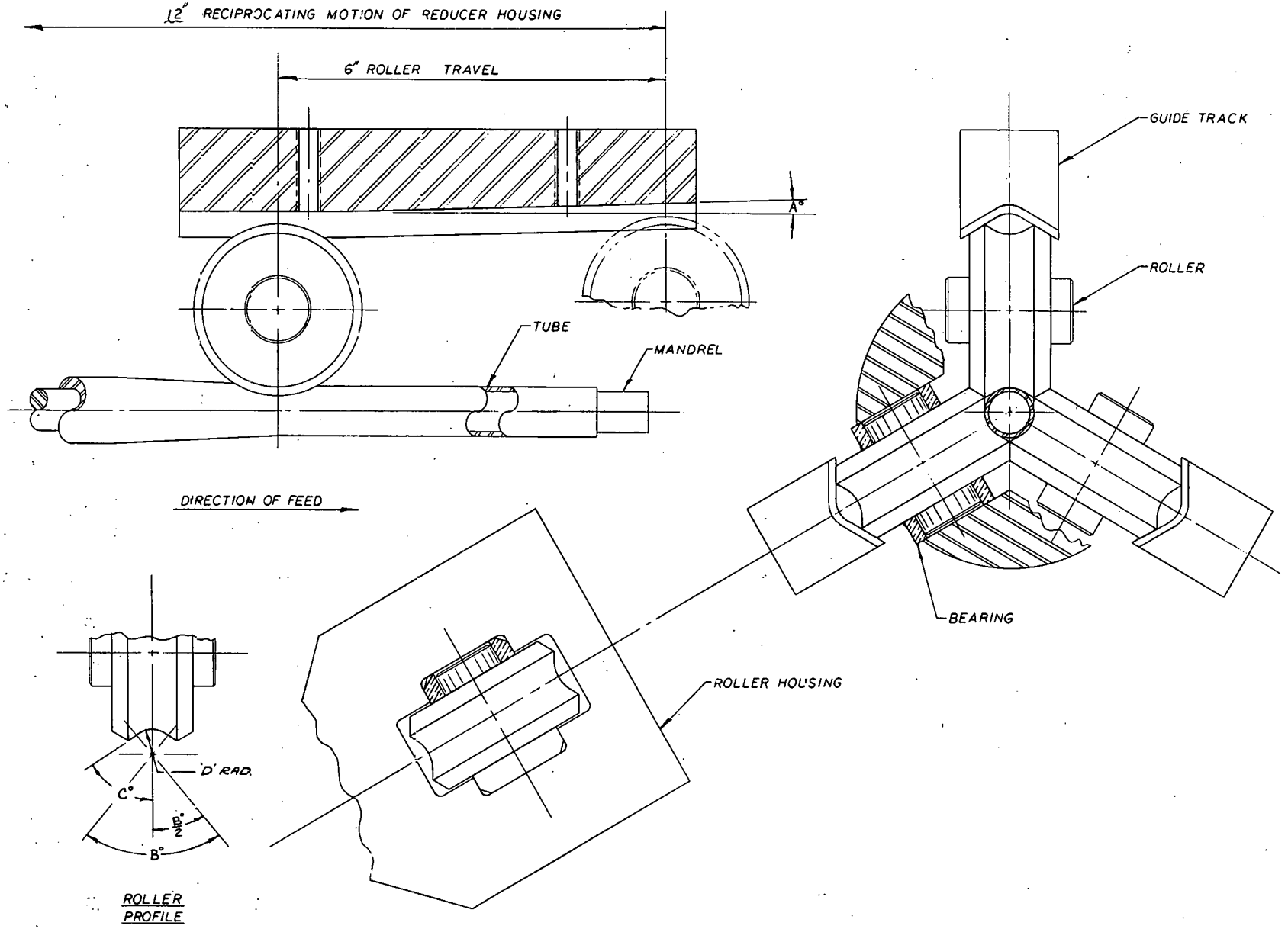

Fig. 17. Roller Arrangement and Operational Details of the ANL Three-roll Tube-reducer

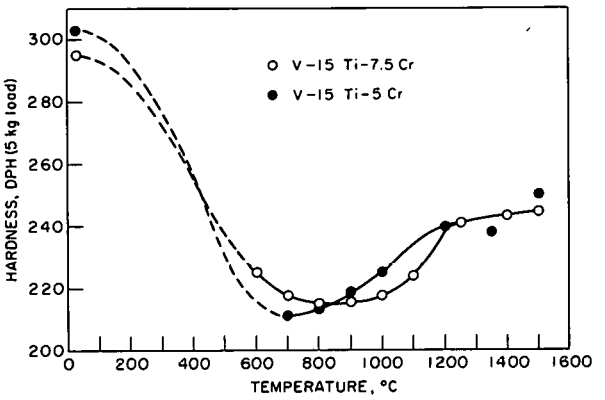

Fig. 18. The Change in Hardness as a Function of 1-hr Anneals for V-15 w/o Ti-7.5 w/o Cr and V-15 w/o Ti-5 w/o Cr

Although the microstructural changes as a function of annealing temperature and the subsequent effect on properties has not been fully evaluated as yet, the fabrication development has proceeded to the point where material is being made available for more definitive testing.

b. Thermal Expansivity of V-15 w/o Ti-7.5 w/o Cr. The linear thermal expansion behavior of V-15 w/o Ti-7.5 w/o Cr was determined between 25 and 960°C. The dilatation specimen was machined from an alloy rod that had been annealed for one hour at 900°C in vacuum and had a density of 5.88 g cm^{-3}.

Values of the mean coefficient of linear expansion are given in Table X for the temperature ranges indicated.

TABLE X. Linear Thermal Expansion of Annealed V-15 w/o Ti-7.5 w/o Cr

Temperature Range (°C)	Mean Linear Expansion Coefficient (10^{-6} $°C^{-1}$)
0-250	9.30
0-500	9.83
0-750	10.42
0-1000	11.28 (extrapolated)

4. Corrosion

a. Fuel-jacket Materials for Sodium-cooled Reactors. Oxidation of samples of V-20 w/o Ti exposed to sodium containing less than 5 ppm oxygen (as measured by vacuum distillation) at 600°C for periods of time up to 32 hr and rotated at about 5 rpm to insure access of oxygen to the surface was linear at 600°C for the entire period of exposure. The rate constant K_l was determined as 3×10^{-3} mg/cm^2 hr.

V-20 w/o Ti exposed under the same conditions at 700 and 750°C (see Progress Report for January 1966, ANL-7152, p. 35) exhibited appreciably different corrosion kinetics. At 700°C, the process was linear ($K_l = 8 \times 10^{-3}$ mg/cm^2 hr) for the first 12 hr of exposure, followed by a transition to a parabolic rate law. At 750°C the process was parabolic for

exposure times between 4 (the time of the first data point) and 32 hr. If a linear process exists at 750°C, the maximum duration is 4 hr.

Exposure of samples at much higher rotational speeds will be undertaken to determine if mass transfer of oxygen in the liquid is the rate-controlling step in the early stages of oxidation.

b. Refractory Metal Alloys for Service Oxygen-contaminated Sodium. Small levitation melts of V-20 w/o Cr-10 w/o Al modified with 1 w/o and 2 w/o Zr or 0.5 w/o and 1 w/o Y (see Progress Report for January 1966, ANL-7152, p. 35) were hot rolled and returned for corrosion testing in sodium. The additions did not appreciably improve the ease of fabrication, but might be more important if vanadium containing more oxygen were used in the alloy preparation. An exposure to 650°C sodium (refreshed oxygen--static autoclave system) containing 25 to 30 ppm oxygen for 7.0 days showed no significant corrosion effect of the addition of 1 w/o Zr or 0.5 w/o Y to the basic composition.

Two one-week experiments have been performed with V-20 w/o Ti in flowing sodium (6.1 m/sec) at 650°C. In the first experiment the post-test oxygen analysis was 20 to 28 ppm. The V-20 w/o Ti samples were badly roughened on the surface and eroded at the leading edges and in a flow pattern back from the edges in contact with the stainless steel holder. The samples lost about 100 μ per side.

In the second experiment the cold-trap temperature was reduced to ~120°C. The post-test oxygen analysis was 15 ppm (oxygen concentration determined by mercury amalgamation). The V-20 w/o Ti samples were in much better condition after this exposure. The surfaces were smooth, but the leading edge of one sample was slightly eroded. The samples lost only 10 to 18 μ per side.

Experiments at lower oxygen levels will be attempted upon completion of minor repairs and modifications to the loop.

5. Irradiation Testing

a. Irradiated EBR-II Fuel Jackets. Additional tube-burst tests of the Type 304 stainless steel jackets from irradiated EBR-II fuel rods (see Progress Report for January 1966, ANL-7152, pp. 36-38) have been made. Tests at 500°C have verified that the top of the jacket tubes is the weakest part. Tests have been made on the top sections of three different jackets. In two cases the top weld was kept intact and the pressure connection to the tube was made elsewhere than at the top. In a third test, the pressure connection was made to the top end after cutting off the plug. In both cases where the top plug was in place, the tube ruptured adjacent

to the weld. In the third test the break was adjacent to the pressure connection at the top of the jacket. The pressures required to break these three specimens were appreciably less than in other tests made along the lengths of the tubes.

One jacket from a fuel rod with 1.2 a/o burnup was cut into five sections for tube burst tests at 700°C. The lowest bursting pressure (270 kg cm^{-2}) occurred with the top section, but this value is in doubt because of a 70°C override on the temperature prior to testing. The maximum bursting pressure (327 kg cm^{-2}) occurred with the middle section. The bottom section showed a considerably lower value (282 kg cm^{-2}) than the peak value. The apparent drop in the burst pressure toward the bottom of the jacket at 700°C is a variation from the pattern exhibited at 500°C.

The specimens tested at 700°C also differed from the tests at 500°C in showing some tendency toward general expansion under pressure. The elongation values at 500°C as determined from post-test measurements of diameter were generally below 1%. After the 700°C tests similar measurements showed elongations as high as 8% (14% for the overheated specimen). The evidence seems to indicate that the irradiation effects are annealing out in tests at 700°C.

b. Irradiation Program for Fast Reactor Fuels

(i) Metal Fuels. Sixty specimens are under irradiation (see Table XI). The specimens being irradiated in CP-5 are from 10 to 15 cm long and are in five instrumented capsules. The specimens in EBR-II are full length (46 cm) and are located in three special subassemblies. There are no metallic fuels being irradiated in the MTR at the present time.

Six new U-15 w/o Pu-12 w/o Zr fuel pins jacketed in iron- and nickel-base alloys were encapsulated and are undergoing irradiation in CP-5. The jacket materials are either Type 304 or Type 316 stainless steel, or Hastelloy-X. The maximum jacket temperature for these specimens is either 530 or 460°C.

The irradiation experiments in the EBR-II have the same status as for the previous month because the reactor has not been operated during this report period.

Capsule ANL-55-8 was removed from MTR and shipped to the alpha-gamma cave, Building 212 at the Illinois site. This capsule contains three full-length EBR-II-type fuel rods. Two of the fuel alloys are U-15 w/o Pu-10 w/o Fz and the other is U-10 w/o Pu-10 w/o Fz. The jacket materials are Nb-1 w/o Zr and vanadium. The maximum jacket temperatures during irradiation were 555°C. The calculated maximum burnups are 3.3 a/o.

TABLE XI. Status of Metal Fuel Irradiations in Progress

Specimen No.	Reactor	Fuel Composition (w/o)	Jacket Composition (w/o)	Jacket ID (mm)	Jacket Thickness (mm)	Maximum Jacket Temp (°C)	Calculated Burnup to Date	
							a/o	f/cm^3 x 10^{-20}
N-15	CP-5	U-19 Pu-14 Zr	V-20 Ti	4.5	0.38	580	5.7	18.8
ND-23	EBR-II	U-15 Pu-10 Zr	V-20 Ti	4.5	0.41	540	1.08	3.97
ND-24	EBR-II	U-15 Pu-10 Zr	V-20 Ti	4.5	0.41	535	1.08	3.97
ND-28	EBR-II	U-15 Pu-9 Zr	304 SS	4.2	0.51	650	0.53	2.00
ND-41	EBR-II	U-15 Pu-9 Zr	304 SS	4.2	0.51	650	0.53	2.00
ND-32	EBR-II	U-15 Pu-9 Zr	316 SS	4.2	0.38	645	0.53	2.00
ND-43	EBR-II	U-15 Pu-9 Zr	Hast.-X	4.2	0.38	645	0.53	2.00
L-18	CP-5	U-15 Pu-12 Zr	Hast.-X	4.2	0.38	460	0.34	1.16
F-35	CP-5	U-15 Pu-12 Zr	304 SS	4.2	0.38	460	0.34	1.16
F-37	CP-5	U-15 Pu-12 Zr	316 SS	4.2	0.38	460	0.34	1.16
L-19	CP-5	U-15 Pu-12 Zr	Hast.-X	4.2	0.38	530	0.34	1.16
F-36	CP-5	U-15 Pu-12 Zr	304 SS	4.2	0.38	530	0.34	1.16
F-38	CP-5	U-15 Pu-12 Zr	316 SS	4.2	0.38	530	0.34	1.16
ND-25	EBR-II	U-14 Pu-12 Zr	304 SS	4.2	0.51	630	0.47	1.64
ND-27	EBR-II	U-14 Pu-12 Zr	304 SS	4.2	0.51	630	0.50	1.74
ND-26	EBR-II	U-14 Pu-12 Zr	316 SS	4.2	0.38	625	0.47	1.64
ND-29	EBR-II	U-14 Pu-12 Zr	316 SS	4.2	0.38	625	0.47	1.64
ND-30	EBR-II	U-14 Pu-12 Zr	316 SS	4.2	0.38	635	0.50	1.74
ND-31	EBR-II	U-14 Pu-12 Zr	316 SS	4.2	0.38	635	0.50	1.74
ND-33	EBR-II	U-14 Pu-12 Zr	Hast.-X	4.2	0.38	630	0.50	1.74
ND-34	EBR-II	U-14 Pu-12 Zr	Hast.-X	4.2	0.38	635	0.50	1.74
ND-35	EBR-II	U-14 Pu-12 Zr	Hast.-X	4.2	0.38	640	0.50	1.74
ND-37	EBR-II	U-14 Pu-12 Zr	Hast.-X-280	4.5	0.38	635	0.50	1.74
ND-39	EBR-II	U-14 Pu-12 Zr	Hast.-X-280	4.5	0.38	635	0.50	1.74
ND-44	EBR-II	U-14 Pu-12 Zr	Hast.-X-280	4.5	0.38	635	0.50	1.74
N-14	CP-5	U-15 Pu-10 Ti	V-20 Ti	4.4	0.38	560	5.0	16.8
NC-17	EBR-II	U-15 Pu-10 Ti	V-20 Ti	4.5	0.41	540	1.08	3.64
NC-23	EBR-II	U-15 Pu-10 Ti	V-20 Ti	4.5	0.51	540	1.09	3.68
N-10	CP-5	U-10 Pu-10 Fz	V-20 Ti	4.2	0.41	530	5.2	19.9
N-11	CP-5	U-10 Pu-10 Fz	V-20 Ti	4.1	0.41	530	5.2	19.9
N-12	CP-5	U-10 Pu-10 Fz	V-20 Ti	4.0	0.41	530	5.2	19.9
CGO2	EBR-II	U-10 Pu-10 Fz	Nb-1 Zr	4.0	0.23	445	0.42	1.60
CGO3	EBR-II	U-10 Pu-10 Fz	Nb-1 Zr	4.0	0.23	440	0.41	1.56
CJO1	EBR-II	U-10 Pu-10 Fz	Nb-1 Zr	4.0	0.23	435	0.40	1.52
PBO2	EBR-II	U-10 Pu-10 Fz	Nb-1 Zr	4.0	0.23	440	0.41	1.56
TC-1	CP-5	U-15 Pu-10 Fz	Nb-1 Zr	4.0	0.23	500	2.4	5.3
C-152 P	CP-5	U-15 Pu-10 Fz	Nb-1 Zr	4.0	0.23	500	2.4	5.3
C-153 P	CP-5	U-15 Pu-10 Fz	Nb-1 Zr	4.0	0.23	500	2.4	5.3
C-155 P	CP-5	U-15 Pu-10 Fz	Nb-1 Zr	4.0	0.23	510	2.4	5.3
C-156 P	CP-5	U-15 Pu-10 Fz	Nb-1 Zr	4.0	0.23	510	2.4	5.3
C-159 P	CP-5	U-15 Pu-10 Fz	Nb-1 Zr	4.0	0.23	510	2.4	5.3
N-7	CP-5	U-15 Pu-10 Fz	V-20 Ti	4.2	0.41	530	5.2	19.9
N-8	CP-5	U-15 Pu-10 Fz	V-20 Ti	4.1	0.41	530	5.2	19.9
N-9	CP-5	U-15 Pu-10 Fz	V-20 Ti	4.0	0.41	530	5.2	19.9
N-13	CP-5	U-15 Pu-10 Fz	V-20 Ti	4.3	0.38	550	4.4	16.7
CAO1	EBR-II	U-15 Pu-10 Fz	Nb-1 Zr	4.0	0.23	450	0.41	1.56
CBO2	EBR-II	U-15 Pu-10 Fz	Nb-1 Zr	4.0	0.38	445	0.42	1.60
CBO3	EBR-II	U-15 Pu-10 Fz	Nb-1 Zr	4.0	0.38	440	0.41	1.56
CBO4	EBR-II	U-15 Pu-10 Fz	Nb-1 Zr	4.0	0.38	440	0.41	1.56
CDO1	EBR-II	U-15 Pu-10 Fz	Nb-1 Zr	4.0	0.23	440	0.41	1.56
CDO2	EBR-II	U-15 Pu-10 Fz	Nb-1 Zr	4.0	0.23	430	0.40	1.52
LAO2	EBR-II	U-15 Pu-10 Fz	Hast.-X	3.9	0.25	430	0.40	1.52
PAO1	EBR-II	U-15 Pu-10 Fz	Nb-4 V	4.0	0.23	435	0.40	1.52
C-93	EBR-II	U-20 Pu-10 Fz	Nb-1 Zr	4.0	0.23	435	0.41	1.56
C-97	EBR-II	U-20 Pu-10 Fz	Nb-1 Zr	4.0	0.23	430	0.40	1.52
C-98	EBR-II	U-20 Pu-10 Fz	Nb-1 Zr	4.0	0.23	430	0.39	1.48
C-99	EBR-II	U-20 Pu-10 Fz	Nb-1 Zr	4.0	0.23	430	0.40	1.52
C-100	EBR-II	U-20 Pu-10 Fz	Nb-1 Zr	4.0	0.23	430	0.40	1.52
C-101	EBR-II	U-20 Pu-10 Fz	Nb-1 Zr	4.0	0.23	435	0.40	1.52
CM-01	EBR-II	U-20 Pu-10 Fz	Nb-1 Zr	4.0	0.38	435	0.40	1.52

(ii) Ceramic Fuel Irradiations. Irradiations of ceramics being conducted in EBR-II are summarized in Table XII. Since EBR-II was not operated in February, there has been no change in the status of these experiments.

TABLE XII. Status of Ceramic Fuel Irradiations in EBR-II

Specimen No.	Fuel Material	Fuel Form	Jacket Material	Max Jacket Temperature (°C)	Burnup	
					a/o	fiss/cc x 10^{20}
SMV-2	UC-20 w/o PuC	Vipac	304 SS	645	1.4	3.7
HMV-5	UC-20 w/o PuC	Vipac	Hast.-X	670	1.4	3.7
NMV-11	$(U_{0.8}Pu_{0.2})C$	Vipac	Nb-1 Zr	645	1.4	3.7
NMP-2	$(U_{0.8}Pu_{0.2})C$	Pellet	Nb-1 Zr	545	0.33	0.86
NMV-4	UC-20 w/o PuC	Vipac	Nb-1 Zr	635	0.47	1.2
NMV-7	UC-20 w/o PuC	Vipac	Nb-1 Zr	605	0.43	1.1
NMV-12	$(U_{0.8}Pu_{0.2})C$	Vipac	Nb-1 Zr	635	0.47	1.2
HMV-1	UC-20 w/o PuC	Vipac	Hast.-X	640	0.42	1.1
HMV-4	UC-20 w/o PuC	Vipac	Hast.-X	670	0.46	1.2
HWMP-1	$(U_{0.8}Pu_{0.2})C$	Pellet	Hast.-X[1]	555	0.32	0.84
HWMV-1	$(U_{0.8}Pu_{0.2})C$	Vipac	Hast.-X[1]	685	0.47	1.2

[1]Has 0.005-in. layer of vapor-deposited tungsten on the ID.

D. General Fast Reactor Fuel Reprocessing Development

1. Skull Reclamation Process

After fuel pins discharged from the EBR-II reactor have been melt refined, a uranium-bearing residue or skull is left in the crucible. The uranium in the skull amounts to 5 to 10% of the original uranium charge. A skull reclamation process is being developed for the recovery and purification of the uranium from the skull. The chemistry and technology that are being accumulated have considerable potential utility for processing plutonium-uranium oxide and carbide fuels. Currently, the skull reclamation process is being tested in remotely operated plant-scale equipment (~4 kg of uranium per batch) comprising a reduction furnace and a retorting furnace.

The final step in the skull reclamation process consists of retorting, or solvent evaporation, to recover the product uranium from the Zn-12 w/o Mg-12 w/o U ingot cast from the product solution that is transferred out of the reduction furnace. Three plant-scale retorting runs (PSR-10, -11, and -12) have been completed with unirradiated Zn-Mg-U ingots from reduction furnace runs SRR-13 and SRR-14 (see Progress Report for December 1965, ANL-7132, pp. 23-24), and run SKR-29 from the previous pilot-scale reduction furnace operations. The runs were conducted in the same thixotropically cast beryllia crucible that had been used in seven

previous retorting runs (see Progress Report for January 1966, ANL-7152, p. 43). The retorting procedure was the same as in previous runs: distillation from the uranium product solution of the magnesium-zinc under vacuum (~10 Torr) at 650 to 750°C, followed by melting of the uranium at ~1200°C to form a button.

In the current runs, the Zn-Mg-U ingots were cleaned before being charged to the crucible in order to remove the residual flux that accompanies the Zn-Mg-U solution during its transfer from the reduction furnace. It was previously shown that failure to remove flux from an ingot before retorting results in a uranium product containing a large quantity of oxide (see ANL-7152, p. 43). Retorting of these ingots resulted in a clean uranium product.

Since the ingots cannot be washed in actual plant operation, separation of residual flux from Zn-Mg-U product solution during transfer from the reduction furnace was investigated. In small-scale experiments, salt flux was successfully removed from molten Zn-Mg alloy when the material was poured through Fiberfrax strainers at temperatures ranging from 600 to 775°C. The Fiberfrax was preferentially wetted by the flux while the clean metal passed through the strainer. On the basis of these tests, a full-scale strainer has been built for tests with the plant-scale reduction furnace.

The uranium product buttons[3] obtained in the retorting of Zn-Mg-U product solutions from four skull oxide-reduction runs (SRR-11 through -14) have been analyzed (by X-ray fluorescence technique) for fission product elements. Analytical results indicate that the overall removal of molybdenum was 60 to 70% and that of ruthenium was 80%. These fission product removals are quite satisfactory. (These values will be checked by wet chemical analyses.)

Operation of the retorting equipment in the three current runs was very satisfactory. Improved control of retorting temperature and pressure eliminated the "bumping" that had occurred in earlier runs. Retention of Zn-Mg alloy by the retorting apparatus was excellent; only negligible amounts of Zn-Mg alloy escaped from the apparatus. At the conclusion of each run, the uranium product button was readily dumped from the beryllia crucible.

2. Processes for Future Fast Reactor Fuels

Compact pyrochemical processes are being developed for processing fast breeder reactor fuels of the ceramic (e.g., oxide or carbide) or metallic types. In current work, the principal emphasis is on salt transport processes. The process and its advantages were discussed in a previous report

[3]The buttons were remelted and then cast to provide samples for analyses.

(see ANL-7152, pp. 43-44). In salt transport processes, the fissile and fertile constituents of a reactor fuel are selectively transferred from one liquid metal solvent to another by cycling a molten salt phase, which acts as a carrier, between the two metal solvents.

To date, most of the experimental work has been carried out with liquid copper-magnesium and zinc-magnesium alloys in mutual contact with molten $MgCl_2$ at 800°C (see ANL-7152, pp. 43-44). The copper-magnesium alloys offer the advantages of good single-stage separation of rare earths from plutonium, good transfer rates of uranium and plutonium, and internal control of the magnesium concentration in the Cu-Mg alloys through the dissolution of excess solid copper in the system as magnesium is transferred into a Cu-Mg alloy.

Another alloy that is being considered in place of the copper-magnesium alloys for the salt transport process is cadmium-zinc-magnesium, which offers the possibility of lowering the operating temperature to ~600°C. Molten 50 m/o $MgCl_2$-30 m/o NaCl-20 m/o KCl (see ANL-7152, p. 44) is being considered as the salt phase. The specific composition of interest for the alloy was at low magnesium concentration and at a cadmium-to-zinc ratio of 9 to 1 that provided maximum uranium solubility in the alloy. In recent work, distribution coefficient data were determined for uranium between 50 m/o $MgCl_2$-30 m/o NaCl-20 m/o KCl and Cd-Zn-Mg. These distribution data together with solubility data for uranium in the metal phase are presented in Table XIII. These data

TABLE XIII. Distribution of Uranium between 50 m/o $MgCl_2$-30 m/o NaCl-20 m/o KCl and Cd-Zn-Mg Alloy

Cadmium to zinc ratio: 9 to 1.
Alloy saturated with uranium except as noted.

Sample No.	Temp (°C)	Metal Phase		Salt Phase	Distribution Coefficient
		Mg (w/o)	U (w/o)	U (w/o)	$(K_d)^a$
1	600	0.28	2.64[b]	3.41	1.29
2	598	0.23	2.80[b]	4.72	1.69
3	650	0.36	5.91	9.50	1.60
4	530	0.25	4.61	5.4	1.17
5	448[c]	0.16	1.76	1.39	0.791
6	500	0.23	4.03	5.1	1.26

[a] $K_d = \frac{\text{w/o U in salt}}{\text{w/o U in metal}}$.

[b] Alloy not saturated with uranium.

[c] The solid phase in equilibrium with the molten alloy is UCd_{11} instead of metallic uranium.

indicate that rapid uranium transfer is possible. However, since the equilibrium uranium concentration in the molten salt is sensitive to small changes of magnesium concentration in the alloy, the magnesium concentration in this alloy must be maintained at a low level (<1 w/o). This might be accomplished by fractional distillation of a side-stream of the Cd-Zn-Mg alloy. With this system, a multistage separation would be required for an adequate removal of rare earth fission products from plutonium.

3. Materials Evaluation

A supporting program to find inexpensive, easily fabricated containment materials for pyrochemical process solutions is under way. Testing of a cast iron crucible was continued in order to investigate the use of cast iron as a container material for a system consisting of Cu-10 w/o Mg-2 w/o U alloy and 50 m/o $MgCl_2$-30 m/o NaCl-20 m/o KCl salt (see ANL-7152, p. 44). After the crucible was exposed for an additional 200 hr (total time, 370 hr) at 800°C to the copper-magnesium-uranium alloy/salt system, no evidence of corrosion or deterioration of the crucible was observed. Metallographic examination of sections of the crucible is in progress. The stability of the uranium solution in this test is also being determined; results of analyses are not yet available.

E. Sodium Technology

1. Components Surveillance Loop

a. Modified Falex Wear Tester. Additional tests were performed with the wear tester now on hand to evaluate its high-temperature performance. A carbon steel shaft was mounted between blocks of 304 stainless steel and the unit was operated in an atmosphere of inert gas at 1200°F.

In the first test, the unit was loaded to 1000 psi. At a velocity of 94.1 in./min, the shaft moved only 2.35 in. before severe galling terminated the test.

In a second test with the same materials and a loading of 275 psi, the shaft moved a distance of 260.1 in. at a velocity of 23.5 in./min before terminating because of galling.

The results of these tests show that the materials exposed to the test are much too plastic at 1200°F to offer good possibilities in bearing construction. The galling failure, even under relatively light loads, shows that the pressure tends to force the welding of the materials at the contact points. Future tests will be aimed at harder and more durable materials at the 1200°F temperature.

2. Dynamic Components Test Loop (DYCOTL)

This loop is nearing completion. A brief resume of its current status follows:

i. All piping welds have been completed.
ii. The loop has been leak tested.
iii. Lagging on the loop is complete and the lagging on the spool piece is almost complete.
iv. All but two pipe hangers have been installed.
v. Some X-ray work remains to be completed.

The 15-hp motor for the sodium-to-air heat exchanger has been operated on emergency and regular power. The speed-control-indicating circuit has been installed and checked for dependability. A speed-indicator readout panel is installed on the main panel for loop control.

The elevator to the deep pit is now interconnected to the new 7.5-kWe gas-electric generator. In case of a major failure of building power, the deep-pit elevator will operate, automatically, on emergency power.

A separate deep-pit fresh-air blower is also interconnected with the emergency power supply. In the event of a major sodium fire and power failure, fresh air may be supplied to the pit by use of a button located on the front of the control panel.

3. Small Static Soak Pots

a. Materials Compatibility Test. At 400°F tests were run for 16 and 48 hr with a lifting technique applied through a strain gauge for each of five loaded 304 stainless steel metal pairs. No indication of sticking at 400°F was found.

The test was repeated at 600°F for 144, 171, and 216 hr. Again no indication of sticking was found.

Tests are being conducted at 1000°F and then will be made at 1200°F.

4. Evaluation of Aeroquip Brazed Fitting

Six 1/2-in. Nicrobrazed joints were received from a vendor. These fittings are of the type used to make remote connections in aircraft tubing except that the joints under study were made of 304 stainless steel and Nicrobraz, which is a high-temperature alloy. The condition of one of the fittings, as received, is shown in Fig. 19.

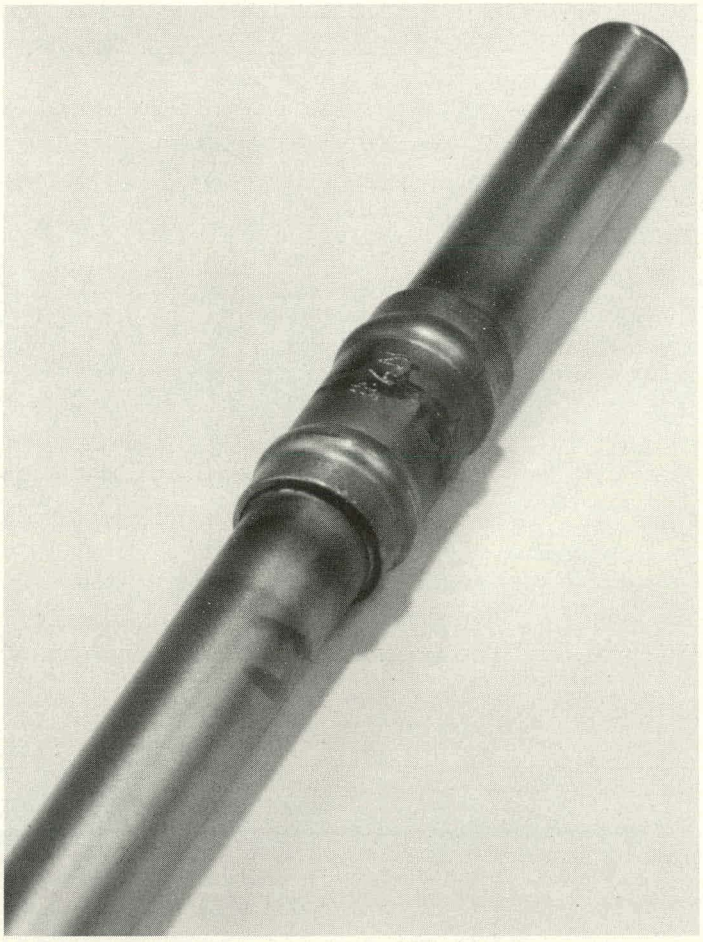

Fig. 19. Brazed Conoseal Fitting before Exposure

Two of the fittings were converted into capsules by welding end caps into the ends of the 10-in. long sections. Prior to closure, sodium was introduced into the capsule in a quantity sufficient to result in an internal pressure of 44.1 psia at 1200°F. Subsequently, the two capsules were placed in a furnace and raised to 1200°F. The atmosphere in the furnace was air so that the external surfaces of the capsules were exposed to atmospheric oxygen. Both capsules were exposed to these conditions for 1380 hr. During this time, the capsules did not release the contents despite appreciable oxidation of the external surfaces. Figure 20 shows the capsule after the exposure in the furnace.

One capsule was sectioned and the sodium reacted from the interior. Subsequently, macro and micro photographs were made of the joint. The examination revealed that the interior surface of the capsule was in excellent condition. Furthermore, the brazed joint was not compromised in any way. No evidence of corrosion was visible; consequently, it was apparent that the capsules could have performed as well for a significantly longer period of time.

A second pair of capsules is now under exposure with a vacuum as the environment immediately surrounding the external surfaces.

The performance of these capsules and the feature permitting remote assembly suggests a number of possible uses for this type of fitting, for example, fuel-element closures, connections in a sodium loop, instrumentation connections, and other attachments in reactor components or experimental systems. The relative simplicity of the fitting could also reduce costs and manipulations necessary in remote operations.

Fig. 20. Brazed Conoseal Fitting after 1380-hr Exposure at 1200°F

5. Evaluation of Type 304 Stainless Steel Tubing

Nine sample tubes of Type 304 stainless steel have been fabricated for 1200°F rupture and tensile tests. These samples (0.493 in. in OD and of 0.014-in. wall) are prepared for ultimate tensile strength, yield strength, percent elongation, and burst strength in 1200°F sodium.

Small segments of these samples will be examined for hardness, sensitization, grain structure, and chemically analyzed for carbon. The sodium used for immersion of these samples will be new, clean sodium of known composition.

In general, the sensitization of the tubing using "clean" sodium for soaking periods of 3, 6, and 9 days is to be measured or determined.

These data will be compared to the rather severe sensitization of 304 stainless steel previously reported (see Progress Report for January 1966, ANL-7152, pp. 48-49). It should be remembered that the earlier observed sensitization of 304 stainless steel tubing was developed from tubing exposed to 1200°F sodium in the small high-temperature loop, which has carbon in the sodium to the extent of about 70 ppm.

Three samples of Type 304 stainless steel tubing are being analyzed for carbon, namely,

a) as received from vendor;
b) a sodium soaked at 1200°F;
c) a different heat as received from the vendor.

The latter tubing was the material used in fabricating the nine samples discussed above. It will be desirable to know the carbon content of the as-received tubular products before soaking in sodium to determine

if a measured, variable carbon content of "as received" tubing can be correlated with observed and measured sensitization of 304 stainless steel after exposure to sodium.

A Filar eyepiece for the Kentron Micro-Hardness Tester has been purchased and used for traverse cross sectional measurements on "as received" EBR-II blanket element tubing. Data on one sample of one heat of "as received" tubing indicates a rather uniform hardness, wall to wall, at four locations across the wall (Rockwell B scale readings of 85, 87, 90, and 87). The Rockwell B readings are converted Knoop hardness numbers, actually measured, of 165, 173, 186, and 165, obtained with a 500-gm load and a Knoop indenter.

Microhardness measurements of the wall thickness of 1200°F sodium-soaked, 1200°F air-heated, and 1200°F argon-heated samples are in progress.

6. Loop Evaluation after Long-time, High-temperature Exposure to Sodium

An evaluation of the performance of Type 304 stainless steel welded pipe which had been exposed to hot sodium at ANL was received from the U. S. Steel Corporation. The pipe was a portion of a loop that was exposed to flowing sodium on the inside at 1200°F for 2069 hr, at 1472°F for 4695 hr, and between 572 and 1200°F for 1000 hr. The outside of the pipe was covered with insulation and thus exposed to air. In the comparison of the material properties between the unexposed and exposed pipe sections, the report shows:

a. a minor reduction in the room-temperature ultimate tensile strength (from 86.8 to 83.5 kpsi);
b. a significant reduction in the room-temperature yield strength (from 45.7 to 35.2 kpsi);
c. a minor reduction in room-temperature ductility (elongation dropped from 64 to 58%);
d. significant microstructural change in the weld metal (partial transformation of delta ferrite to sigma);
e. precipitation of carbides around the grain boundaries;
f. chemical environmental reactions [both the inside and the outside surfaces were nitrided to a depth of about 0.001 in. The nitride phase was substantially harder than the matrix, Brinell 255 versus 180. The more heavily nitrided inner case (0.24%) initiated cracking of the wall in bend tests].

The chemical analysis shows that the material was probably a low-carbon, austenitic stainless steel whose inner and outer surfaces were carburized 0.063 to 0.082% C during the manufacture of the pipe. Nickel

and chromium contents were 10.3 and 18.3%, respectively; in composition, the 304 SS material just meets the lower limits of low-work-hardening AISI Type 305 stainless steel. Grain growth during the exposure period was nominal, an increase from grain size 8 to 7. Evidence of austenitic metallurgical instability, other than precipitation of carbides, was lacking.

The results of the U. S. Steel Company examination of the ANL pipe in part support the selection of the nickel-rich (11.5/12/5% Ni) AISI Type 305 SS for the 1200°F FARET pressure vessel. The conversion of delta ferrite to sigma phase with long-time exposure at high temperature as noted in the report was anticipated; therefore, proposed FARET welding requirements limited the ferrite content of the weld metal. The nitriding of the 304 SS exterior was expected, but the 0.001-in. nitriding of the pipe interior wall was not anticipated, although it was known that air had mixed with the argon atmosphere during sample withdrawal.

In addition to the acquisition of the above metallurgical data, from July of 1964 to February 1966, an analysis of impurities which might be in the sodium in the 304 SS forced-circulation loop has been conducted. The values of the principal metallic impurities measured by spectrochemical analysis are as follows for several different analyses made over a period of time:

Spectrochemical Analysis

(values in ppm)

	Al	Cu	Fe	Ni	Cr	V
a. Impurity range in new, clean sodium	8	2	2	2	-	4
b. Sodium sample at ~8000 hr before	24					1500
removal of pipe for U. S. Steel	40	750	15	8	-	2000
analysis						
c. Sodium sample from drain tank	2	3	40	-	-	-
d. Sodium sample from loop after drain	3	4	40	-	-	-
and refill #1						
e. Sodium sample from loop after drain	25	100	16	4(?)	-	1300
and refill #2						

Analysis of item d was obtained before a stressed vanadium exposure run was made. Analysis of item e was obtained after a stressed vanadium sample exposure run was made.

The carbon content of the sodium was measured after removal of the U. S. Steel Company specimen sample of pipe. A value of 77 ppm of carbon was found.

The oxygen content of the system was measured only after the 2-in. pipe specimen was removed at the end of 7764 hr of service in hot sodium. A standard ANL plugging meter was used to measure the oxide content. The plugging temperature of this system operating at 600°C was approximately 530°C.

The unusually high plugging temperature of 530°C corresponds to the highest measured quantity of sodium oxide in sodium as presented by the Mine Safety Appliance Company's solubility curve in the July 1955 Liquid Metals Handbook, p. 8. A plugging temperature of 530°C corresponds to 0.22 w/o oxygen or about 2200 ppm. The adverse oxide condition can be explained by the fact that at no time has a sodium oxide-removal system been incorporated into the loop. Only recently has a dump tank been used to study the effect of system "drain and refill."

From the work described above, these general conclusions may be drawn:

a. The lack of cold-trap and hot-trap devices on the engineering loop would not be duplicated in a fast reactor, and therefore both the metallurgical condition of the pipe and the chemical quality of the sodium should be more adverse for the engineering system than for a commercial fast reactor system.

b. The metallurgical data and the analysis of the impurities in the sodium are in general agreement, i.e., both the results of the U. S. Steel Company metallurgical analysis and the lack of large increases in Fe, Ni, and Cr in the sodium, support each other.

7. Separation of Particulate Carbon by Centrifugation

Previous experiments (see Progress Report for February 1965, ANL-7017, p. 70) on separation of particulate carbon from liquid sodium at 200°C by centrifugation (2000 rpm, 300 to 625 g) indicated that the particles, if present, were in the submicron range. Recent experiments have shown that much larger centrifugal forces are effective in sedimenting such particles.

For these experiments, a 56 w/o Na-44 w/o K alloy, which is liquid at room temperature (m.p. 19°C), was substituted for sodium because the high-speed centrifuges available could not operate above the melting point (98°C) of sodium. The alloy was sealed in stainless steel centrifuge tubes in a helium-atmosphere glovebox and (1) centrifuged at 17,000 rpm (~35,000 g) for 40 min, then slowed to a stop over the next 20 min; or (2) centrifuged at 40,000 rpm (~150,000 g) for $3\frac{3}{4}$ hr, of which the final $1\frac{1}{2}$ hr was at 0°C in order to freeze the alloy while spinning. In both cases,

the centrifuge tubes were tilted to the rotor axis (34 and 20°, respectively). After centrifugation, the tubes were cooled in liquid nitrogen and opened within the glovebox for sampling. Samples could not be taken from specific locations in the solid alloy because of its extreme brittleness. Thus, the alloy was allowed to liquefy and samples were withdrawn by pipette from the top of the liquid. The results of the carbon analyses are given below:

	Carbon (ppm)
Before centrifugation	76, 53, 36, 43
After centrifugation	
at 17,000 rpm	22, 33
at 40,000 rpm	23, 34

Statistical analysis of these data indicates that at the 95% confidence level there is a difference in carbon contents of the original and centrifuged alloys. The separations obtained may not represent the maximum achievable: redistribution of carbon particles by convection and vibration could have occurred during the melting and sampling steps. Further experiments with liquid Na-K alloys will be carried out to determine if sufficient information on particle size can be obtained to warrant extension of this work to liquid sodium.

II. GENERAL REACTOR TECHNOLOGY

A. Experimental Reactor and Nuclear Physics

1. Multiplication Process in Proportional Counter

The multiplication process of 4π-recoil proportional counters has been investigated in the region of high gain by examination of the single-electron response distribution (see Progress Report for January 1966, ANL-7152, pp. 50-51). The experimental arrangement (see Fig. 21) is similar to that employed by Curran, Cockroft, and Angus.[4] With such an arrangement, the response of the proportional counter to single electrons can be determined. Ultraviolet quanta enter the counter through the quartz window, traverse the active volume of the counter gas, and create photoelectrons on the opposite side counter wall. Once created, a photoelectron will drift toward the center (anode) wire of the counter, initiating an electron avalanche which is subsequently detected. Measurement of the response distribution which arises from these single-electron events permits a study of the statistics of the multiplication process.

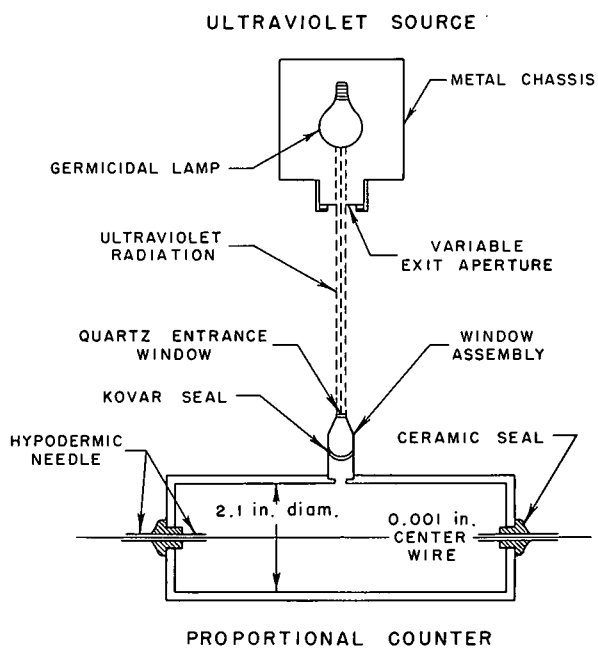

Fig. 21. Experimental Arrangement of Proportional Counter, Window Assembly, and Ultraviolet Source for the Measurement of Single-electron Response Distributions

Some single electron spectra obtained in this region are displayed in Fig. 22. These figures present the measured distribution $P(\nu)$ in normalized form:

$$\nu = n/\bar{n},$$

where n and $\bar{n}$ are the final number and average final number of electrons in the avalanche, respectively. It is evident that the single-electron response distribution is not constant, but changes with anode voltage. Consequently, one can conclude that the electron branching process in proportional counters is not invariant with respect to the average final number of electrons in the avalanche.

[4]Curran, S. C., Cockroft, A. L., and Angus, J., Phil Mag. 10, 929 (1949).

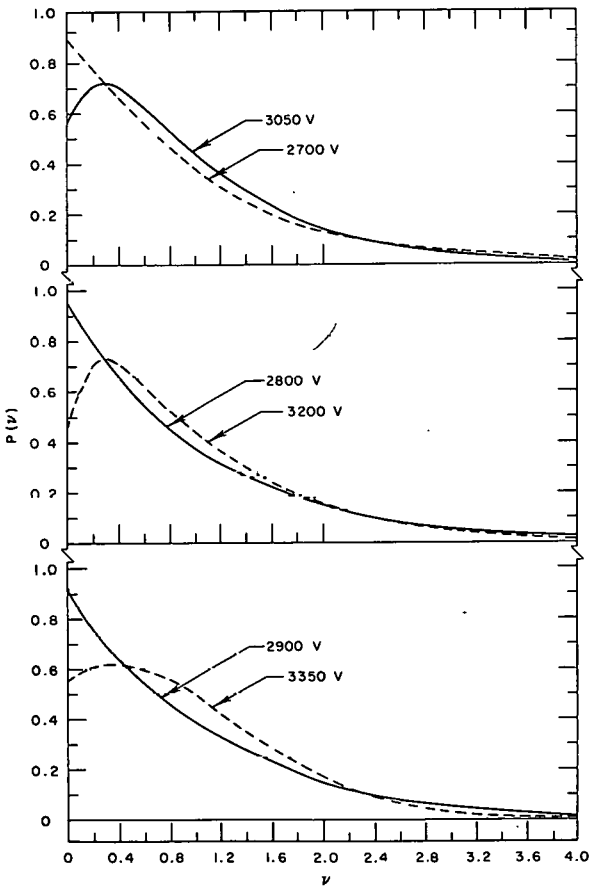

Fig. 22. Single-electron Spectra Obtained at Different Anode Voltages in a One-atmosphere Methane-filled Proportional Counter

B. Theoretical Reactor Physics

1. Reactor Computations

In computing average cross sections in the unresolved resonance region, averages must be taken over statistical distributions of neutron and fission widths. In the case of fission, for example, the average cross section at an energy E* may be written as

$$\bar{\sigma}_f(E^*) = \frac{\int_0^\infty \int_0^\infty P_n(x)\, P_m(y)\, y\Gamma_f J(\xi,\beta)\, dx dy}{\int_0^\infty \int_0^\infty P_n(x)\, P_m(y) \int_{-D/2}^{D/2} \frac{1}{\psi + \sigma_p} d\xi dx dy}$$

where P_n and P_m denote Porter-Thomas distributions of m and n degrees of freedom.

The evaluation of the triple integrals is most widely accomplished by the method of Greebler and Hutchins,[5] in which the distribution functions are approximated by trapezoids of equal area. This method has undesirable features in that the area of each trapezoid must be computed by iteration, and a fairly large number of points must be used to achieve adequate accuracy. About ten trapezoids are needed to obtain 1% accuracy for a distribution with one degree of freedom.

An alternative method is the use of a Gauss-Laguerre quadrature formula. The exponential term in the Porter-Thomas distribution is extracted and used as the weighting function in the Gauss-Laguerre formula. The use of a formula of this type yields 1% accuracy with only five points. This results in a savings of computation time by a factor of two.

2. Effective Potential Scattering Cross Section for Use in the Single-level Breit-Wigner Formula

The total cross section for a given isotope may be computed from the single-level formula

[5]Greebler, P., and Hutchins, B. A., Proc. Seminar on Physics of Fast and Intermediate Reactors, Vienna (1961).

$$\sigma_T(E) = \sigma_0\left[\frac{\Gamma_a}{\Gamma}\left(\frac{E_0}{E}\right)^{1/2} + \frac{\Gamma_n}{\Gamma}\right]\psi(\xi, x) + \left(\sigma_0\sigma_{pg}\frac{\Gamma_n}{\Gamma}\right)^{1/2}\chi^{(\xi,x)} + \sigma_p;$$

$$x = 2(E - E_0)/\Gamma.$$

The potential scattering cross section σ_p which appears in this expression is frequently taken to be the average value of the total cross section at low energies distant from any resonances. If an attempt is made to reconstruct the curve of measured total cross section using this value for σ_p along with measured resonance parameters, agreement with the measured total cross section is poor at energies which are not close to resonance peaks. This occurs because the interference contribution to the total cross section can be fairly large in relation to the magnitude of σ_p, when this expression for the total cross section is used at energies which are distant from resonance peaks.

For example, a potential scattering cross section of about 13 b is needed to give good agreement with the measured total cross section of U^{238} at low energies. This calculation was made with the use of the resonance parameters measured by Garg.[6] This high value for σ_p is needed to compensate for the interference term in the expression for the total cross section which is large and negative at energies below a resonance peak. At fairly high energies, the use of σ_p = 13 b leads to calculated values which are slightly high in relation to the measured total, and the use of σ_p = 10 b (the apparent average value of σ_T in BNL-325 at low energies) leads to calculated values which are slightly low.

A similar behavior is noted for sodium. Here the total cross section at low energies is influenced by the 2.8-keV resonance. A σ_p of about 5 b is needed to calculate the measured total of about 3.2 b at low energies. In the case of sodium, it has been found[7] that the agreement with experiment may be improved over a wide energy range by using spin-dependent potential scattering cross sections.

3. Cross-section Evaluations

The programs LEGENDRE, PØLYWØLY, ØSCAR, and CØAGØGØ, used in the study of angular distributions of scattering, have been consolidated into one program, SAD. The subroutine used for the transformation of Legendre expansion coefficients from the laboratory to the center-of-mass system of coordinates has been replaced by a more accurate subroutine obtained from the Atomics International code, CHAD.[8] Also, the CHAD code, written originally in Fortran-IV, has been transformed to 3600 Fortran, and test problems have been run successfully.

---

[6]Garg, J. B., et al., Phys. Rev. 134, 985 (1964).

[7]Stephenson, T. E., BNL-961 (T-401) (1965).

[8]Berland, R. F., CHAD, Code to Handle Angular Data, NAA-SR-Memo 11231.

4. ZPR-7 Physics Analysis

Calculations of bucklings (B^2) and various microparameters were carried out for the final two Hi-C lattices studied in the ZPR-7 critical assembly. These lattices had a pitch of 1.349 cm in a square array with either aluminum or stainless steel (SS) clad. The atom ratio (of hydrogen to uranium-238) of about 4.15 makes these lattices the least undermoderated lattices studied with Hi-C fuel. GAM-I constants for three fast groups and THERMØS constants for the thermal group were calculated. The computed B^2 for the aluminum-clad assembly was 9.303×10^{-3} cm^{-2} for the case in which the B-1 approximation was used in GAM-I, and 8.994×10^{-3} cm^{-2} for the P-1 approximation case. The experimental value was 9.182×10^{-3} cm^{-2}. Not enough fuel was available to make the SS-clad lattice critical without an external driver zone, so no experimental B^2 is available for comparison with calculations.

5. Treatment of Source Discontinuities

The effect of discontinuities in the external source in numerical solution of the diffusion equation has been analysed for the case of 1-group 1-dimensional slab geometry.

$$[D(x)\,\phi'(x)]' - \sigma(x)\,\phi(x) + S(x) = D\phi'' + D'\phi' - \sigma\phi + S = 0. \qquad (1)$$

Here, $\sigma(x)$ includes both absorption and fission contributions, and may be either positive or negative. This example illustrates some essential program difficulties which will be encountered in solving more complicated problems.

The treatment avoids, to begin with, such simplifying assumptions as constancy of diffusion coefficient, cross section, and external source, and will thus apply as well to more realistic models than those in current use. It leads to the fundamental consistency condition which must be satisfied at every point x_0:

$$\gamma S + \mu D\gamma\phi'' + \mu\phi''\gamma D + \mu\phi'\gamma D' - \mu\sigma\gamma\phi - \mu\phi\gamma\sigma = 0, \qquad (2)$$

where μ_F is the mean value of the quantity F on opposite sides of x_0, and γ_F is the jump in F at x_0; i.e.,

$$\mu_F = \lim_{\epsilon \to 0} \left\{ \tfrac{1}{2} F(x_0 - \epsilon) + \tfrac{1}{2} F(x_0 + \epsilon) \right\}$$

and

$$\gamma_F = \lim_{\epsilon \to 0} \left\{ F(x_0 + \epsilon) - F(x_0 - \epsilon) \right\}.$$

In the neutron-diffusion interpretation of Eq. (1), S is the external source, ϕ the flux, $D\phi'$ the current, $\sigma\phi$ the net loss rate from the group, including the effects of capture and fission, and D the diffusion coefficient. The last two are ordinarily determined almost entirely by the composition and their values, and the jumps at the boundaries are fixed by considerations other than the external source. Under these conventions, discontinuity in the source reflects itself in discontinuities in the flux or its derivatives. Neutron-conservation arguments ordinarily are used to require continuity of flux and current. Under these assumptions the only possible function in which an arbitrary discontinuity can occur to compensate the arbitrary jump in the source is the second derivative of the flux, ϕ''. With the assumptions of continuity of flux and current, the discontinuity in the second derivative is given by

$$\gamma_{\phi''} = -\gamma_S/D \tag{3}$$

in regions where the cross sections and diffusion coefficient are continuous, and

$$\gamma_{\phi''} = (-\gamma_S + \phi\gamma_\sigma - \mu_{\phi''}\gamma_D)/\mu_D \tag{4}$$

at boundaries between such regions.

The implications of this analysis for finite difference, or, indeed for any numerical method of integrating Eq. (1), are clear. Since all numerical integration schemes for second-order differential equations assume the boundedness of at least the third derivative, it is no safer to ignore discontinuities in the external source than it would be to ignore discontinuities in the material. At any point of discontinuity, the integration should be stopped and restarted with new boundary conditions. Under the assumptions of continuity of flux and current, these new boundary conditions can be obtained from use of Eq. (3) or (4).

The method of carrying out this change of boundary conditions is entirely analogous to that used for changes of materials, for which the condition of Eq. (4) must be satisfied even if $\gamma_S = 0$. There is thus no need to discuss the technique in detail other than to remark that the program must provide for discontinuities in source across the region boundaries, as well as for discontinuities in diffusion constant and cross sections, and that the user must provide region boundaries at every point where he wishes a discontinuity in the external source.

6. Hybrid Computer Techniques

A hybrid computer has been created by linking components of a PACE electronic analog to components of a PDP7 digital computer. This hybrid is considered to be analog-computer oriented because of the nature

of the problems which are being solved. It could as easily be digital-computer oriented if the major portion of the computing effort were vested in digital components.

The types of problems being solved involve coupled nonlinear partial differential equations. The analog components of the hybrid solve partial differential equations as a function of discrete space and continuous time. The digital components function as memory, as function generators, and as computers of analog subroutines.

This hybrid is currently limited by physical equipment. The largest problem which has been succesfully solved is a set of coupled equations consisting of the equations of two-dimensional heat flow (radial and axial), reactivity feedback (Doppler, expansion, and voids), and the six-group, space-independent, neutron kinetics equations.

The two-dimensional representation of this problem results in a set of forward-coupled (along the axis since axial heat conduction is insignificant) nonlinear partial differential equations. Similar differential equations in this set are solved sequentially by programming only one of them on analog components and using the memory of the digital computer to provide the initial conditions for each succeeding equation. To do this, an iterative procedure is necessary whenever there is feedback in the closed loop. This is made possible by use of the digital component for temporary storage and transfer.

This iterative procedure has converged very rapidly in problems considered to date. This convergence is predicted by consideration of the principle of contraction mapping. Large conservation of analog components through employment of this multiplexing process is thus made possible only by hybridizing the computations.

The problems which have been programmed for the hybrid and studied to date are:

1. The significance of variable thermal conductivity and its gradient in nuclear fuels
2. The effect of internal radiative heat transfer in ceramic fuels upon the transient behavior of fast reactors
3. Power excursions in fast cores with strong Doppler feedback
4. The frequency response of ceramic fuels to periodic power fluctuations
5. The effect of coolant flow upon fuel temperature
6. The convergence rate of closed sets of nonlinear partial differential equations.

7. The ARC System

The interface specifications among various computational modules have been revised and updated to accommodate the changes in the system organization and to add to convenience. Based on these interface specifications, the programming of various neutronics and related modules are underway.

In addition, progress is being made in the following aspects:

(1) System Operation--Several possibilities of system operation are being studied. This study will eventually develop a system that meets all the peculiar requirements of ARC.

(2) DATAPOOL--The study of the organization and functioning of DATAPOOL goes in parallel with that of the system operation, as the organization of the DATAPOOL must be made such that the system operation is not only feasible, but also efficient. The results of the preliminary study of the system operation have already lead to some basic changes in the order and number of hierarchy levels in the DATAPOOL.

(3) Control Input--Various possible modes of inputting the information for use with some "standard" types of computations are being studied.

(4) Burnup Module--Preliminary specifications regarding the general capabilities of the Burnup Module (and associated modules) for the ARC System is under study.

Conventionally, determining the equilibrium initial atomic concentration vector $\underline{n}$ for a given fuel-management policy involved an iteration procedure. The following analytical procedure is under investigation for the possible use in the new burnup module which is being developed for use in the ARC System.

Let $\underline{n}$ be a KM-dimensional vector for the initial atomic concentration of the form

$$\underline{n} = \text{col.}\left\{n_1^1, n_2^1, \ldots, n_M^1, \ldots, n_1^K, n_2^K, \ldots, n_M^K\right\}, \tag{1}$$

where superscripts refer to regions, the subscripts to nuclides, K is the number of regions, and M the number of nuclides. After one irradiation step for a given burnup time, thus for a fixed burnup matrix $\underline{B}$, the nuclide concentration will be

$$\underline{p} = \underline{B}\,\underline{n}. \tag{2}$$

Define the following matrices:

$\underline{D}$ → a diagonal matrix such that $\underline{D}\,\underline{p}$ gives the amount of nuclides removed from reactor for transfer to other regions, for reprocessing, etc.

$\underline{C}$ → a diagonal matrix such that $\underline{C}\,\underline{D}\,\underline{p}$ gives the amount of nuclides to be "sold" out.

$\underline{G}$ → a diagonal matrix such that $\underline{G}\,\underline{D}\,\underline{p}$ gives the amount of nuclides to be reprocessed.

$\underline{A}$ → "transfer matrix," such that $\underline{A}(\underline{I}-\underline{C}-\underline{G})\underline{D}\,\underline{p}$ gives the direct transfer into various regions.

$\underline{R}$ → "recovery matrix," such that $\underline{R}\,\underline{G}\,\underline{D}\,\underline{p}$ gives the amount of reprocessed nuclides that is recovered. $\underline{R}$ takes into account the radioactive decay of nuclides as well as the factor associated with the reprocessing efficiency.

$\underline{E}$ → "distribution matrix," such that $\underline{E}\,\underline{R}\,\underline{G}\,\underline{D}\,\underline{p}$ gives the distribution of recovered nuclides into various regions.

In addition, define a K-dimensional vector $\underline{q}$, called the "makeup vector," such that the element q^k of $\underline{q}$ is the total number of nuclides to be added to the k^{th} region before each irradiation step in order to satisfy the conservation relation of all nuclides in each region. Further, the "feed matrix" $\underline{F}$ is defined such that $\underline{F}\,\underline{q}$ is a KM-dimensional vector, whose element h^k_m denotes the amount of nuclide m to be added in region k.

When all operations are completed, the nuclide concentration for the next irradiation step is given by generalizing to i^{th} step:

$$\underline{n}^{i+1} = \underline{X}\,\underline{n}^i + \underline{F}\,\underline{q}^i, \tag{3}$$

where

$$\underline{X} = (\underline{I}-\underline{D})\underline{B} + \underline{A}(\underline{I}-\underline{C}-\underline{G})\underline{D}\,\underline{B} + \underline{E}\,\underline{R}\,\underline{G}\,\underline{D}\,\underline{B}. \tag{4}$$

Notice that the vector $\underline{n}^i$, for all i, must satisfy the conservation relation

$$\underline{S}\,\underline{n} = \underline{c}, \tag{5}$$

where $\underline{S}$ is a (KXKM)-matrix such that the element c^k of $\underline{c}$ is given by

$$c^k = \sum_{m=1}^{M} n^k_m. \tag{6}$$

From Eqs. (3) and (5),

$$\underline{S}\,\underline{n}^{i+1} = \underline{c} = \underline{S}\,\underline{X}\,\underline{n}^{i} + \underline{S}\,\underline{F}\,\underline{q}^{i}, \tag{7}$$

from which

$$\underline{q}^{i} = (\underline{S}\,\underline{F})^{-1}\,[\underline{c} - \underline{S}\,\underline{X}\,\underline{n}^{i}]. \tag{8}$$

By use of Eq. (8) in Eq. (3),

$$\underline{n}^{i+1} = \underline{X}\,\underline{n}^{i} + \underline{F}(\underline{S}\,\underline{F})^{-1}\,[\underline{c} - \underline{S}\,\underline{X}\,\underline{n}^{i}], \tag{9}$$

which describes the behavior of the vector $\underline{n}$ as the sequence of fixed irradiation-fuel management steps proceed, i.e., the information regarding the approach to equilibrium.

Now, suppose that above process reached an equilibrium. Then, from Eq. (3),

$$\underline{n}^{eq} = \underline{X}\,\underline{n}^{eq} + \underline{F}\,\underline{q}^{eq}, \tag{10}$$

or

$$(\underline{I} - \underline{X})\underline{n}^{eq} - \underline{F}\,\underline{q}^{eq} = \underline{0}. \tag{11}$$

Combination of Eqs. (11) and (5) yields

$$\left[\begin{array}{c|c} (\underline{I} - \underline{X}) & -\underline{F} \\ \hline \underline{S} & \underline{0} \end{array}\right]\left[\begin{array}{c} \underline{n}^{eq} \\ \hline \underline{q}^{eq} \end{array}\right] = \left[\begin{array}{c} \underline{0} \\ \hline \underline{c} \end{array}\right]. \tag{12}$$

Therefore,

$$\underline{\tilde{n}}^{eq} = \left[\begin{array}{c|c} (\underline{I} - \underline{X}) & -\underline{F} \\ \hline \underline{S} & \underline{0} \end{array}\right]^{-1}\left[\begin{array}{c} \underline{0} \\ \hline \underline{c} \end{array}\right], \tag{13}$$

if the inverse exists and where

$$\underline{\tilde{n}}^{eq} = \left[\begin{array}{c} \underline{n}^{eq} \\ \hline \underline{q}^{eq} \end{array}\right], \tag{14}$$

which gives the equilibrium initial atomic concentration and the makeup directly without iteration.

C. High-temperature Materials Studies

1. Ceramics

a. (Th-U-Pu) Phosphides. Studies have continued on the high-temperature compatibility of UP with the following refractory metals: Ti, Zr, Nb, Ta, Mo, and W (see Progress Report for January 1966, ANL-7152, pp. 56-57). Samples containing equivalent mole percentages of UP and these metals were heated in the melting point furnace to obtain liquidus temperatures for these compositions. The results are given below:

Composition	Liquidus Temperature (°C)	Composition	Liquidus Temperature (°C)
UP-Zr	2055	UP-Mo	2395
UP-Ti	2110	UP-Ta	2405
UP-Nb	2380	UP-W	2574

The liquidus temperatures represent complete melting of the compositions and are considerably higher than those at which liquid first appeared. Nevertheless, these results parallel the compatibility observations previously reported. UP reacted extensively with Zr and Ti at 1800°C, at which temperature the pellets melted. Samples containing Nb and Mo exhibited considerable melting and vaporization at 2000°C. The composition UP-Ta was relatively stable up to 2200°C, but melted at this temperature. UP and tungsten showed no reaction at 2200°C. Interestingly, the above results generally follow the order of melting points of the pure metals.

Studies of the system UP-UN have continued. Melting experiments conducted in helium and nitrogen showed that the liquidus temperatures were affected by the atmosphere used. Use of pressurized nitrogen was necessary for the UN-rich side of the system to suppress formation of uranium, which depressed the melting temperature. However, compositions at the UP end of the system were shifted toward higher UN contents through reaction with the nitrogen atmosphere, and melted at lower temperatures than in helium. Use of mixed gases in the same proportions as the P/N ratios of the samples did not solve the problem, since the helium was inert whereas the nitrogen was quite reactive in the temperature range used (2200 to 2850°C). Use of sealed tungsten containers might conceivably solve this problem.

b. Development of Thermal Diffusivity Rig for Ceramic Materials. Thermal-diffusivity and heat-capacity techniques are being used to determine the heat-transfer properties of ceramics. The method requires disc-shaped samples, approximately 1.9 cm in diameter by 0.2 to 0.3 cm thick. These samples must be prepared from high-purity material that must not become contaminated during fabrication. The samples must also be uniform

in structure and porosity, and free from microcracks. To this end several techniques for fabrication of disc samples have been investigated.

Attempts to prepare discs by cold-pressing and sintering have had limited success. Many of the samples had laminations or center cracks that interferred with the measurements. Center cracks were eliminated by a slow firing procedure. The laminations persisted, however, and were found to be due to the pressure release when the compact was pushed from the die.

In order to obtain crack-free samples isostatic pressing was attempted. The method consisted of loading powder into a section of rubber hose, of 1.9-cm ID, with a 1-cm wall thickness, and with a rubber stopper closing one end. When the appropriate amount of powder was loaded, a second stopper with a hole drilled in its center was pushed into the open end. The length of hose was adjusted before the start of the operation so that the stoppers would contact the powder. A thin-walled metal tube, 0.155 cm in diameter, was then pushed into the stopper hole, and the entire assembly was placed in a plastic bag and evacuated. When evacuation was complete, the metal tube was removed from the stopper without breaking the connection to the vacuum system. The opening used for evacuation was then heat sealed, and the bag and its contents were isostatically pressed at 21 kg/mm^2. Samples were free from laminations. This technique, which was conducted with uranium sulfide powder, is presently being adapted for plutonium-glovebox operation. Development of this procedure should enable us to study the effects of porosity on high-purity materials.

2. Liquid-metal Corrosion

a. Polarization Studies. High oxygen concentration in glovebox helium caused interruption of polarization experiments. The oxygen leak has been repaired, and the glovebox is again in operation. Two observations relating to solutions of problems necessary for successful study in this area are discussed in the following.

The first concerns verification of the efficacy of the glovebox cold trap in reducing oxygen concentration in helium from the range of 25 ppm (an incidental value existing when the observations began) to less than 0.33 ppm, a value appreciably lower than that corresponding to the vapor pressure of oxygen at liquid nitrogen temperatures. The low concentration was maintained in spite of additional in-leakage of oxygen at an estimated rate of 0.5 ppm/min. The trap contains coconut charcoal in a copper vessel immersed in liquid nitrogen and is regenerated periodically by heating and evacuation. It was not empirically determined if the charcoal was more effective in obtaining this performance than would be an equal area of other thermally conductive materials.

The second development concerns a mechanical method of stripping corrosion film from zirconium electrodes after overnight exposure to oxygenated sodium (or oxygen gas) near 540°C. An effective stripping method has been needed to evaluate the weight of corrosion film present on electrodes where weight-gain measurements are questionable because of oxygen dissolution into "uncorroded" sample metal underlying films and also because of the possibility of some film loss to the sodium environment.

The novel method employs glass microbeads carried by a high-velocity gas stream impinging on the corroded surface. The stripping mechanism appears to involve localized shattering of brittle corrosion product by impinging microbeads and removal of resulting debris by the gas stream. Uncorroded metal absorbs the impact shocks and is relatively unaffected except for alteration of surface texture. The maximum diameter of spherical glass beads employed was about 0.15 mm, the mean sphere size being considerably smaller. An Industrial Airbrasive Unit was used to generate the gas-bead stream. The velocity of nitrogen carrier gas in the nozzle orifice of 0.46- to 0.51-mm diameter is estimated by the manufacturer to be near 1100 ft/sec. About 5 min were required to strip a 15-cm^2 area with a nozzle-to-surface distance of 1.9 cm and the stream held normal to the surface.

Thinner corrosion films than those noted above were removed only very slowly, due probably to the cushioning effect of underlying metal. Relatively thick films (of thickness corresponding to 1 mg/cm^2 of oxygen) were similarly affected only slowly or unaffected; perhaps a higher impact energy (by use of larger beads) would have been more effective. A film weight loss corresponding to 0.4 mg oxygen/cm^2 was determined for one of the samples whose film thickness was in the optimum range for the stripping technique described.

Some sparking was seen as glass beads struck stripped zirconium, indicating loss of unoxidized metal. This amount was found to be 0.6 mg total for the 15-cm^2 area during a second 5-min period of treatment similar to that of stripping. A third 5-min treatment resulted in loss of another 0.6 mg. This loss is thus small and reproducible.

The stripping method was further applied to stainless steel corroded in 540°C steam and to 1100 aluminum corroded in 70°C water. Corrosion films were readily removed. There was little weight change observed when uncorroded samples of the same materials were subjected to the same treatment. This method of stripping thus appears applicable to a number of corrosion problems and displays a potential for use in quantitative studies. A more detailed report[9] has been prepared and submitted to Corrosion for publication.

---

[9]Youngdahl, C. A., "Mechanical Stripping of Corrosion Samples," submitted to Corrosion (February 1966).

b. Lithium Corrosion Studies at Elevated Temperatures. Titanium is an effective nitrogen getter in lithium. The solubility of titanium in lithium containing 55 ppm of nitrogen is about 15 ppm at 930°C (PWAC-356). The behavior of titanium in lithium at higher temperatures and its interaction with multicomponent liquid-metal systems is not yet known. It is thought that by obtaining this information, insight into corrosion-preventive measures applicable to lithium systems could be gained. The results of exploratory tests are described below.

In the initial titanium-lithium test at 1200°C, in which molybdenum was the container, a weight loss of 27.3 mg/cm^2 of titanium was observed over a period of 7 days. A needlelike surface structure associated with high-microhardness measurements indicated some impurity diffusion had occurred. Chemical analysis of post-test lithium samples showed a nitrogen content of 15 ppm, compared with an initial nitrogen content near 50 ppm. No significant surface change of the molybdenum capsule was observed after test.

Under similar test conditions and exposure time, a test was made with an addition of 1.5 a/o silicon to the lithium. Silicon is considered to be of interest because it is a powerful deoxidizing agent, is very soluble in lithium, and $MoSiO_2$ is a very effective oxidation barrier. The weight loss of titanium was slightly reduced to 23.3 gm/cm^2 over the same 7-day period. The nitrogen content of post-test lithium was 25 ppm (initial nitrogen content was the same as in the previous test). Microhardness measurements indicated no surface irregularities on the titanium. However, an unidentified, rather brittle layer developed on the inner surface of the molybdenum. Such a result has not been experienced previously.

In view of the different results of these tests, it is noted that silicon may significantly affect the behavior of titanium in lithium. Interesting questions include the effect of silicon on the solubility limit of nitrogen or oxygen in lithium and the nature of the layer on the molybdenum.

It is expected that the addition of selected additives may have profound effects on the corrosion of materials in high temperature lithium. Exploration of these systems will be continued.

3. Irradiation Testing

A series of irradiations are in progress. A summary of the irradiations of ceramic fuels in progress is shown in Table XIV.

TABLE XIV. Status of High-temperature Fuel Irradiations in Progress

Specimen No.	Fuel Composition (w/o)	Jacket Composition (w/o)	Jacket ID (mm)	Jacket Thickness (mm)	Maximum Jacket Surface Temp (°C)	Calculated Burnup to Date	
						a/o	$f/cm^3 \times 10^{-20}$
MV-2	UC-20 PuC	Nb-1 Zr	6.5	0.30	650	4.6	15
MV-3	UC-20 PuC	Nb-1 Zr	6.5	0.30	760	5.1	17
MV-5	UC-20 PuC	Nb-1 Zr	6.5	0.30	750	4.8	16
MV-6	UC-20 PuC	Nb-1 Zr	6.5	0.30	660	5.1	17
S-7	US	Nb-1 Zr	6.5	0.30	530	3.4	8.6
S-8	US	Nb-1 Zr	6.5	0.30	690	5.4	13
S-9	US	Nb-1 Zr	6.5	0.30	710	5.4	13
S-10	US	Nb-1 Zr	6.5	0.30	670	5.4	13
S-15	US	Nb-1 Zr	6.5	0.30	560	2.5	6
S-16	US	Nb-1 Zr	6.5	0.30	690	4.4	10.6
S-17	US	Nb-1 Zr	6.5	0.30	680	3.1	7.5
S-18	US	Nb-1 Zr	6.5	0.30	790	4.9	12

The capsule irradiation program for the vibratorily compacted UC-20 w/o PuC specimens calls for nominal burnup levels of 2, 5, and 10 a/o at jacket surface temperatures of 600, 800, and 1000°C. Irradiations have been completed at the 2 and 5 a/o burnup levels at 600°C, although the 2 a/o specimens did not all quite achieve this burnup or temperature. Specimens for the 10 a/o level at 600 and 800°C are now in MTR.

The 5 a/o, 1000°C capsule which was inserted into the MTR on January 10, 1966 had to be removed from the reactor after one cycle because of inability to maintain the gas annulus atmosphere under a static test. Burnup for each specimen is estimated to be 0.3 a/o (1.0×10^{20} fiss/cc). The maximum cladding temperatures attained were 860°C. A comparison of the specimens from this capsule and those with higher burnups will yield information on any predominantely thermal effects which may occur in the UC-20 w/o PuC system.

Another 1000°C capsule has been shipped to the MTR and is awaiting insertion.

D. Other Reactor Fuels and Materials Development

1. Fast-neutron Irradiation of Jacket Materials

Twelve capsules containing a total of 60 tube-burst specimens and 112 stress-rupture-type specimens are being irradiated in EBR-II as partial loadings in two subassemblies. The neutron flux is to be 2.5 x 10^{15} n/cm^2-sec. During this report period the status of these capsules did not change because the reactor was not operated. The capsules are identified in Table XV.

TABLE XV. Status of Irradiations of Jacketing Materials in EBR-II

Capsule Number	Material	Type of Specimen	No. of Specimens	Loading Date	Tentative Removal Date	Accumulated Exposure (n/cm^2)	Maximum Specimen Temp (°C)
AS-1	V-20Ti	Tube-burst	12	12-65	5-68	3.3 x 10^{21}	540
AS-2	V-20Ti	Tube-burst	12	12-65	5-68	3.3 x 10^{21}	540
AS-3	Hast-X	Tube-burst	12	12-65	5-68	3.3 x 10^{21}	540
AS-4	Hast-X	Tube-burst	12	12-65	5-68	3.3 x 10^{21}	540
AS-5	304 SS	Tube-burst	12	12-65	5-68	3.3 x 10^{21}	540
AS-6	V-20Ti	Stress-rupture	16	12-65	5-68	3.3 x 10^{21}	580
AS-7	Hast-X	Stress-rupture	16	12-65	5-68	3.3 x 10^{21}	580
AS-8	304 SS	Stress-rupture	16	12-65	5-68	3.3 x 10^{21}	580
AS-9	V-20Ti	Stress-rupture	16	11-65	4-68	6.6 x 10^{21}	590
AS-10	Hast-X	Stress-rupture	16	11-65	4-68	6.6 x 10^{21}	590
AS-11	304 SS	Stress-rupture	16	11-65	4-68	6.6 x 10^{21}	590
AS-12	V-20Ti	Stress-rupture	16	11-65	4-68	3.3 x 10^{21}	580

2. Hydrogen Embrittlement in Irradiated Steels

A study is being made of possible hydrogen embrittlement in irradiated steels. Tensile tests and stress-rupture tests of unirradiated steels 4340 and 212 B have been completed.

Type 4340 is a high-strength (19,000 kg cm^{-2} UTS) steel which clearly shows its susceptibility to delayed failure by hydrogen embrittlement in a stress-rupture test at room temperature. Hydrogenated notched tensile specimens of 4340 failed in minutes or a few hours with loads corresponding to one-half to one-third their tensile strength. The hydrogen charge was not high enough to produce blistering of the steel, but was more than sufficient to produce delayed failure.

These tests were used to demonstrate the reproducibility of the electrolytic hydrogen charging, cadmium plating, and baking techniques used to load the specimens with hydrogen. Efforts to measure the amount of hydrogen put in by the charging process by vacuum annealing have been unsuccessful thus far. Many difficulties have been reported in the literature relative to this measurement. The apparatus has provided semi-quantitative information on the rate of outgassing at various temperatures.

This is helpful in explaining behavior of specimens after aging and long periods of time under stress.

Control tests with 212 B pressure-vessel steel revealed that tensile strengths of the specimens agreed with data furnished by the supplier. Unirradiated specimens charged with hydrogen behave just as do uncharged controls in tensile tests. The yield stress is about 4200 kg cm^{-2} for these specimens, or about 60% of the ultimate tensile stress. In stress-rupture tests failure was observed instantly at the ultimate tensile strength (~7000 kg cm^{-2} or 100,000 psi) for notched-bar specimens. A delayed failure took place after a few hours with a load representing 95% of the ultimate tensile stress. No failures were observed at or below 90% of the ultimate.

All preparations have been completed for testing of irradiated specimens (see Progress Report for August 1965, ANL-7090, pp. 39-40). A small hot cell has been equipped with a stress-rupture machine and all the apparatus for charging, plating, and baking the specimens. These operations have been performed in this cell on some of the control specimens.

The irradiated capsule containing the specimens has been opened in a hot cell. The NaK used as a heat transfer bond was successfully cleaned away and the specimens were identified.

Tensile tests of irradiated specimens disclosed that the tensile strength of the 4340 went up about 5% as a result of the irradiation. This result is based on a shaped tensile specimen. The load corresponded to a stress of 20,000 kg cm^{-2} based on initial cross-sectional area. Some reduction of area took place, but has not yet been measured.

The irradiation raised the yield stress of 212 B by almost 70% and the ultimate tensile stress by about 30%. The exposure was calculated to be enough to raise the NDT temperature well above room temperature. Thus, tests for delayed failure of hydrogen-charged specimens will be performed on steel that is considered brittle at room temperature. The effect of hydrogen on this steel will be compared with that observed in the unirradiated steel.

3. Nondestructive Testing

a. Elastic Moduli of High-temperature Materials by Ultrasonics. The elastic constants of four small V-15 w/o Ti-7.5 w/o Cr samples were calculated from ultrasonic data as follows:

Longitudinal wave velocity	$(6.08 \pm 0.04) \times 10^5$ cm/sec
Shear wave velocity	$(2.75 \pm 0.01) \times 10^5$ cm/sec
Density	5.88 g/cm^3
Young's Modulus	$(12.19 \pm 0.09) \times 10^{11}$ dyne/cm^2
Shear Modulus	$(4.45 \pm 0.03) \times 10^{11}$ dyne/cm^2
Poisson's Ratio	0.371 ± 0.002

The samples, which were measured in the as-rolled condition, have now been annealed at four different temperatures and will be remeasured.

Another stainless steel 304 rod has been received from the shops, and measurements at high temperature will be made on it.

b. Ultrasonic Instrument and Transducer Development. Efforts to uncover a suitable backing material for ultrasonic transducer probes that contain ceramic piezoelectric materials have continued.

Additional samples of sintered Type 316 stainless steel (316 SS) and fiber Type 302 stainless steel (302 SS) have been received. The 316 SS samples are fine-particle discs with densities of about 65 and 75% theoretical. The 302 SS samples, as received, were square sheets of Type A fibers with densities of 66, 74, and 93% theoretical. Subsequently, two discs were pressed from each 302 SS sheet. Longitudinal velocity measurements of these samples are in process.

Two sintered nickel discs, 70 and 78% dense, were also received this month. Preliminary measurements of the longitudinal velocities have been made. The 78% dense sample has an acoustic impedance, Z, of about 32×10^6 kg/m^2-sec. Medium attenuation was observed in this sample. These results indicate that sintered porous nickel holds promise as a backing material for ultrasonic probes with ceramic piezoelectric transducers.

The continuous-wave Schlieren system for visualization of ultrasonic vibrations was reassembled this month. Several new or improved components were introduced into the system. The capability of the present system is demonstrated in Fig. 23. The ultrasonic beams are the white areas. The transducer probes are at the top of the pictures.

c. Development of a Neutron-image-intensification System. A second postirradiation annealing study of an irradiated, clad fuel pin was completed. The results of this run were superior to those obtained in the first study in that improvement of image quality was apparent. Analysis of the results is now in progress.

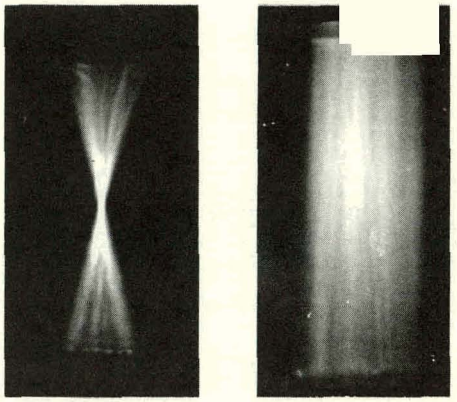

43516 (a) 1X 43517 (b) 1X

Figure 23

Schlieren Photographs of Two Ultrasonic Transducer Probes. (a) ANL 0.4 Mc cylindrically-focused (no lens) lead zirconate-titanate. (b) Automation Industries 5 Mc lead metaniobate.

Even with the improved image quality of this second run, further image sharpness is desired. Attempts to photograph the image directly off the output phosphor screen of the intensifier tube are now being made, and comparisons of such results with television photographs will be made.

d. Thermal Conductivity of Irradiated Fuel as a Function of Burnup and Temperature. The thermal-pulse method of measuring thermal diffusivity and conductivity is being utilized to determine the thermal properties of irradiated fuel pins as a function of burnup. This method will enable the diffusivity and conductivity to be measured in both the axial and radial directions at many points along the fuel pin and, thus, will indicate any anisotropy in the thermal properties as well as any variation of these properties in the axial and radial directions along the length of the fuel pin.

The last half of the irradiated uranium-5 w/o Fs specimens (see Progress Report for November 1965, ANL-7122, p. 54) have been received and transferred into the hot cell. Room-temperature measurements of the thermal diffusivity and thermal conductivity are in progress.

E. Engineering Development

1. Boiling Liquid-metal Technology

a. Niobium-1% Zirconium Loop. The Nb-1% Zr loop has been completely wrapped with a 0.004-in. layer of Nb-1% Zr foil, except for the heavy-walled pump tube. The entire loop, support structure, heater assemblies, and condenser shutters have been assembled and transferred to the proper position in the vacuum chamber facility. Connections are being made to the pressure taps, sodium fill and flowmeter cooling lines, electrical power and thermocouple leads, and the shutter drive. This assembly work and final loop insulation are being carried out in the clean atmosphere provided by the plastic cover and filtered air supply.

The sodium piping system has been heated to 350°F. Eight leaks in the valves, some in the gaskets and some in the valve bodies, were found. This system must be leaktight. Repairs are in progress.

Of approximately 60 thermocouple assemblies received from the vendor, 29 were acceptable, although none meet the original specifications.

Acceptability was determined by radiograph, resistance check, and thermal cycling (see Progress Report for January 1966, ANL-7152, p. 64). A minimum of 36 assemblies is required prior to initial loop operation.

The clean room used for assembly of the loop and support structure will be used for storage and for future assembly of loop components requiring a clean atmosphere (e.g., assembly of high heat flux and transient heaters). Preliminary design of a heater for transient boiling experiments is underway.

b. Heater Experiments

(i) Electron-bombardment Heater Experiment. This experiment is designed to gain experience with electron-bombardment heating and to investigate geometric and mechanical factors involved in the construction of a high heat flux heater. The present design incorporates a sodium pool boiler with a sixteen inch heated length. Although the information obtained from this experiment is being used primarily in the design of a high temperature, high heat flux electron-bombardment heater, basic information pertinent to the pool boiling of sodium from a vertical cylinder may also be gleaned.

Extended operation of the electron-bombardment heater experiment has shown that the 200-kW, high-voltage power supply is not adequate for use with electron-bombardment heating for long time periods at lower power levels. Modifications of the present power supply which will enable operation from 0.5 to 200 kW are now being examined. Also, a filter system is being designed to eliminate a high-voltage arcing problem in the power supply, caused by dust buildup on components located within the power supply.

2. General Heat Transfer

a. Heat Transfer in Double-pipe Heat Exchanger. A paper entitled "Mathematical and Practical Aspects of Heat Transfer in Double-pipe Heat Exchangers," which summarizes nearly all of the work done at ANL under this category of research, has been accepted for presentation at the "Third International Heat Transfer Conference," Chicago, Aug. 8-12, 1966. The paper has been completed and will be published in the conference preprint volumes well in advance of the actual meeting date. The ABSTRACT of the paper is as follows:

A mathematical analysis of heat transfer in double-pipe heat exchangers, based on first principles rather than on the use of heat transfer coefficients, is generalized to include laminar or turbulent flows, various geometrical configurations, and both cocurrent and countercurrent operation. Practical aspects concentrate on accurate predictions of overall

heat transfer rates and include consideration of a quantity called the "Effectiveness Coefficient" for this purpose. Procedures for the interpretation of experimental data, derived from the analysis, are also suggested.

(i) Countercurrent Turbulent Liquid-metal Flow. As part of the continuing study of computational procedures for application of the available formal mathematical solution for predicting heat transfer and temperature distributions in counter-flow heat exchangers, several alternate procedures (e.g., see Progress Report for December 1965, ANL-7132, pp. 43-44) have been reformulated for the plug-flow parallel plane exchanger. The formulation will be used to perform "computer experiments" for comparison of the various procedures on a common basis. The simple case chosen--plug flow in parallel plane ducts--eliminates many complications which, at the present stage, are not important for comparisons of the computational procedures.

Improvements of the existing mercury flow loop have been completed, and a test-section (double-pipe heat exchanger) design has been selected for construction.

F. Chemical Separations

1. Fluidization and Volatility Separations Processes

a. Recovery of Uranium and Plutonium from Low-enrichment Fuels: Laboratory Support Work

(i) Fluorination of UO_2-PuO_2-Fission Product Pellets. Development studies are being performed in a 2-in.-dia fluid-bed reactor to determine the optimum conditions for fluorinating UO_2-PuO_2 pellets containing fission products. Two runs (Pure-15 and Pure-16) were carried out to evaluate the effect of programming the temperature of the fluid bed during recycle-fluorination on the uranium and plutonium retention on the fluid-bed material. In each run a 2-in.-deep fluidized-packed bed of UO_2-PuO_2-fission product pellets (650 g pellets and 1100 g alumina containing 0.6 g CsF) was fluorinated according to the sequence: (1) a two-zone oxidation-fluorination step for 3 hr at 450°C, (2) a once-through fluorination step for 1 hr at 450°C while the fluorine concentration was increased from 10 to 90 v/o, (3) a recycle-fluorination step with 90 v/o fluorine while the bed temperature was increased from 450 to 550°C in increments of 5°C/9 min in run Pure-15 and 5°C/18 min in run Pure-16, and (4) a recycle-fluorination step with 90 v/o fluorine at 550°C to give a total recycle-fluorination time of 8 hr. The concentration of plutonium in the final alumina bed was 0.025 w/o in run Pure-15 and 0.034 w/o in run Pure-16. Since the residual plutonium concentrations in these runs were higher than those achieved in several previous runs employing two-zone

oxidation-fluorination followed by other recycle-fluorination schemes (see Progress Report for December 1965, ANL-7132, p. 45), it appears that increasing the bed temperature from 450 to 550°C in small increments following the two-zone oxidation-fluorination step does not lead to increased plutonium removal from the bed material.

To improve removals of plutonium from beds of alumina containing CsF in runs in which the alumina bed is used only once, a newly developed two-step procedure was employed in two experiments. Preliminary results from these experiments indicate that the concentration of plutonium on the alumina is reduced to a satisfactory level (0.009 w/o) by the two-step procedure. In the experiments, UO_2-PuO_2-fission product pellets were reacted in the following manner in an alumina fluid bed containing cesium fluoride: (1) the pellets were pulverized by oxidation with 20 v/o oxygen for 3 hr at 450°C, and (2) the uranium and plutonium oxides were fluorinated with 10 v/o fluorine for 2.5 hr at 300°C and for 3 hr at 350°C, and the residue was subjected to recycle fluorination with 90 v/o fluorine for 3 hr at 350°C, for 6 hr while the bed temperature was increased from 350 to 550°C in increments of 5°C/9 min, and finally for 3 hr at 550°C. Additional experiments are under way to optimize the conditions for the two-step procedure.

A separate test was performed in the 2-in.-dia fluid-bed reactor with a 2-in.-deep fluidized-packed bed of pellets (0.6 g cesium fluoride added to 1100 g alumina) to demonstrate the use of BrF_5 as a selective fluorinating agent for the conversion of uranium to UF_6. In this process, the pelleted fuel is first pulverized by reaction with oxygen and then fluorinated with BrF_5 to form volatile UF_6 and nonvolatile PuF_4. Plutonium is recovered as PuF_6 in a subsequent step by reaction with fluorine. In this test, the pellet fuel was oxidized for 4 hr with 20 v/o oxygen in nitrogen at 450°C. The uranium was next fluorinated with 11 v/o BrF_5 in nitrogen for 1.8 hr at 300°C. The recycle-fluorination step with fluorine for the volatilization of plutonium was carried out as follows: 1 hr at 300°C while the fluorine concentration was increased from 10 to 90 v/o; 2 hr at 300°C with 90 v/o fluorine in nitrogen, 5 hr with 90 v/o fluorine while the bed temperature was increased from 300 to 550°C in increments of 10°C/12 min, and 2 hr at 550°C with 90 v/o fluorine. The residual plutonium concentration in the final alumina bed was 0.007 w/o after a total of 10 hr of recycle-fluorination. This result is similar to that obtained in a previous test (see Progress Report for January 1966, ANL-7152, pp. 67-68) in which, after a total of 13 hr of recycle-fluorination at temperatures of 300 to 550°C, the final plutonium concentration in the alumina bed was 0.006 w/o. These data indicate that the BrF_5 process can achieve satisfactory residual plutonium levels in the alumina bed in the presence of cesium by the use of a suitable recycle-fluorination scheme.

b. Recovery of Uranium and Plutonium from Low-enrichment Fuels: Engineering Work

(i) Engineering-scale Alpha Facility. Preparations are in progress for the next experiment involving the fluorination of UO_2-PuO_2 pellets to a mixture of UF_6 and PuF_6, and the separation of plutonium from the UF_6-PuF_6 mixture by thermal decomposition of PuF_6 to solid PuF_4 in a fluid-bed reactor.

Chemical analyses of the UF_6-PuF_6 feed stream and of the UF_6 off-gas from the thermal decomposer during the second test (see Progress Report for January 1966, ANL-7152, pp. 68-69) indicate that essentially complete decomposition of PuF_6 occurred in the fluid-bed decomposer. The plutonium concentration in the mixed hexafluoride gas stream decreased from 0.05 w/o in the feed to <0.001 w/o in the off-gas.

(ii) Process Development Studies for Uranium Dioxide Fuels. Studies have continued in a 3-in.-dia fluid-bed reactor to investigate alternative schemes for processing uranium dioxide fuels. Three tests were performed to study (1) the effect of prefluorination temperature on the extent of conversion of the alumina bed material to fluoride, and (2) the effects of operating conditions on the fluorination of large quantities of uranium fines.

When sintered alumina is exposed to fluorine at a given temperature level the concentration of fluoride in the alumina reaches an equilibrium value after about 4 hr. In a test in which sintered alumina was exposed to 67 v/o fluorine at 20, 450, and 550°C (4 hr at each temperature level), the concentrations of fluoride in the alumina bed at the end of each interval were 0.09, 0.06, and 1.2 w/o, respectively.

Two tests were performed to determine satisfactory operating conditions for fluorinating large quantities of uranium oxide fines. At the end of one test, a minor portion of the final bed was found to be caked. Analyses of the data from this run and previous runs involving fluorination of uranium oxide fines suggest that the formation of a cake might result from a combination of high temperature in the fluid bed, low gas velocity in the bed, and low concentrations of fluorine in the off-gas stream. Excess fluorine in the off-gas can be achieved by reducing the fluorine utilization through reduction in the fluorination temperature or through an increase in gas velocity. These conditions were successfully applied in the second run, which involved the fluorination of 2.3 kg of uranium oxide fines in a 2.9-kg alumina fluid bed. The fluorination was carried out at 350°C with 12 v/o fluorine in nitrogen as the fluidizing gas. The superficial gas velocity in the fluid-bed reactor was 1.5 ft/sec. The fluorination was completed in 2.5 hr, during which period the UF_6 production rates averaged 50 lb/(hr)(sq ft). The alumina bed material at the end of the run was free flowing.

2. General Chemistry and Chemical Engineering

a. Preparation of Ceramic Fuels for Fast Reactors. There are two motivations for studying the preparations of ceramic fast reactor fuels. The first is to make well-defined materials for further experimental work; the second is to develop preparation procedures which economically fit into an appropriate fuel cycle. Both objectives may, however, be served by a single research program.

The Chemical Engineering Division at Argonne has carried on for several years a small effort on the synthesis of ceramic fuels, particularly carbides (see Reactor Development Program Progress Reports for February 1964, ANL-6860, p. 80; July 1965, ANL-7082, p. 46; and November 1965, ANL-7122, p. 65). In the past few months the program on the synthesis of carbide fuels has been expanded. The discussion below concerns program planning and presents a summary of the most pertinent experimental results.

The fluidized-bed technique appears to be especially attractive for preparation of carbide fuels because it affords efficient gas-solids contacting and because a powdered product is obtained. Two fluidized-bed processes are being developed for preparing carbides: (1) carburization of hydrided uranium-plutonium alloy with hydrocarbon-hydrogen gas mixtures to form (U,Pu)C, and (2) conversion of $(U,Pu)O_2$ to (U,Pu)C by reaction with carbon or methane. The former problem is requiring the larger effort, whereas the latter is a small effort aimed at developing methods of closing the carbide fuel cycle. The process for reacting uranium-plutonium alloy with methane or propane has been developed to the point where the ultimate success of producing (U,Pu)C by this process appears to be assured, as noted by the experimental progress described below. Considerations of the process steps indicate that the cost of producing (U,Pu)C by this method will be moderate.

The fluidized-bed process to convert $(U,Pu)O_2$ to (U,Pu)C is in the planning and design stage. One source of $(U,Pu)O_2$ for this process would be the product of the fluoride volatility fuel reprocessing cycle. It is contemplated that carbon will be blended with the oxide during conversion of UF_6-PuF_6 to $(U,Pu)O_2$, after which the $(U,Pu)O_2$-carbon mixtures will be converted in a high-temperature (1500 to 1700°C) fluidized bed to the monocarbide. An alternative approach would be to react a methane-hydrogen gas mixture with $(U,Pu)O_2$ particles in a high-temperature fluidized bed. It is believed that formation of carbides, rather than carbon coating of the oxide particles, can be attained by proper selection of the process variables. Either of these oxide-conversion processes is potentially capable of producing dense spherical particles which would be suitable for the vibratory compaction method of fuel densification.

(i) Thermobalance Studies. A detailed discussion of the reaction thermodynamics for formation of UC and (U,Pu)C by reaction of the metal or alloy with hydrocarbon gases was given in ANL-7122, p. 65. Excessive carburization of (U,Pu)C by the reaction

$$2(U,Pu)C + CH_4 \rightleftharpoons (U,Pu)_2C_3 + 2H_2$$

can be prevented by maintaining the CH_4 concentration at less than the equilibrium value for the above reaction. Thermobalance experiments are being conducted in order to determine a more precise value than can be obtained by calculations based on currently available free energy data. A rough indication of the rate of reaction is also obtained in these experiments.

An Ainsworth recording thermobalance installed in a plutonium glovebox has been utilized for these experiments. A length of fine platinum wire, fastened to the balance pan, suspends a platinum dish holding a metallic sample in a quartz furnace tube. The furnace tube is heated by a resistance furnace. The procedure consists of reacting about 3 g of metal with hydrogen in the thermobalance to yield a finely divided hydride and then reacting the hydride with a hydrogen-hydrocarbon mixture. The carburizing gas flow is begun as soon as hydriding is complete in order to prevent sintering as the temperature is raised. The change in weight of the sample is recorded as a function of time.

Runs were carried out in which uranium-20 w/o plutonium alloy samples were reacted with propane-hydrogen or methane-hydrogen gas mixtures at 650 to 750°C. (At thermodynamic equilibrium, it is immaterial, for a given C:H ratio for the gas phase, whether propane or methane is used.) The operating conditions and the composition of the products resulting from a number of these runs are shown in Table XVI.

TABLE XVI. Thermobalance Experiments on Preparation of Uranium-Plutonium Carbide by the Metal-Hydrocarbon Reaction

Conditions: Approximately 3 g of U-20 w/o Pu alloy hydrided and then reacted with hydrocarbon-hydrogen mixtures at the temperatures indicated below; a gas flow rate of 1.4 to 3.1 liters/min; 1 atm pressure

Reaction Conditions					Product Compositions		
		Reaction Time (min)			X-ray Analysis		(w/o)
Temp (°C)	Reagent Gas[a]	To Completion[b]	Total	Weight Gain (% of Theory)[c]	Major	Minor	Carbon[d]
670	1.6 v/o C_3H_8	200	200	105	XC[e]	-	4.72
700	3.2 v/o C_3H_8	120	120	91	XC	-	4.80
700	4.2 v/o C_3H_8	100	100	-	XC	-	4.62
750	1.0 v/o C_3H_8	125	270	113	XC	X_2C_3	4.69
750	1.5 v/o C_3H_8	52[f]	90	98	XC	-	4.07
750	1.5 v/o C_3H_8	210	400	107	XC	X_2C_3	4.88
750	1.5 v/o C_3H_8	-	215	102	XC	X_2C_3, XO_2	4.26
750	1.0 v/o CH_4	180	370	108	XC	X_2C_3, XO_2	4.17
750	2.0 v/o CH_4	85	290	114	XC	X_2C_3	5.04

[a] The balance is hydrogen.
[b] Estimated time for completion of reaction measured from the time temperature reached 500°C until the rate of change of weight became very low.
[c] Based on formation of pure (U,Pu)C.
[d] Carbon content of stoichiometric (U,Pu)C is 4.80 w/o.
[e] Face-centered cubic structure with lattice parameter of about 4.96 Å, a value which is within the range that might be expected for a uranium-plutonium monocarbide solid solution.
[f] A second hydriding was performed, thereby reducing the particle size and resulting in a faster carbiding rate.

The differences in reaction rates as a result of variation of temperature and gas composition were not large as compared with those produced by random variations in the reactivity of the hydrided alloy. However, increasing the hydrocarbon concentration did appear to increase the reaction rate slightly. Most of the runs were conducted with a gas composition which would be expected to be in equilibrium with carbon or the sesquicarbide. However, only small amounts of sesquicarbide formed in runs that were continued for several hours beyond the completion of the formation of the monocarbide (as indicated by weight gain of the sample). The low rate of formation of the sesquicarbide is attributed to a low rate of diffusion of carbon through UC_2.

It is noted that the sesquicarbide did form (although in small amounts, as observed above) even at the lowest hydrocarbon concentration (1 v/o methane) when the experiments were continued appreciably beyond the time that the reaction to form UC was completed. This indicates that a methane concentration of 1 v/o is too high for equilibrium of the gas with the monocarbide.

In a recent experiment carried out at 770°C, carbiding was initiated with a hydrogen-0.9 v/o methane gas mixture. The reaction proceeded as usual to the stoichiometric weight gain and beyond, indicating that at these conditions $(U,Pu)_2C_3$ was the equilibrium phase. However, when the methane concentration was lowered to 0.75 v/o, the weight stabilized at the value representing (U,Pu)C. This result indicated that $(U,Pu)_2C_3$ and (U,Pu)C were in equilibrium at 0.75 v/o The free energy change for the reaction

$$C + 2(U, 20\,w/o\,Pu)C \rightleftharpoons (U, 20\,w/o\,Pu)_2C_3$$

was calculated to be -4.4 kcal/mole of $(U, 20\,w/o\,Pu)_2C_3$. Further experiments of this type are planned in order to determine the equilibrium gas phase composition at various temperatures and plutonium concentrations and with reactant gases containing lower concentrations of impurities than has been possible with the existing equipment.

These thermobalance experiments indicate that, at a temperature of 770°C and a pressure of 1 atm, the methane concentration must be 0.75 v/o or less in order to prevent formation of higher carbides. It is expected on the basis of thermodynamic considerations that, by raising the total pressure to 10 atm, the partial pressure of methane could be increased almost 100-fold (from 0.0075 to about 0.7 atm) without formation of the sesquicarbide. This is a satisfactorily high value for the fluidized-bed process in which the gas flow rate is limited by the free-fall velocity of the finer particles.

(ii) Fluidized-bed Studies. The experimental program for the preparation of UC and (U,Pu)C by the fluidized-bed technique is directed toward exploring the operating conditions which appear most likely to yield stoichiometric monocarbides at high production rates. These conditions are: temperature, 700 to 900°C; pressure, 5 to 10 atm; and fluidizing gas, 2 to 10 v/o methane in hydrogen. The six fluidized-bed reactors for this program are in various stages of development from conceptual design to near the termination of operation, as shown in Table XIX. Because of the additional complications in operating experimental equipment with plutonium, experiments for testing equipment design and operational concepts for carbide fuel production will first consist of preparing UC, since these experiments can be carried out in an open hood. This is the reason for the extensive preparations for synthesis of UC.

Installation of a $2\frac{1}{2}$-in.-dia reactor (designated "Semiworks Reactor" in Table XXII) which can be used with the above ranges of conditions for preparation of UC on a 2-kg scale has been completed, and the reactor is now undergoing "shakedown" runs. This reactor, constructed of Type 304 stainless steel, has a jacketed heating section which is pressurized with argon in order to balance the internal pressure and thus minimize the stress on the heated wall. The off-gas from the reactor will be discarded in initial tests but, at a later date, equipment to recirculate the gas will be installed. A similar reactor (designated "Production Reactor" in Table XVII) is being designed for preparation of (U,Pu)C.

TABLE XVII. Status of Fluidized-bed Reactors

Reactor	Feed Material	Product	Capabilities: Capacity (kg/batch)	Capabilities: Temp (°C)	Capabilities: Pressure (atm)	Purpose, Status
UC Preparation						
Small-scale Reactor	U	UC	0.3	750	3	To demonstrate process and test gas compositions; experiments to be discontinued soon.
Semiworks Reactor	U	UC	2	900	10	To test process and designs concepts; "shakedown" runs in progress.
Oxide Converter	UO_2	UC	1	2000	10	To demonstrate process for various methods of carbon addition; design is under way.
(U,Pu)C Preparation						
Demonstration Reactor	U-Pu	(U,Pu)C	0.8	800	5	To demonstrate process by producing high-purity (U,Pu)C; "shakedown" runs beginning.
Production Reactor	U-Pu	(U,Pu)C	2	900	10	To demonstrate process on semiworks scale and produce (U,Pu)C for irradiation and fabrication studies; design is under way.
Advanced Fuel Preparation						
UN Reactor	U	UN, U(C,N), etc.	0.3	1000	1	To demonstrate preparation of UN and of UC-containing additives; "shakedown" runs under way (under low priority).

The reactors for producing UC are to be operated within an air-atmosphere hood, as noted above, with only normal industrial precautions required. (The exception is the small-scale reactor, which has been operated in a helium-atmosphere glovebox.) However, these reactors

must be unloaded in a high-purity inert atmosphere. In the case of the semiworks reactor, the product is pneumatically conveyed to a container which is transferred to a glovebox for unloading.

The reactors for producing (U,Pu)C are designed to be operated in gloveboxes which contain a high-purity helium atmosphere, in order to minimize oxidation of the product during unloading. Two interconnected gloveboxes containing 250 cu ft of helium are now being used for this process. The atmosphere in these boxes is maintained at a low impurity level (as low as 3 ppm water and 5 ppm oxygen in recent tests) by a purification system which utilizes an activated charcoal trap cooled by liquid nitrogen.

During this period of equipment construction, UC has been synthesized in a $1\frac{1}{2}$-in.-dia fluidized-bed reactor (designated "Small-scale Reactor" in Table XVII) which is capable of operation at near-atmospheric pressure and at temperatures up to 750°C. The purpose of these experiments was to demonstrate that a stoichiometric monocarbide of low oxygen content could be obtained by the fluidized-bed technique. In these experiments, 100 to 200 g of uranium rods were hydrided at 250°C to form fine UH_3 powder suitable for fluidization. This powder was dehydrided and converted to UC by heating at 600 to 750°C while fluidizing with a propane-hydrogen gas mixture. The temperature was maintained at the final level for 5 to 20 hr to complete the reaction. Near-stoichiometric UC with an oxygen content as low as 0.08 w/o was produced in recent experiments. Results from some of these runs are shown in Table XVIII.

TABLE XVIII. Uranium Monocarbide Experiments in a Fluidized Bed

(200-g scale; run duration, 10 hr)

Temperature (°C)	Propane in Fluidizing Gas[a] (v/o)	Product Composition				
		Carbon		Oxygen		Uranium[b]
		a/o	w/o	a/o	w/o	a/o
600	3	47.2	4.5	2.5	0.32	50.3
700	1.5	48.6	4.6	0.8	0.10	50.6
700	9	56.5[c]	6.2[c]	0.5	0.08	43.0

[a]The balance is hydrogen. The following C_3H_8 concentrations in hydrogen were calculated for C:H ratios equivalent to the equilibrium gas compositions in the systems CH_4-H_2-UC-UC_2 and CH_4-H_2-UC_2-C:

Temperature (°C)	C_3H_8 Concentration (v/o)	
	UC-UC_2	UC_2-C
600	5.5	8.6
700	2.0	3.6

[b]Calculated by difference.

[c]Carbon deposition on the reactor walls indicated that the product for this run probably had a high free-carbon content, as expected (see footnote a).

The carbon contents of the products from the first two runs in the table were very close to the stoichiometric value of 50 a/o (4.8 w/o) carbon. These runs were conducted under carburizing conditions which would be expected to yield the monocarbide (see footnote a in Table XVIII). The third run produced hyperstoichiometric carbide, as was to be expected because of the high propane concentration.

Work is also in progress to develop techniques for pressing and sintering (U,Pu)C in order to obtain kilogram quantities of pellets for irradiation and chemistry studies of the fuel. This work is being carried out in a facility closely associated with the fluidized-bed unit to avoid exposure of the fluidized-bed product to air in transfers from preparation equipment to pressing and sintering equipment. An automatic press has been purchased for installation in an inert-atmosphere glovebox for these studies. Two sintering furnace, one loaded from the bottom of a glovebox in the two-glovebox system described above, are now operable.

In summary, it is believed that UC or (U,Pu)C powder of low oxygen content and near-stoichiometric carbon content can be routinely prepared by the fluidized-bed process when equipment currently being designed has been completed. Such powder would be suitable for pressing and sintering into fuel pellets without need for an intermediate grinding step.

G. Plutonium Recycle Program (EBWR)

1. Theoretical Calculations

The unpoisoned plutonium zone in the EBWR with control and safety rods removed had been found experimentally to have a multiplication constant of 1.001 when loaded with 22 assemblies. A four-group, two-dimensional diffusion-theory calculation, by means of the CANDID-2D code, made for this configuration yielded a multiplication constant 1.008. Microscopic cross sections for the three fast groups were obtained by use of the GAM code and for the thermal group by use of the Argonne Revised THERMØS code, which permitted successive spectrum-weighted homogenizations of the complicated EBWR cells. In this calculation the control-rod followers were assumed to be made of Zircaloy; actually, the lower 15 in. of the followers are stainless steel. Calculations will be made to estimate the reactivity effect due to the stainless steel.

III. ADVANCED SYSTEMS RESEARCH AND DEVELOPMENT

A. Argonne Advanced Research Reactor (AARR)

1. Reactor Physics Experiments

Measurements summarized in this report period include earlier experiments with the 810 fuel foils and 810 boron-stainless steel poison strips reactor core loading (~41.4 kg U^{235}/425 g B), and experiments with the present full core loading of 1215 standard fuel foils (~62.1 kg U^{235}) and 1620 B-SS poison strips (~850 g B).

The experiments with the former (810/810) loading included:

(a) effects of beam-tube interaction on neutron-beam intensity;

(b) vertical traverses of U^{235}-fission activity, at various distances from partially inserted in-core control blades;

(c) azimuthal traverses of U^{235}-fission activity near control-blade followers;

(d) a study of the feasibility of using a (modified) peripheral control blade for automatic regulation of reactor power.

The experiments with the newer (1215/1620) loading included:

(a) available excess reactivity;

(b) reactivity-control capacities of the control blades;

(c) reactivity coefficient of voids in the Internal Thermal Column (ITC).

Working with two square aluminum-walled through-tubes (4 in. x 4 in. OD; 1/8-in. wall thickness), beam-tube interaction was measured for two different radial locations of the tubes and for two different thicknesses of beryllium between the tubes. In each case, the two tubes were placed one above the other, with the longitudinal axes coplanar. Whether the tubes were placed against an outer face of the reactor core, or placed with 2 in. of beryllium between the tubes and the core, a 4-in. beryllium thickness between the tubes provided essentially complete separation. With 2 in. of beryllium between the beam tubes and the core, and only 2 in. of beryllium between the tubes, the intensity of the collimated neutron beam in one voided tube was reduced by approximately 16% when the beryllium filler was withdrawn from the other through-tube. It must be expected that with much larger voids in the beryllium, representing beam tubes and their environment, interaction effects of beam tubes will be much larger when beam tubes are in close proximity.

The results of vertical traverses and azimuthal traverses of U^{235}-fission activity near control channels in the 810/810 system indicated that for in-core blades the control blade absorber depressed the power as far as halfway through an adjacent fuel assembly. Similarly, in the vicinity of control-blade followers, there was substantial power peaking. The peaking dropped off roughly exponentially with distance from the follower, but persisted until the middle of the adjacent fuel assembly. With a 0.2-in.-thick aluminum blade follower, the percentage increase in power at the control channel was approximately twice as large as for a SS follower of the same thickness. These measurements will be repeated in the 1215-fuel-foil loading, which is much closer to the reference design AARR.

Activation mappings (U^{235} fission) in the 810/810 system indicated that there would be no pronounced power tilt in the core if a peripheral control blade were used as a regulating blade. However, there is a substantial reduction in the level of thermal-neutron flux in the beryllium nearby, even as far as 3 to 5 in. The present choice of a regulating blade is between a single in-core-blade position and a single peripheral-blade position. Before making a choice, additional measurements will be made, this time in a loading more closely approximating the reference design system, both for an in-core blade and for a peripheral blade.

With the three tubes in the beryllium reflector filled with beryllium, the measured available excess reactivity of the 1215/1620 system was 2.2%. The aluminum walls of the beam tubes caused a reactivity loss of 0.3%. The inferred net reactivity of the system with a clean reflector therefore is $2\frac{1}{2}$%, in comparison with a computed value of ~$4\frac{1}{2}$%.

The reactivity-control capacities of control blades are smaller in the 1215/1620 system than in earlier, lighter core loadings of fuel and poison. The measured worths of control blades are reported in Table XIX, as positive values. For convenience, a summary is given in Table I of control-blade worths in all 4 core loadings so far studied. The worth of control-blade No. 3 in the 1215/1620 system appears to be unreasonably low, and it will be remeasured.

TABLE XIX. Reactivity Worths (%) of Hafnium Control Blades with Aluminum Followers

Control-blade Type[a]	Blade No.	Reactivity Worth (%)			
		315 Core	615/420 Core	810/810 Core	1215/1620 Core
A	1	-	-	1.3	1.15
A*	3	-	-	-	1.00
B	2 or 4	-	1.52	1.43 ± 0.01	1.15
B*	6	-	-	-	1.22
C	7, 9, or 11	-	-	1.30 ± 0.05	1.01 ± 0.01
C*	7	-	-	-	1.04
D	8, 10, or 12	1.8 ± 0.1	1.66	1.43 ± 0.01	1.12 ± 0.01
D*	10	-	-	-	0.93

[a]A- and B-type control blades are peripheral blades. They are $7\frac{1}{2}$ in. wide and 0.20 in. thick, except those marked with asterisks, which are 0.15 in. thick because of removal of 0.05 in. of stainless steel shim plate. Orientation distinguishes A from B. C- and D-type blades are 6-in. wide, in-core blades.

For distributed void in the ITC, and small percentages of void, the positive reactivity coefficient of ITC void with the 1215/1620 loading is 0.04%/% void. This is only ~0.9 as much as the coefficient in the 615/420 and 810/810 systems. The corresponding computed coefficient is ~0.03%/% void.

In the preceding Monthly Progress Report (January 1966) ANL-7152, p. 73, it was reported that the reactivity of the system was decreased slightly when the SS follower replaced the zirconia-SS portion of specimen S3 in the in-core position. This is an error as the sign of this reactivity change should be positive, not negative.

2. Theoretical Reactor Physics

A computational study has been made of the reactor physics characteristics of the Internal Thermal Column (ITC) in the preliminary physics reference design system. In this system, the inner radius of the fuel zone is 6.8 cm. The study surveyed reactivity effects and flux-depression effects of volumes of aluminum as a diluent for irradiation samples, and also of the additional neutron poison in purely absorbing samples in the ITC. To evaluate the relative merits of reducing the radial dimension of the ITC, a comparison study was made for a 5.8-cm-radius ITC. In the latter case, the fuel zone was thickened simply by increasing the thickness of the ungraded-fuel zone by 1 cm. The graded fuel zones were kept at the same thicknesses in both studies.

For an ITC containing only full-density H_2O (no aluminum and no samples), the total thermal-neutron flux at the center of the ITC is only a few percent smaller for the smaller ITC than for the 6.8-cm-radius ITC. In more detail, the peak group-15 neutron flux (0.1-0.4 eV) is 10% larger in the smaller ITC; the peak group-16 flux (0-0.1 eV) is 5% smaller. In the 5.8-cm-radius ITC, the ratio of computed peak neutron fluxes is

$$\phi_{16}^{(0)}/\phi_{15}^{(0)} \simeq 4.0.$$

A more realistic case is one in which the ITC is loaded with samples. If 25% of the entire "active" ITC volume (within the axial bounds of the active core zone) is filled with aluminum, for the 6.8-cm-radius ITC the computed group-16 peak flux is 25% smaller than for the case of 100% water in the ITC. The peak group-15 flux is reduced by only a few percent. The addition of poisoning equivalent to 1 g natural boron in this ITC volume causes a further reduction of ~12% of the original total thermal-neutron flux (groups Nos. 15 and 16), mostly in group No. 16. This additional neutron poisoning has the absorption equivalent of twice that of the aluminum added, or approximately 40 cm^2 of neutron poison in the "active" ITC, in group No. 16. The computed reactivity effect of 1 g boron in the ITC is ~-0.3%.

The same total aluminum volume in the 5.8-cm-radius ITC would occupy roughly 35% of the smaller ITC. If pure aluminum occupied 25% of the active volume of the smaller ITC, the peak total thermal-neutron flux per unit power would be approximately 10% lower than in the larger ITC with the same percentage of aluminum. Increasing the pure aluminum content to 40% in the smaller ITC would reduce this peak thermal-neutron flux by 25%, relative to the peak ITC flux for the case of 25% aluminum in the ITC. Poisoning by capturing samples would lower the peak flux still further.

In summary, a comparison can be made of the ratio, R, of the computed peak total thermal-neutron flux, per unit reactor power, in the ITC's, with the assumptions that: (a) the same total volume of aluminum is introduced; and (b) the total (sample) poisoning is equivalent to 1 g natural boron:

$$R \equiv \frac{\text{Peak thermal neutron flux: 6.8-cm-radius ITC}}{\text{Peak thermal neutron flux: 5.8-cm-radius ITC}} \simeq 1.3.$$

For the ITC's filled with H_2O (no aluminum and no samples) this ratio is ~1.0.

There are certain advantages to working with the smaller ITC. One important benefit is that the increase in core size plus the decrease in ITC size gives a net reactivity gain of ~2.1%. A second advantage of the smaller ITC is a computed reduction in the maximum positive reactivity effect of voiding in the ITC.

At this writing, it appears that if the reduction in peak thermal-neutron flux can be tolerated in the smaller ITC, there are some marked advantages to reducing the ITC radius. As a cautionary note, if the AARR were to be used more nearly as a production facility during a particular core cycle, there would be substantially less ITC volume for loading of samples.

3. Core Structure

Preliminary stress studies of the AARR core support grid have been completed. Results indicate that a stainless steel grid will not be required and that a much less expensive aluminum alloy grid can be used. Since the reactor will be refueled by means of insertion and removal of a complete core package several times a year, the use of a substantially less expensive core support grid is considered to be quite important. Also, the problem of gamma heating in the grid structure is reduced if aluminum is used instead of stainless steel.

Tests were conducted with an actual core support grid made from aluminum (aluminum was chosen for these tests because a test section machined from aluminum cost 1/3 to 1/2 that of stainless steel) in the apparatus

shown in Fig. 24. Hydraulic jacks were used to load each dummy fuel end fitting. Two independent pumps and manifold arrangements were required to handle the two different sizes of end fittings and their respective net load contribution to the core support grid.

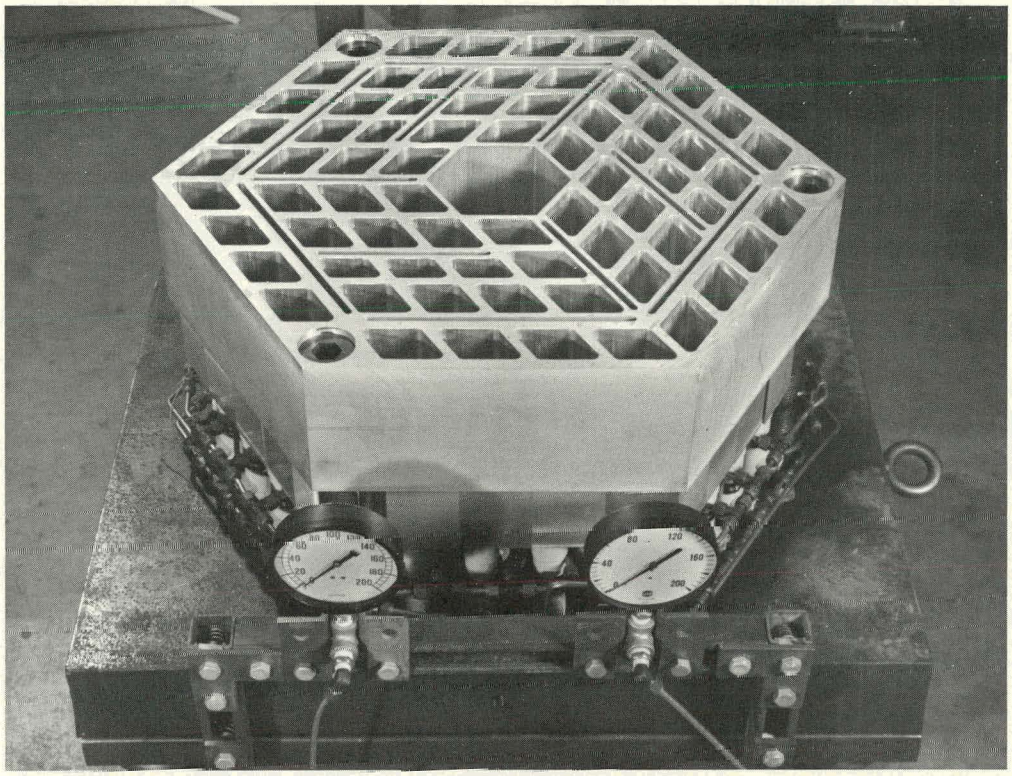

Fig. 24. AARR Grid-plate Stress-analysis Facility. Full-size aluminum grid plate in test position.

In the initial tests the deflection of the structure was determined by use of a reduction in pressure loading proportional to the difference of the modulus of elasticity between SS-347 and Cast Aluminum 6061. In the fully loaded condition (i.e., equivalent to a 125-psi pressure drop across the SS-347 grid and fuel) the maximum deflection occurred in the edge of the central hexagonal hole of the ITC. Maximum deflection at the equivalent full load was approximately 0.010 in., slightly more than the 0.006-0.008-in. deflection desired to maintain alignment of fuel and structures attached to the plate.

Photo-stress analysis was used to determine the areas of maximum stress, which were found to occur at the three junctions of the two outer control-rod slots and the inner control-rod slots remote from the three hold-down bolts (i.e., there are six such junctions--three are adjacent to the bolts, three are remote from the bolts). Detailed analysis of these areas by photo-stress techniques showed the stresses at these points, though greater than at any other place on the plate, were sufficiently low so as to be difficult to measure.

An attempt was made to measure the magnitudes of the stresses. By means of strain gauges, the maximum stress encountered in the surface of the core support plate under the full pressure load appeared to be less than 3800 psi.

The results of this series of tests leads to a proposal that a second aluminum core support grid, is with a web-section depth of ~10 instead of the present 6 in., be used. It is expected that the tests with this second aluminum grid will demonstrate that the deflections and stresses are sufficiently low so as to obviate the need for stainless steel.

4. Fuel and Materials Development

a. Fuel-element Test Materials. A sandwich-type fuel-element structure of depleted UO_2 dispersed in a stainless steel "picture frame" was tested. The core of the element is 37 w/o UO_2 dispersed in Type 304-B stainless steel, and was fabricated by a pressing and sintering process. The facings of low-cobalt-type 347 stainless steel were hot rolled onto the core.

The fuel element was machined into test specimens oriented longitudinal and transverse to the direction of rolling (the long dimension of the fuel element). Three types of tests were conducted with these specimens to determine the mechanical properties of the sandwich material.

In order to use sandwich analysis to determine core properties of this material, an accurate facing thickness value is needed. Photos of the microstructure of the sandwich were taken at various levels of magnification. In all cases there was no visible difference in the stainless structure from the edge to the center of the sandwich. UO_2 particles were dispersed throughout the center. With the UO_2 particles along the edge as a guide (the facings are void of UO_2), an estimate of the thickness of the facings was made. It appears that the facings are each 6 mils wide. Due to the uncertainty of this value, the uncertainty of the stainless microstructure, consistency, and the use of the material as a sandwich rather than just the core, the effective mechanical properties of the sandwich as a unit were reported instead of those of the core alone.

b. Type of Testing and Results

(i) Tensile Tests. The specimens were loaded in an Instron tensile testing machine, and curves of tensile load versus strain obtained. These curves were not linear for strain levels above 700 μin./in., as expected of stainless steel.

The data were very consistent from specimen to specimen, varying by less than 4%. Young's modulus for the longitudinally oriented

specimens was 21.5 x 10^6 psi, and for the transversely oriented specimens 23.5 x 10^6 psi. For most calculations of strengths of materials, such a difference in modulus in two directions is not great enough to justify treatment of the material as anisotropic.

Solid stainless steel specimens (cut from the picture frame) had a modulus of approximately 28 x 10^6 psi. With this value for the facing material, assumed to be 6 mils thick (see Section III.A.4.a), Young's modulus of the core was calculated. For the transverse specimens, the core modulus was 21.4 x 10^6 psi and for the longitudinal was 18.5 x 10^6 psi. Since the facing thickness is only an estimate, the modulus values can only be considered to be order-of-magnitude numbers and should not be used for calculations of core strength.

The ratio of strain in the direction of loading to strain in the transverse direction as measured by strain gauges is an approximation of Poisson's ratio for the material. Considerable scatter was evident in the data for this ratio, but no difference could be determined between the transverse and longitudinal directions of the original element. A value of 0.25 is a reasonable average value of Poisson's ratio for the material.

(ii) Bending Tests. The specimens were loaded as simply supported beams in such a manner as to produce constant strain in the center span. Deflection and strain were measured and plotted versus load applied. Values of the deflection were 22.9 x 10^6 psi for the longitudinal specimens and 26.2 x 10^6 psi for the tangential specimens. The strain-gauge data yielded values of 22.8 x 10^6 longitudinal and 24.4 x 10^6 psi tangential for the Young's modulus of the material in bending.

(iii) Dynamic Testing. Dynamic tests of two types were conducted. The first tests consisted of mounting the beams as cantilevers and exciting them so that the natural resonance frequency could be determined. By means of the relation between natural frequency and Young's modulus, values of moduli were calculated. Young's modulus of the longitudinally oriented specimens was 22.2 x 10^6 psi and for the tangentially oriented specimens 25.5 x 10^6 psi. The damping factor, calculated from the ratio of the strain amplitude, was approximately 0.006.

The second tests consisted of attaching a large cylindrical mass to the cantilever and twisting the released mass, allowing the system to respond as a torsional pendulum. From the natural frequency of the system, the shear modulus was calculated. The longitudinally oriented specimens had a shear modulus of 9.4 x 10^6 psi and those transversely oriented 9.8 x 10^6 psi. Because of the complex behavior of a rectangular cross section subjected to torsion, such shear-modulus values may not be appropriate for other types of loading. However, the data were consistent (deviating from test to test by $<2\%$).

c. Conclusions. For calculations of bending strength and critical flow velocity the usual sandwich analysis assumptions must be modified. The normal assumptions are that the facings act as plates bending about a neutral axis through the centroid of the entire section and the core has no bending strength. Obviously the core has bending strength, since the approximate Young's modulus of the core was of the order of 10^6 psi.

Further, the relations are normally modified to allow for reduction of the resultant values since the core is not infinitely rigid in shear. This shear action in the core allows deformation about some other neutral axis than the one through the centroid. With a Young's modulus of the order of 10^6 psi, the additional term allowing for this deflection due to shear has a very small value. In fact, a magnitude of 10^3 psi is required to allow this term to have any significance in the geometrical arrangement under investigation. Certainly deviations in the facing thickness assumed could not reduce the calculated core modulus by a factor of 10^3.

A more appropriate assumption for fuel-element calculations would be that the sandwich material behaves as solid stainless steel strip with a modulus of elasticity of 21.5×10^6 or 26.2×10^6 psi, whichever produces the most conservative result for the analysis being performed.

It should be further noted that the ratio of the modulus in the transverse direction to that in the longitudinal direction (1.14) is not enough to justify the assumption of anistropy for this material in any but the most exact analysis. Therefore the sandwich material can be assumed to be isotropic with a Poisson's ratio of 0.25.

5. Reactor Vessel

a. Design. A preliminary draft of the technical specifications for the procurement of the AARR vessel was completed. Preliminary drawings of the vessel elevation, top head, and belt-line penetrations have also been completed to illustrate the design described in the draft specifications.

Since the coolant-outlet nozzle is located below the core, the current vessel design incorporates an internal thermal shield which serves as an overflow weir to prevent the drainage of the vessel in the event of a rupture in the discharge line. The vessel internals and support are arranged so that coolant flows down through the core and reflector, then upward between the thermal shield and reflector shroud, and finally downward to the exit nozzle via the annulus formed by the thermal shield and vessel wall. A horizontal divider plate above the core and thermal shield separates the vessel into two interconnected chambers (via the core passages).

This modification of earlier designs permits raising the inside surface temperature of the belt-line section to the coolant exit temperature, or sufficiently above the nil ductility temperatures within the vessel wall.

The vessel is supported from the lower section to permit access to the beam-tube connections. With the vessel supports well below the core support structure, the problem of radiation hardening of the steel is eliminated. Upper vessel guide members are incorporated to permit axial expansion while limiting radial displacements.

b. Pressure Pulse. The ultimate strength of the AARR pressure vessel when subjected to pressure pulses has been investigated under slowly applied internal pressure and sudden applied shock loading. In both cases, the shell was assumed to act as an ideal membrane in which the elastic strains and the bending strength are neglected, and the shell material was assumed to be a rigid, strain-hardening, plastic solid. Due to the presence of nozzles at the midsection of the vessel, the maximum permissible strain ϵ is restricted to one-third of the ultimate strain ϵ_u to ensure no premature rupture occurring at nozzles and welds. This restriction is believed to be conservative since test results[10] show that all vessels with multiple nozzles are capable of deforming without rupture to strains greater than $1/3\ \epsilon_u$.

In the quasi-static analysis, it is further assumed that the profile of the deformed shell is a circular arc.[11] The strain rates ϵ for such a loading are usually low and moderate. The stress is, therefore, only a function of strain. According to the deformation theory,[11] the maximum allowable internal pressure that the AARR vessel is capable of containing is 6,000 psig.

The spectrum of the accidental nuclear excursion is quite large in both peak flux and total energy released. Furthermore, accidents can occur under a variety of conditions, especially in the case of coolant loss. Hence, for the purpose of the dynamic analysis, it was postulated: (1) that the nuclear excursion will occur under the most adverse conditions, (2) that the energy flux of the excursion is comparable to that of TNT detonation, and (3) that the vessel is completely filled with coolant. Under these conditions the shock loading is so rapid that the stress becomes a function of both the strain ϵ and the strain rate $\dot{\epsilon}$. Based on the proposed TNT Containment Law,[10] it is estimated that the maximum charge weight of TNT that the vessel is capable of containing is about 110 lb. For this charge

---

[10] Wise, W. R., Jr., and Proctor, J. F., Explosion Containment Laws In Nuclear Reactor Vessels, NOLTR 63-140, U. S. Naval Ordnance Laboratory (Aug 1965).

[11] Weil, N. A. and Salmon, M. A., Studies of Reactor Containment Structures, Report ARF-8262, Armour Research Foundation (1964).

the corresponding maximum peak pressure of the shock wave is approximately 27,600 psig. The investigation showed that although the vessel wall will deform plastically and the excessive deformation may render the vessel inoperable, a catastrophic failure will not occur.

6. Experimental Facilities

The detail design for the fabrication of the beam-tube prototypes for test has been completed. The blind beam-tube assembly and the through-tube assembly are shown in Fig. 25. Basically, the design is similar to an earlier version (see Progress Report for July 1964, ANL-6923).

The blind beam tube comprises six major subassemblies: (1) an aluminum blind beam tube, (2) a stainless steel beam-tube adapter, (3) a stainless steel biological-shield-alignment liner, (4) a collimator adapter, (5) the bolt-breach connectors, and (6) a pool (bellows) seal. The subassemblies perform the following major functions within the integrated assembly:

a. The beam tube penetrates the reactor vessel and furnishes a collimated beam of high-intensity neutrons from the core to the experimental face. The beam tubes are designed to be replaceable. Environmental conditions within the vessel require that the tubes be designed to withstand (1) a collapsing pressure of 800 psig, (2) thermal stresses created by gamma heating, and (3) irradiation damage from sustained exposure.

b. The stainless steel beam-tube adapter serves as a transition piece between the reactor nozzle and beam tube. In addition, it extends from the vessel nozzle to the experimental face and forms a support housing for internal shielding. The adapter after installation will be semipermanent, and removal is not intended unless damage to sealing surfaces occurs. Installation of the beam tube is accomplished by connection to the adapter rather than to the nozzle. This is done to reduce the possibility of damage to the vessel nozzle. A damaged seat on the beam tube adapter is easily remedied by replacement of the adapter.

c. The biological-shield-alignment liner is designed to compensate for installation misalignment between the vessel and biological shield liner.

d. The collimator adapter provides a connection for the installation of the experimenter's collimator.

e. The bolt-breech connectors are designed to facilitate rapid remote assembly or disassembly of the beam-tube components.

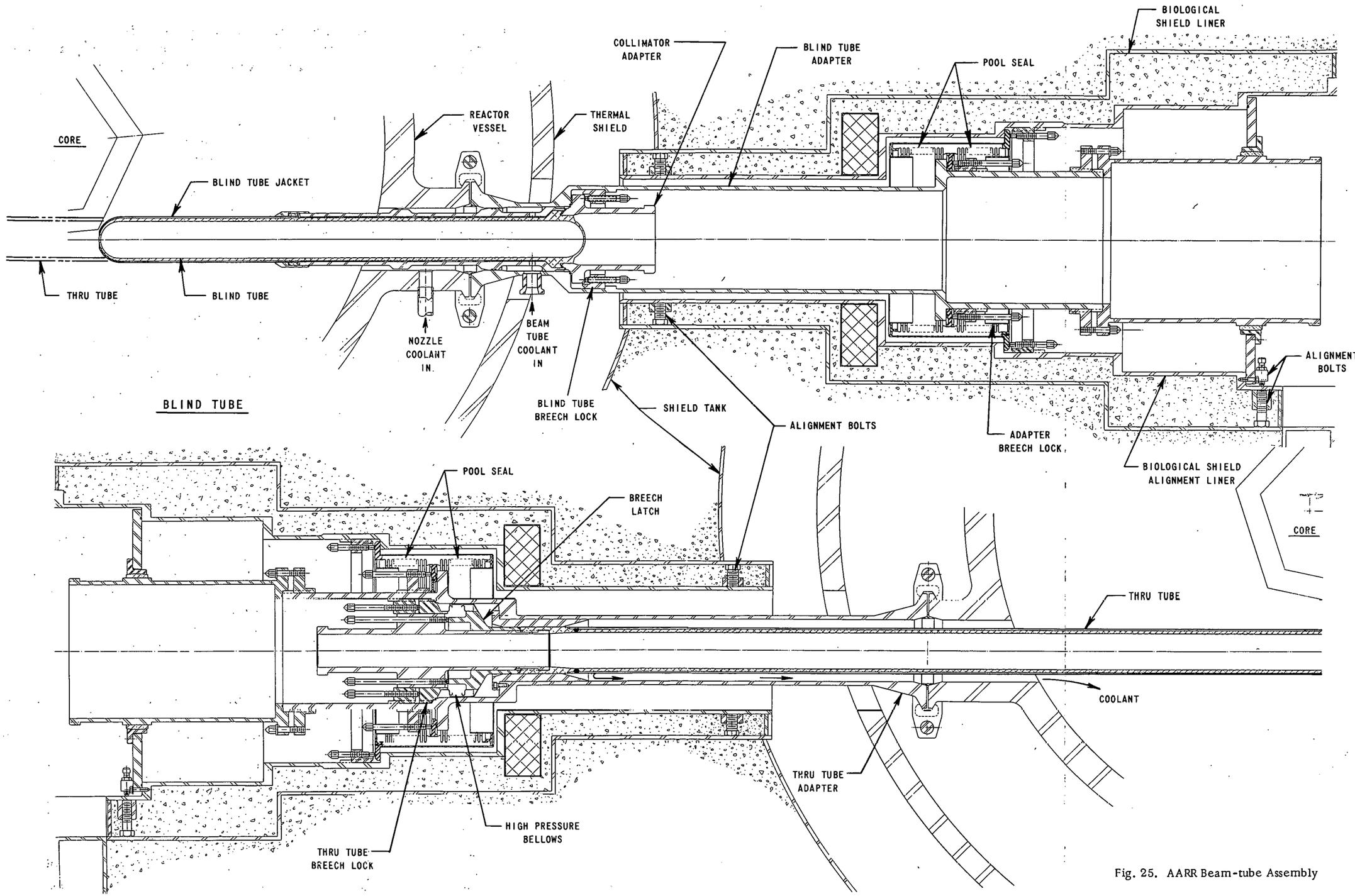

Fig. 25. AARR Beam-tube Assembly

f. The pool (bellows) seal, in addition to forming a barrier for the reactor pool water, compensates for thermal expansion and for vertical and lateral movement between the reactor vessel and biological-shield-alignment liner.

The design of one end of the through-beam-tube assembly is similar to the blind beam tube. However, the opposite end is modified to provide a connector for securing and sealing the end of the through-beam tube which has been inserted through the vessel. The connector features a high-pressure bellows seal which also allows for axial thermal expansion of the through-beam tube. To prevent catastrophic leakage in the event of a rupture in the high-pressure bellows, a split-ring seal is incorporated as a backup.

Briefly, the blind beam tube consists of an aluminum pressure tube encased in thin-walled aluminum jacket. Both jacket and tube are inserted into an aluminum sleeve which lines the opening in the reflector. The sleeve is sealed to the reflector shroud. Cooling water enters through the beam-tube adapter and flows through the annulus formed by the tube and jacket toward the tip of the blind beam tube. At this point, the flow reverses, enters the annulus formed by the sleeve and jacket, and ultimately discharges into the reactor vessel. Coolant flow through the through-beam tube is basically the same except that the coolant is discharged into the vessel at the opposite end of the tube.

7. Material Compatibility and Corrosion

The tests in which a 6061 aluminum specimen was subjected to a heat flux of 100,000 Btu/hr-ft^2 were terminated after a 2000-hr exposure. The specimen was cut from the electrodes, and the edges were milled off to expose the water-cooled surfaces. The surfaces of the specimen were smooth and light gray in color. There was no evidence of film spallation as was observed on the first specimen exposed at the higher temperature. A detailed examination of the specimen will be made, including metallographic sectioning to determine accurately the thickness of the corrosion product film.

The following table lists the temperatures that existed along the specimen, the observed temperature increase during the run, and the oxide thicknesses calculated assuming a thermal conductivity of 1.3 Btu/hr-ft-°F.

Distance from Inlet End (in.)	Temp at Water Interface (°F)	Bulk Water Temperature (°F)	Δt Across Oxide (°F)	Oxide Thickness (mils)
1.00	190	125	13	0.51
1.25	190	126	13	0.51
2.25	190	132	15	0.58
3.25	193	137	18	0.70
3.25	196	137	16	0.62
4.25	197	143	19	0.74
5.25	202	148	24	0.94
5.50	201	149	23	0.90

The first stainless steel specimen was installed in the loop, and a short run was made to demonstrate that the specimen can be tested at a heat flux of 4×10^6 Btu/hr-ft^2. Before a long-term run can be made with the test facility, various orifice plates, additional coolers, and a temperature recorder of greater range than currently exists must be installed. The long-term run should begin during the next month.

IV. NUCLEAR SAFETY

A. Reactor Kinetics

1. Irradiated Fast Reactor Oxide Fuel Pins

The development of mixed oxide fuel has a high priority because of the promise of achieving high burnup at high operating temperatures with this material in fast reactors. However, the state of knowledge of oxide behavior under accident conditions is presently well below that available for the EBR-II Mark-I metallic fuel. Some of the questions relating to the safety of fast reactor oxide fuel include:

(a) What fuel movements can occur short of actual failure that could cause serious rates of reactivity increase?

(b) Can fuel slumping occur rapidly and coherently?

(c) Can other types of physical movements occur?

(d) What are the mechanisms of fuel failure?

(e) What forces influence the fuel movements?

(f) What dominant mechanisms affect coolant pressures?

(g) What roles are played by fission gases and the structural changes resulting from irradiation of the fuel?

The behavior of fast reactor-type (gas-bonded), EBR-II-size UO_2 pins under transient nuclear heating to failure has been studied in TREAT experiments.[12] The tests were conducted with samples contained in an inert gas atmosphere. Cladding thermocouples and high-speed motion-picture photography were used to follow the pin behavior. The general pattern of results was consistent with the physical properties of the oxide. Since the experiments were primarily to investigate phenomena associated with fast reactor oxide fuel under accident conditions, $(U + Pu)O_2$ was not used, nor were studied the effects of appreciable steady-state irradiation, such as fission gas trapped in the fuel structure, fission gas buildup inside the cladding, and formation of central voids or other structural changes.

Ten steady-state-irradiation capsules, each containing two steel-clad, gas-bonded half-length EBR-II-size UO_2 pins have been irradiated in the Materials Testing Reactor (see Progress Report for April 1965, ANL-7045, p. 65). The fuel was 93% dense, and had a ratio of oxygen to uranium of 2.00. These are the first fast reactor oxide fuel samples to be irradiated to appreciable burnup in the ANL Fast Reactor Safety program. The first seven capsules have been removed from the testing

[12] Dickerman, C. E, et al., ANL-6845 (Jan 1965).

reactor and disassembled in the ANL hot lab. They cover a range of nominal burnups of 0.7 to 3 a/o. The remaining three capsules are scheduled to reach 6 a/o burnup. Maximum calculated fuel temperature was 2330°C, although the actual maximum in each pin would be expected to change during irradiation with position, fuel burnup, and changes of fuel structure. Visual examination disclosed no failures in the 14 pins, nor visible cladding deformations. Spot checks of cladding dimensions on each of the pins with a micrometer showed that cladding outer diameters were unchanged. The Al-0.1 w/o Co monitor wires which were wrapped around the specimens during the irradiation will be radiochemically analysed. Neutron radiographs have been taken, using the Juggernaut reactor, in order to determine the internal structure of the pins. (This is necessary for those pins to be run in TREAT if the pretransient structure is to be known.) In the case of control specimens to be destructively examined, radiography is necessary for direct comparison against the TREAT pins and in case of possible structural damage during disassembly.

Significant structural changes, indicating that exposure levels were in the range specified, are seen in the neutron radiographs. Figure 26 shows seven of the pins. Central voids are clearly visible. Some lateral cracking has occurred, but the pellet-pellet interfaces are not as prominent as the cracks.

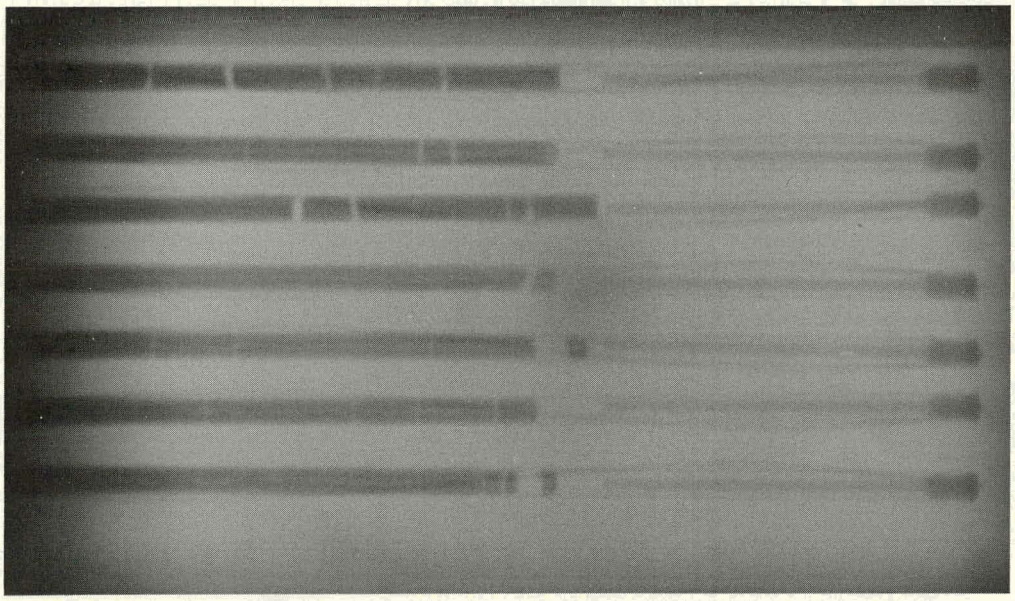

Fig. 26. Neutron Radiographs of a Portion of Irradiated Oxide Specimens, Showing the Typical Post-irradiation Internal Structure

Because of the relative lack of detailed information on this type of oxide fuel pin irradiated at high power ratings, one pin from each two-pin capsule is scheduled for destructive, detailed examination as a control specimen. Coarse gamma-ray scanning at 1-cm intervals over the fuel lengths were made. Continuous gamma scans are also being made.

2. Fast Reactor Safety

a. Coolant (Water) Expulsion Studies. The maximum energy input rate of the system has been reached (about 110 kW) and other parameters are now being studied, notably the annular gap.

The correlations of a large mass of data now available, are still inchoate. Several high-speed motion pictures have been analyzed and expulsion velocities of about 5 m/sec were observed.

The collection of data should be completed within two months which will allow more emphasis on analysis and correlation.

b. Superheat Experiments. This experiment is designed to measure the degree of liquid superheat required to initiate nucleate boiling in sodium under various conditions simulating a reactor environment. Typical parameters will be systematically varied to determine their independent and combined effects upon the liquid superheat necessary to initiation nucleation: pressure, dissolved gas content, heat flux, and surface characteristics.

Assembly of this experiment is underway. Four superheat test vessels and the containment vessel have already been fabricated. Completion of assembly awaits the arrival of the high-temperature, fast-response piezioelectric pressure transducer which is necessary for the measurement of pressure transients during sudden void formation. Also, some of the recording instrumentation for this experiment has not been received.

c. Sodium Expulsion Experiment. In this experiment, it is planned to investigate the mechanism of coolant expulsion in a simulated reactor environment. Hence, this experiment includes the measurement of void distribution, expulsion velocities, pressure transients, and liquid superheats during coolant expulsion.

A preliminary design evaluation of this sodium expulsion experiment has been initiated. Preliminary drawings of the experimental apparatus are being made.

d. Critical Flow Studies. Calculations of the progression of accidents in sodium-cooled reactors reveal that critical flow may exist in the core and lead to detrimental effects, such as voidage of the coolant channel, shock phenomena, and pressure buildup.

The design and construction of experiments to study critical flow of different fluids are continuing. Final design of the sodium loop and the water loop to be used in the low-pressure region (0-15 psia) has been completed. Fabrication of individual components for the loops and layout of the instrumentation have been initiated.

3. Containment Program

A literature survey has uncovered a number of computer programs, mostly from Livermore Radiation Laboratory, which can be adopted to reactor safety studies. These programs were originally developed for the Plowshare program, but are sufficiently general to include arbitrary equations of state. The one-dimensional codes handle material behavior ranging from pure elastic up through the high-pressure hydrodynamic region. In addition, mechanisms such as crushing, compaction, and crack propagation are included so that these programs can also be used in excursion studies. The two-dimensional codes handle only the elastic-plastic, plastic, or hydrodynamic phases. These programs will be adapted to the Argonne computers.

By use of a new finite Hankel transform, the following problems have been solved:

a. the radial vibration of an infinitely long, thick, elastic circular shell when the surfaces have tractions which are arbitrary functions of time;

b. radially symmetric vibrations of a thick, elastic spherical shell with surface tractions as in (a);

c. extension of (a) and (b) to the case of N concentric shells. This corresponds to the containment idea of multiple regions for protection.

The solutions were obtained in closed form. However, before any numerical results can be obtained, the frequency equations must be solved so that the displacements and stresses can be calculated.

B. TREAT

1. Operations

A sample of prototype SEFOR fuel that had previously been irradiated to a burnup of 10 MWd/ton was subjected to seven transient irradiations for the General Electric Company.

Two metal-water reaction samples (CEN-218 and CEN-219), consisting of four Zircaloy-2 clad, vibratory-compacted UO_2 rods, were irradiated in room temperature water. These are the first metal-water reaction experiments run in TREAT with vibratory-compacted UO_2.

Two metal-water reaction experiments were run in transparent capsules to obtain photographic data on the behavior of aluminum-clad, plate-type fuel elements when they are heated above the melting point of aluminum prior to contact with water. One sample was aluminum-uranium alloy of the SPERT 1-D type, and the other was an HFIR-type cermet plate.

A total of eleven transients were run to test the transient characteristics of samples of a rocket reactor fuel being developed by Argonne.

2. Large TREAT Loop

The contractor completed installing insulation on the heated systems in the sodium equipment room. Interconnection of the electrical heaters is in progress.

Reassessment of the damage to the sodium-filling tank (see Progress Report for January 1966, ANL-7152, p. 90) indicated that the tank is usable and will be available for filling the TREAT system when required.

C. Chemical and Associated Energy-transfer Problems in Reactor Safety

1. Metal-Water Reactions

a. Scale-up Metal-Water Experiments in TREAT with UO_2-core Fuel Clusters. An experiment has been performed in TREAT in which three Zircaloy-2-clad, UO_2-core fuel pins were melted while suspended above a pool of water. The purpose of this experiment was to simulate certain aspects of a loss-of-coolant accident in which a break in a primary-system water pipe of a nuclear power reactor would result in the fuel elements being left in contact with steam at high temperature. (A calculational study estimating the extent of the subsequent cladding-water reaction was reported in the Progress Report for April 1965, ANL-7045, pp. 67-69.)

The experimental assembly used was that previously described for scale-up experiments (see Progress Report for November 1964, ANL-6977, p. 83). However, the experiment differed from the previous UO_2-core, scale-up transients which simulated power excursion incidents (see Progress Report for September 1965, ANL-7105, p. 81) as follows:

(1) The fuel cluster consisted of 3 pins (of 0.42-in. dia by $5\frac{5}{8}$ in. long) rather than 9.

(2) The pins were located above a pool of water rather than submerged in it.

(3) The meltdown was achieved during a "flat-top" transient rather than a pulse.[13]

[13]In the "flat-top" transient, fission heating remained reasonably constant over a period of about 12 sec. In a pulsed transient, the time scale for heating is about 1 sec, with a Gaussian-shaped power-time heating curve.

The results of this experiment are summarized in Table XX. In this meltdown, 38 w/o of the fuel cluster dropped into the water, although the larger particles tended to be retained above the water by the autoclave supporting structure. (Table XX shows that a smaller average particle size of the residue was collected in the water compared with that of the residue remaining above the water.) The extent of cladding-water reaction was 40% as determined by the total amount of hydrogen released; however, it was not apparent that cladding which dropped into the water had more extensively reacted than the cladding which remained on the supporting structure. All of the hydrogen produced was assumed to be formed by reaction of the Zircaloy cladding. The reaction of the UO_2 core with water would be

TABLE XX. Results from In-pile (TREAT) Meltdown Experiment CEN-217-S: UO_2-core Zircaloy-2-clad Fuel Cluster Subjected to Flat-top Transient

Fuel Cluster	
No. of Pins[a]	3
Cladding[b]	Zircaloy-2
Weight, g	336[c]
Transient	
Type of Incident Simulated[d]	Loss of Coolant
Fission Energy Input, cal/g UO_2	560
Time of Heating, sec	12
Peak Adiabatic UO_2 Temperature, °C	3300 (vapor region)
Results	
Metal-Water Reaction, %	40
Peak Pressure Rise, psi	87
Chemical Energy Release, % of Total Energy	26
Average Particle Size of Residue (d_{sv}),[e] mils	
Residue remaining above water	240
Residue in water	50
Total residue	91
Appearance of Fuel after Meltdown	Complete destruction; molten UO_2 ran out, leaving sections of hollow cylinders of the Zircaloy cladding.

[a] Ten pellets of UO_2 (10% enriched with U^{235}) per pin. Overall pin dimensions were 0.42 in. in diameter by $5\frac{5}{8}$ in. long.

[b] 25-mil-thick cladding; 3-mil gap between core and cladding; helium bonded.

[c] 254 g of UO_2 and 82 g of Zircaloy-2.

[d] The fuel pins were suspended above ambient temperature water.

[e] $d_{sv} = \frac{\Sigma n_i d_i^3}{\Sigma n_i d_i^2}$ where n_i = number of particles with diameter d_i.

expected to become significant only after the cladding was completely oxidized, since the presence of excess hydrogen greatly suppresses the UO_2-water reaction. The chemical energy contributed by the reaction corresponded to 26% of the total energy (i.e., the contribution of the nuclear energy of the transient was 74%).

The oscillograph records of the temperature and pressure measurements from the experiment are shown in Fig. 27. The sequence of events deduced from the figure and from the appearance of the residue may be summarized as follows:

Time (sec)	Energy Input (cal/g UO_2)	Event
0	0	Initiation of fission heating.
7	360	Thermocouple on the Zircaloy cladding records 2430°C and fails, indicating that fuel slumping has begun.
~8.2	480	Pressure rises rapidly owing to the formation of steam and/or evolution of hydrogen, indicating that fragments of fuel are probably entering the water.
~9.3	500	Thermocouple in the water records rapid temperature rise, indicating that the fuel has made contact with the thermocouple (temperature recorded in excess of 1000°C).
12	560	End of heating; pressure rises only very slowly, indicating end of the reaction.

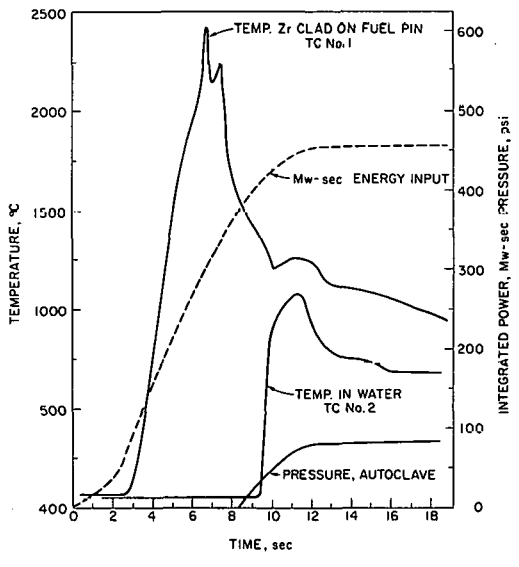

Fig. 27. Oscillograph Record of TREAT Transient CEN-217S

One of the most interesting and possibly significant points in connection with this experiment was the final appearance of the meltdown residue. This was the first time that portions of the cladding were found still in their original cylindrical form, but with the UO_2 core not present. Evidently, the UO_2 had melted and flowed out of the cladding. A photograph of the major portion of the residue is shown in Fig. 28. The observed extent of zirconium-water reaction agrees well with the previously published correlation from meltdown experiments in TREAT in which the fuel pins were submerged in water (see Progress Report for September 1965, ANL-7105, p. 81).

Fig. 28. Residue from Zircaloy-clad, UO_2-core Fuel Pins after TREAT Transient Simulating a Loss-of-coolant Incident

Since the energy developed in this experiment (560 cal/g UO_2) was high enough to vaporize the UO_2 adiabatically and the time scale (12 sec) was relatively short, the experiment was not an exact simulation of a loss-of-coolant accident. Therefore the extent of reaction is not directly comparable to what might be expected in such a situation. Nevertheless, the residue shown in Fig. 28 gives some indication of the meltdown model that must be considered in the analysis of this type of incident.

D. Plutonium Volatility Safety

1. Environmental Contamination Control

A program has been established to investigate various aspects of environmental contamination control as related to the reprocessing of reactor fuel materials by fluoride volatility techniques. Several experimental programs which are already under way are related to this study. These programs involve the study of the removal of plutonium hexafluoride from cell exhaust air by hydrolysis and filtration, and bench-scale fluid-bed studies with irradiated fuel materials. In the studies with irradiated fuels, particular attention is directed toward obtaining information related to the behavior of volatile fission product species in process-gas streams. Other investigations which have been recently started are concerned with the development of systems for the effective removal of fluorine, interhalogens, and hydrogen fluoride from process off-gas streams, and studies related to the chemistry of tellurium fluorides, particularly the removal of tellurium hexafluoride from gas streams by reaction with activated alumina or soda lime.

V. PUBLICATIONS

Papers

Spectrophotometric Determination of Ruthenium with 1-Nitroso-2-Naphthol
Gwendolyn Kesser, R. J. Meyer, and R. P. Larsen
Anal. Chem. 38(2), 221-224 (February 1966)

Fast Reactor Stability and Safety
J B. Nims, A. E. Klickman, R. B. Nicholson, R. R. Smith, and J. A. Thie
Proc. American Nuclear Society National Topical Meeting on Fast Reactors, Detroit, April 26-28, 1965. ANS-100, pp. 213-224

The Remote Fabrication of Reactor Fuels
A. B. Shuck, A. L. Lotts, and Kirk Drumheller
Reactor Technology. Selected Reviews--1965, ed. L. E. Link U. S. Atomic Energy Commission Publication TID-8541, pp. 71-148

Irradiation Behavior of Metallic Fuels
J. H. Kittel, T. K. Bierlein, B. R. Hayward, and W. C. Thurber
Proc. 3rd Intern. Conf. on Peaceful Uses of Atomic Energy, Geneva, August 31-September 9, 1964. United Nations, New York, 1965, Vol. 11, pp. 227-234

Fabrication of Solid Fuels for Fast Reactors
R. E. Macherey, H. W. Alter, and A. A. Shoudy
Proc. 3rd Intern. Conf. on Peaceful Uses of Atomic Energy, Geneva, August 31-September 9, 1964. United Nations, New York, 1965, Vol. 10, pp. 180-189

Effect of Flow Passages on Two-phase Critical Flow
T. C. Min, H. K. Fauske, and Michael Petrick
Ind. Eng. Chem. Fundamentals 5(1), 50-55 (February 1966)

Fast Reactor Test Facility (FARET) and Initial Experimental Program
W. R. Simmons, P. J. Persiani, and T. R. Bump
Fast Reactor Technology, Am. Nucl. Soc. Natl. Topical Meeting, Detroit, April 26-28, 1965. ANS-100 (Suppl.), pp. 37-55

Report on Argonne National Laboratory's Activities
R. C. Goertz
Proc. 1964 Seminars on Remotely Operated Special Equipment, Jackass Flats, Nevada, November 4-5, 1964. USAEC Report CONF-641120, Vol. II, pp. 41-47

Some Work on Manipulator Systems at Argonne National Laboratory, Past, Present, and a Look at the Future
R. C. Goertz
Proc. 1964 Seminars on Remotely Operated Special Equipment, Germantown, Md., May 26-27, 1964. USAEC Report CONF-640508, Vol. I, Parts I and II, pp. 27-69

ANL Reports

ANL-6417 THE FABRICATION AND TESTING OF DEPLETED URANIUM BLANKET SLUGS FOR EBR-II
W. R. Burt, Jr., R. D. McGowan, and C. H. Bean

ANL-6893 FABRICATION AND EVALUATION OF THORIA-URANIA FUEL MATERIAL
E. D. Lynch and J. H. Handwerk

ANL-6898 ENGINEERING DEVELOPMENT OF FLUID-BED FLUORIDE VOLATILITY PROCESSES. Part 3. Fluid-bed Fluorination of Uranium Dioxide Fuel Pellets
L. J. Anastasia, J. D. Gabor, and W. J. Mecham

ANL-7025 CRITICAL TEMPERATURES AND DENSITIES OF THE ALKALI METALS
Ira G. Dillon, P. A. Nelson, and B. S. Swanson

ANL-7035 A PRELIMINARY EVALUATION OF THE USE OF HIGH-TEMPERATURE PROCESS HEAT AS PART OF A TOTAL NUCLEAR-ENERGY SOURCE
L. J. Gordon and J. F. Marchaterre

ANL-7055 CHEMICAL ENGINEERING DIVISION SEMIANNUAL REPORT, January-June 1965

ANL-7062 GLASSY MATERIALS FOR NUCLEAR REACTOR APPLICATIONS
E. D. Lynch

ANL-7073 SELF-SUSTAINED HYDRODYNAMIC OSCILLATIONS IN A NATURAL-CIRCULATION TWO-PHASE-FLOW LOOP
Kamal C. Jain

ANL-7094 REVIEW OF STATUS OF SELF-DIFFUSION IN US, UN, UO_2, AND UC
C. M. Walter

ANL-7097 THREE-DIMENSIONAL STRESS CONCENTRATION AROUND A CYLINDRICAL HOLE IN A SEMI-INFINITE ELASTIC BODY
Carl K. Youngdahl and Eli Sternberg